



Melt Extruded Drug Formulations for Individual Dosing by the Solid Dosage Pen

Inaugural-Dissertation

zur Erlangung des Doktorgrades
der Mathematisch-Naturwissenschaftlichen Fakultät
der Heinrich-Heine-Universität Düsseldorf

vorgelegt von

Eva Julia Laukamp

aus Hannover

Düsseldorf, Dezember 2014

aus dem Institut für Pharmazeutische Technologie und Biopharmazie
der Heinrich-Heine-Universität Düsseldorf

Gedruckt mit der Genehmigung der
Mathematisch-Naturwissenschaftlichen Fakultät der
Heinrich-Heine-Universität Düsseldorf

Referent: Prof. Dr. Jörg Breitzkreutz
Korreferent: Prof. Dr. Dr. h.c. Peter Kleinebudde

Tag der mündlichen Prüfung: 21.01.2015

“I keep on making what I can't do yet
in order to learn to be able to do it.”

Vincent Van Gogh in a letter to his brother Theo (September 1885)

Publications

Parts of this thesis have already been published in peer-reviewed journals or at conferences:

K. Wening, E.J. Laukamp, M. Thommes, J. Breitzkreutz, *Individual oral therapy with immediate release and effervescent formulations delivered by the Solid Dosage Pen*, J. Pers. Med. 2012, 2(4), 217-231

E.J. Laukamp, M. Thommes, J. Breitzkreutz, *Hot-melt extruded drug-loaded rods: evaluation of the mechanical properties for individual dosing via the Solid Dosage Pen*, Int. J. Pharm. 2014, 475, 344-350

E.J. Laukamp, A.-K. Vynckier, J. Voorspoels, M. Thommes, J. Breitzkreutz, *Development of sustained and dual drug release co-extrusion formulations for individual dosing*, Eur. J. Pharm. Biopharm. 2015, 357-364

E.J. Laukamp, M. Thommes, J. Breitzkreutz, *Micropellet-loaded rods with dose-independent sustained release properties for individual dosing via the Solid Dosage Pen*, work in progress

E.J. Laukamp, M. Pein, M. Thommes, J. Breitzkreutz, *Carbamazepine modification in Mini-moulds: A question of analytical selectivity or formulation and production?*, Talk, 6th Annual PSSRC Symposium, Lisbon 2012

E.J. Laukamp, M. Pein, M. Thommes, J. Breitzkreutz, *What you see is what you get? – Raman spectroscopy as a PAT-tool for hot melt extrusion*, Talk, 7th Annual PSSRC Symposium, Lille 2013

E.J. Laukamp, M. Thommes, J. Breitzkreutz, *Small-scale production of hot-melt ram-extrudates via a high pressure capillary rheometer*, Talk, 7th Polish-German Symposium on Pharmaceutical Sciences, Gdańsk 2013

E.J. Laukamp, A.-K. Vynckier, M. Thommes, J. Breitzkreutz, *Development of sustained and pulsatile release co-extrusion formulations for individual dosing*, Talk, 9th PBP World Meeting, Lisbon, 2014

E.J. Laukamp, M. Thommes, J. Breitzkreutz, *Excipient screening for individually dosing by the Solid Dosage Pen*, Poster, 4th EuPFI Conference, Prague 2012

E.J. Laukamp, M. Thommes, J. Breitzkreutz, *Small-scale production of hot-melt ram-extrudates via a high pressure capillary rheometer*, Poster, 7th Polish-German Symposium on Pharmaceutical Sciences, Gdańsk 2013

E.J. Laukamp, M. Thommes, J. Breitzkreutz, *Immediate-release carbamazepine formulations for individual dosing by the Solid Dosage Pen*, Poster, 5th EuPFI Conference, Barcelona 2013, PCCA-Poster Award

E.J. Laukamp, M. Thommes, J. Breitzkreutz, *Small-scale melt extrusion with a high pressure capillary rheometer: A predictive tool for cuttable drug-loaded rods for individual dosing*, Poster, AAPS Annual Meeting, San Antonio, 2013

E.J. Laukamp, M. Thommes, J. Breitzkreutz, *Micropellet-loaded rods for individual dosing via the Solid Dosage Pen - Combining advantages of monolithic and multiparticulate dosage forms*, Poster, 6th EuPFI Conference, Athens 2014

E.J. Laukamp, M. Thommes, J. Breitzkreutz, *Are school children capable to utilise the Solid Dosage Pen? - A study of the mechanical properties versus the pinch strength*, Poster, 6th EuPFI Conference, Athens 2014

Table of Contents

1.	Introduction	1
1.1.	Opportunities and Challenges of Individual Dosing	1
1.2.	The Solid Dosage Pen.....	2
1.3.	Manufacturing of Rods for the SDP.....	2
1.4.	Carbamazepine as Model Drug.....	4
1.5.	Excipients for the Formulation Development	7
2.	Aims and Outline.....	9
3.	Results and Discussion	11
3.1.	Small-Scale Production Techniques.....	11
3.1.1.	Introduction and Objectives.....	11
3.1.2.	Mini-Moulds.....	11
3.1.3.	Ram-Extrudates.....	12
3.1.3.1.	Ram-Extrusion via a High Pressure Capillary Rheometer	12
3.1.3.2.	Mechanical Properties.....	16
3.1.3.3.	Dissolution Studies	21
3.1.3.4.	Addition of Pore Formers	24
3.1.4.	Solid State Properties	26
3.1.5.	Summary.....	33
3.2.	Drug-Loaded Rods	35
3.2.1.	Introduction and Objectives.....	35
3.2.2.	Extrudates.....	36
3.2.2.1.	Hot-Melt Extrusion via a Twin-Screw Extruder	36
3.2.2.2.	Mechanical Properties.....	37
3.2.2.3.	Interindividual Manual Forces	40
3.2.2.4.	Dissolution Studies	41
3.2.2.5.	Application of the Solid Dosage Pen.....	42
3.2.2.6.	Uniformity of Dosage Units	44
3.2.2.7.	Stability Studies.....	45
3.2.2.8.	Influence of the Mechanical Properties on the Mass Uniformity	46
3.2.3.	Co-Extrudates.....	49
3.2.3.1.	Formulation Development	49
3.2.3.2.	Hot-Melt Co-Extrusion via Connected Twin-Screw Extruders.....	52
3.2.3.3.	Mechanical Properties.....	55
3.2.3.4.	Dissolution Studies	56
3.2.3.5.	Solid State Properties	61
3.2.3.6.	Application of the Solid Dosage Pen.....	63

3.2.3.7.	Uniformity of Dosage Units.....	63
3.2.3.8.	Stability Studies.....	65
3.2.4.	Summary	68
3.3.	Micropellet-Loaded Rods	69
3.3.1.	Introduction and Objectives	69
3.3.2.	Feasibility Study	69
3.3.3.	CBZ Layering on Micropellets.....	73
3.3.3.1.	Layering Process	73
3.3.3.2.	Particle Size Measurements and Surface Properties	75
3.3.3.3.	Dissolution Studies.....	76
3.3.4.	Sustained Release Coating of CBZ Micropellets.....	77
3.3.4.1.	Coating Process.....	77
3.3.4.2.	Particle Size Measurements and Film Properties	79
3.3.4.3.	Dissolution Studies.....	81
3.3.4.4.	Pressure Compatibility.....	84
3.3.4.5.	Matrix Compatibility	85
3.3.5.	Embedding of Micropellets into Rods	87
3.3.5.1.	Ram-Extrusion via a HPCR.....	87
3.3.5.2.	Mechanical Properties	89
3.3.5.3.	Disintegration Time and Dissolution Studies	91
3.3.5.4.	Application of the Solid Dosage Pen	95
3.3.5.5.	Stability Studies.....	96
3.3.6.	Summary	98
4.	Summary	99
5.	Zusammenfassung	101
6.	Experimental Part.....	105
6.1.	Materials.....	105
6.2.	Methods	107
6.2.1.	Manufacturing Methods.....	107
6.2.1.1.	Production of CBZ Modification I and CBZ Dihydrate.....	107
6.2.1.2.	Melting and Moulding	107
6.2.1.3.	Small-Scale Ram-Extrusion	107
6.2.1.4.	Hot-Melt Extrusion of Extrudates.....	108
6.2.1.5.	Hot-Melt Co-Extrusion.....	109
6.2.1.6.	Immersion of Extrudates.....	109
6.2.1.7.	CBZ Layering on Micropellets.....	110
6.2.1.8.	Sustained Release Coating of CBZ Micropellets.....	110
6.2.1.9.	Ram-Extrusion of Micropellet-Loaded Rods.....	111

6.2.2.	Feasibility Study.....	112
6.2.3.	Analytical Methods.....	112
6.2.3.1.	Maximum Cutting Force of the Extrudates	112
6.2.3.2.	Tensile Strength and E-modulus of the Extrudates	113
6.2.3.3.	Tensile Strength of the Micropellets	114
6.2.3.4.	Microscopy.....	114
6.2.3.5.	Dynamic Image Analysis.....	115
6.2.3.6.	Disintegration Time.....	115
6.2.3.7.	Dissolution Testing.....	115
6.2.3.8.	X-Ray Powder Diffraction (XRPD).....	116
6.2.3.9.	Fourier Transform-Infrared Spectroscopy (FT-IR).....	116
6.2.3.10.	Differential Scanning Calorimetry (DSC).....	117
6.2.3.11.	Raman Spectroscopy.....	117
6.2.3.12.	CBZ Equilibrium Solubility and Partition Coefficient	118
6.2.4.	Application of the Solid Dosage Pen.....	119
6.2.4.1.	Dosing.....	119
6.2.4.2.	Mass Variation.....	119
6.2.4.3.	Content Uniformity	119
6.2.4.4.	Uniformity of Dosage Units	119
7.	Bibliography.....	121
8.	Danksagung.....	131

Abbreviations

API	active pharmaceutical ingredient
aPMMA	amino-polymethylmethacrylate, Eudragit® E, basic butylated methacrylate copolymer (Ph. Eur.)
AV	acceptance value (Ph. Eur. 2.9.40)
BCS	Biopharmaceutics Classification System
CBZ	carbamazepine
CBZ I	carbamazepine modification I
CBZ III	carbamazepine modification III
CBZ DH	carbamazepine dihydrate
CHMP	Committee for Medicinal Products for Human Use
CI	confidence interval
DF	degree of freedom
DIA	dynamic image analysis
DSC	differential scanning calorimetry
DU	dose unit
EMA	European Medicines Agency
E-modulus	Modulus of Elasticity, Young's modulus
FDA	United States Food and Drug Administration
F_{\max}	maximum cutting force [N]
FT-IR	Fourier transform-infrared spectroscopy
GABA	gamma aminobutyric acid
HME	hot-melt extrusion
HPC	hydroxypropyl cellulose
HPCR	high pressure capillary rheometer
HPMC	hydroxypropyl methylcellulose, hypromellose
HPMC AS	hydroxypropyl methylcellulose acetate succinate
HSM	hot stage microscopy
IQS	inter-quartile span
log P	octanol-water partition coefficient
MCC	microcrystalline cellulose
MM	Mini-moulds

MPLR	micropellet-loaded rod
M_w	mean molecular weight [g/mol]
PCL	poly(ϵ -caprolactone)
PEG	polyethylene glycol, macrogol
PEO	polyethylene oxide, high-molecular macrogol
Ph. Eur.	European Pharmacopoeia
PM	Physical mixture
POL	poloxamer 188
PTFE	polytetrafluoroethylene, Teflon [®]
PVAc	polyvinyl acetate, Kollicoat [®] SR 30 D
PVA-PEG	polyvinyl alcohol-polyethylene glycol graft polymer, Kollicoat [®] IR
PVP	polyvinyl pyrrolidone, povidone
RH	relative humidity [%]
R^2	determination coefficient
SA	stearic acid
SD	standard deviation
SDP	Solid Dosage Pen
SEM	scanning electron microscopy
SNV	standard normalised variance
$T_{\text{barrel optimal}}$	optimal barrel temperature [°C]
TEC	triethyl citrate
t_{equil}	equilibration time of the barrel [min]
T_{extr}	extrusion temperature (barrel temperature) [°C]
T_g	glass transition temperature [°C]
T_m	melting temperature [°C]
USP	United States Pharmacopoeia
v_{piston}	piston velocity [mm/min]
WHO	World Health Organization
XRPD	x-ray powder diffraction

1. Introduction

1.1. Opportunities and Challenges of Individual Dosing

Individual dosing of medicines is a key topic in paediatrics and geriatrics (Breitkreutz and Boos, 2007; Standing and Tuleu, 2005; Stegemann et al., 2010) as well as in personalised medicine (Florence and Lee, 2011; Ingelman-Sundberg et al., 2007).

The demand for flexible dosing has been investigated and most recently accessible systems and development approaches have been categorised according to their dose flexibility and expenditure (Wening and Breitkreutz, 2011). Recently, delivery devices for the administration of paediatric formulations have been reviewed and have been discussed by the European Paediatric Formulation Initiative (Walsh et al., 2011).

The repertory for individual oral dosing so far includes liquid drug formulations like suspensions or solutions as well as solid multiparticulate dosage forms like granules, pellets or (mini-)tablets. Measuring can be achieved via partition of monolithical forms or accumulation of multiple drug carriers (Wening and Breitkreutz, 2011).

Due to stability concerns or drug solubility, liquid oral dosage forms are frequently limited (Breitkreutz et al., 1999). Dosing devices like spoons, cups, or syringes for liquid drug formulations often fail in measuring appropriate doses (Griessmann et al., 2005; Sobhani et al., 2008; Tanner et al., 2014).

In contrast, solid monolithic dosage forms may provide a stable and easy dosing approach (EMA/CHPM, 2013) and the acceptance of uncoated mini-tablets as oral solid single dosage forms, for instance, was shown to be superior to syrup (Klingmann et al., 2013; Spomer et al., 2012). However, the number of dose-strengths needed to treat patients appropriately is increased by applying solid single dosage forms (Salunke et al., 2011).

One common strategy of dose adaption for peroral applications is the splitting of tablets. By means of divisible tablets a limited number of fixed parts may be administered (Kayitare et al., 2009). But this approach may involve difficulty of breaking, imprecise dosing, loss of drug-loaded mass, and potentially lead to the formation of potent dust (van Santen et al., 2002).

Due to these still existing challenges in individual dosing, innovative drug formulation concepts and novel devices or dispensing systems are needed. For the compliance of patients, acceptance as well as safe and easy handling of such devices, both from the patients' and caregivers' perspectives, were demanded (Salunke et al., 2011). Moreover, principal requirements in the field of pharmaceuticals like dosage conformity and specified drug release properties, which have to be independent of the delivered individual dose, have to be taken in mind.

The superior target to overcome challenges of individual dosing would be the provision of one dosage form and one corresponding device which meet the requirements of all patient groups.

1.2. The Solid Dosage Pen

A novel dosing device, a “dosing stick for rod-shaped tablets”, was patented in 2002 for the individual dosing of medicines for oral administration (Schoemakers and Grummel, 2002). Based on this idea, a prototype of the device has been constructed and evaluated (Wening and Breitzkreutz, 2010; Wening et al., 2012). This device - called the Solid Dosage Pen (SDP) - consists of an adjusting screw for dose definition, a feeder- and a cutting mechanism, a sample outlet and a sealing cap (Figure 1).



Figure 1: Solid Dosage Pen, adjusting screw for dose definition (a), feeder mechanism (b), drug-loaded rod (c), cutting mechanism and sample outlet (d) and sealing cap (e)

A drug-loaded rod, which may be manufactured via extrusion technologies, is placed into the shaft of the device and made individual dosing by cutting slices of pre-defined heights possible. Finally, these individually dosed tablet-like slices can directly be administered. Due to the possibility to refill the delivery device for reuse, costs of the system could be reduced to an acceptable value. Therefore, the SDP may combine low expenditure with high dose flexibility according to the classification of Wening et al. (2011).

1.3. Manufacturing of Rods for the SDP

Melt extrusion represents a promising drug delivery technology as matrix formulations in which the drug is homogeneously embedded may be produced (Breitenbach, 2002; Crowley et al., 2007; Repka et al., 2007). Moreover, melt extrusion has proved to be a suitable technology to produce drug-loaded rods as dosage forms for the SDP (Wening and Breitzkreutz, 2010; Wening et al., 2012).

Extrusion processes include amongst others ram-extrusion and screw-extrusion:

For ram-extrusion, materials are introduced into a heated cylinder and after an initiation period to soften the materials, a ram (or a piston) presses the soft materials through the die and transforms them into the desired shape (Crowley et al., 2007).

Rod-shaped dosage forms manufactured via ram-extrusion have already been described in literature (Grassi et al., 2003; Perissutti et al., 2002; Pinto and Silverio, 2001; Quintavalle

et al., 2007). For example, a cylindrical sustained-release dosage form with 3 mm diameter and 5 mm length was developed by means of a ram-extrusion process by Grassi et al. (2003) and ram-extrusion was proposed as manufacturing technique for a potential rapid release dosage form by Perissutti et al. (2002).

Due to the discontinuous process, ram-extruders may be operated with small quantities of material and thus have outstanding properties for early development. Nevertheless, some drawbacks, like the poor temperature uniformity within the extrudate or lower homogeneity, as compared to extrudates processed by screw extrusion, have to be faced (Crowley et al., 2007).

For pharmaceutical applications, twin-screw extruders are widely utilised as they include distributive and dispersive mixing as main advantages over ram-extrusion (Crowley et al., 2007). Mixing, melting, and shaping are continuously performed as a one-step process. So far, the drug-loaded rods for the SDP have been manufactured on a twin-screw extruder via wet-extrusion or melt-extrusion (Wening and Breitzkreutz, 2010; Wening et al., 2012).

Hot-melt co-extrusion has recently been proposed for various peroral, subcutaneous as well as intra-vaginal pharmaceutical applications (Fischer, 2008; Groenewegen, 1999; Iosio et al., 2008). Via co-extrusion, more than one layer, for instance a core and a concentric coat (Dierickx et al., 2013; Dierickx et al., 2012; Quintavalle et al., 2008; Vynckier et al., 2014a) or a multi laminar structure (Müllers et al., 2013; Oliveira et al., 2014), can be manufactured. Bi-layered pellets have been prepared by a co-extrusion and spheronisation process (Iosio et al., 2008; Pinto et al., 2001). In 2003 a “polymer release system” based on a polymer (mixture) - typically including polyethylene oxide (PEO) - and a water-insoluble coating, which tailors the dissolution behaviour of an included active pharmaceutical ingredient (API), was patented (Fischer et al., 2003). In a first review, the requirements, challenges, and opportunities of the co-extrusion technique have been highlighted and an overview of the co-extrusion equipment and downstream processing is given (Vynckier et al., 2014b).

Quintavalle et al. (2007 and 2008) manufactured cylindrical co-extrudates with controlled drug release via melt-extrusion. They utilised a laboratory scale vertical ram-extruder with a specially modified head. It was demonstrated that the drug release properties can be tailored through a suitable selection of the dimensions of the cylinder and the formulation of the core and the coat layer.

Lately, co-extrusion with two twin-screw extruders connected by a co-extrusion die was proposed to manufacture fixed dose combination mini-matrices (2 mm in length and 3 mm in diameter) for oral application (Dierickx et al., 2012; Vynckier et al., 2014a).

More recently, dual drug release formulations were successfully produced via co-extrusion (Dierickx et al., 2013). The term “dual release” has been introduced in literature and means in this context the superposition of two release kinetics resulting in a biphasic dissolution profile. Two different polymer combinations were utilised to obtain multilayer

mini-matrices. The drug release could be tailored by varying the drug-loading within the core and the coat.

In conclusion, co-extrusion offers various opportunities for the development of solid peroral dosage forms. Nevertheless, this technique includes some challenges, like finding functional polymer combinations for the desired dissolution characteristics, having a similar extrusion temperature and melt viscosity for the extrusion process, and achieving sufficient adhesion between the layers (Dierickx et al., 2013; Dierickx et al., 2012; Vynckier et al., 2014a; Vynckier et al., 2014b). Until now, co-extrusion technologies have not been used for the purpose to produce drug-loaded rods for the SDP and so far, a combination of immediate and sustained release characteristics of a drug in one formulation for the SDP has not been realised.

The SDP has been introduced for individual dosing of monolithic, tablet-like drug carriers sliced from a drug-loaded rod. The formulations provided both immediate and sustained release characteristics (Wening and Breitzkreutz, 2010; Wening et al., 2012). But as a drawback, the extent of the drug release prolongation for sustained release formulations depended on the dose of the monolithic sliced drug carriers due to square root kinetics or non-Fickian diffusion mechanism of the prolongation (Wening, 2011). Multiparticulate solid dosage forms like coated pellets (Kayumba et al., 2007) permit dose-independent dissolution characteristics, but often lack the ease of administration (Wening and Breitzkreutz, 2011).

Lately, peroral drug delivery systems for administration of multiparticulates have been proposed: Sustained release coated pellets have been embedded into tablet-shaped matrices made from macrogol (polyethylene glycol, PEG) with different molecular weights (Schmidt and Bodmeier, 2001). Moreover, Schilling and McGinity (2010) prepared monolithic matrices containing enteric-coated micropellets. Multiparticulates of different mechanical strength (granules, pellets and drug-layered spheres) were embedded into six hydrophilic polymers (PEGs, PEOs and poloxamers) by single-screw hot-melt extrusion. As oral drug delivery systems, flat-faced tablets were cut from the extruded strand (diameter 6 mm). Matrices containing up to 40 % particles met the requirements for delayed-release dosage forms of the United States Pharmacopoeia (USP) and stability over storage was proven due to the low tendency of the carrier to migrate into the enteric film.

1.4. Carbamazepine as Model Drug

In this work, carbamazepine (CBZ) was utilised as model drug. CBZ is administered as an anticonvulsive drug in a wide range of doses for the medical treatment of children, adults, as well as elderly people suffering from seizures and other epileptic episodes (Kearns et al., 2003; Rowan et al., 2005).

The molecule stabilises the inactivated state of voltage-gated sodium channels leaving the affected cells less excitable (Ragsdale et al., 1991; Willow et al., 1985). The drug has also been shown to modulate γ -amino butyric acid (GABA)-receptors (Granger et al., 1995).

Both the incidence and prevalence of epilepsy are particularly high among children and elderly people. Figure 2 illustrates the incidence of unprovoked seizures in industrialised countries according to Cloyd et al. (2006). Besides, the age-specific incidence of status epilepticus shows a bimodal distribution, with the highest rates in infants and the elderly (Cloyd et al., 2006).

The World Health Organization (WHO) listed CBZ on the “Model List of Essential medicines” (18th edition, April 2013, final amendments October 2013) attesting its global relevance in treatment.

The therapeutic dose for adults was described to be 5 - 8 mg/kg twice a day (Kearns et al., 2003). As the clearance of CBZ from plasma was discovered to be higher in children than in adults, Kearns et al. suggested higher weight-adjusted doses for infants and children (3 - 10 mg/kg body weight three times a day). Exemplarily, for a 6-year-old child weighing 20 kg, this regimen results in single doses of 60 - 200 mg. At present, there are immediate release tablets of 200 mg CBZ and sustained release tablets of 150, 200, 300, 400, and 600 mg CBZ available as well as a liquid formulation in form of a suspension (5 ml = 100 mg CBZ).

The therapeutic range of CBZ is described to be between 4 and 12 mg/L in plasma (Eadie, 1998). Above 12 mg/L ataxia and diplopia may already appear. For patients with a multiple anticonvulsive therapy adverse effects have been described to exist for even lower plasma concentrations. Moreover, considerable inter-patient variability in the relationship between seizure control and effective drug concentration were reported. Therefore, for optimal seizure control, a dosing regimen giving the best response and the fewest adverse reactions for each individual patient has to be found (Carlsson et al., 2005).

According to the commentary on the European Pharmacopoeia further dose adaption is necessary for the start and for the set-off of the therapy with CBZ due to the adaption of the potency and the adverse effects of the drug. Therapeutic drug monitoring is advised for the start of the therapy and after dose adaptations within the treatment.

The CBZ metabolism was described to happen predominantly hepatic and to depend largely on CYP 3A4 (Kerr et al., 1994). Furthermore, CBZ induces CYP 3A4 itself, increasing the elimination of CBZ, which plays a role for multiple applications in the course of the therapy.

To conclude, individual dosing of CBZ would be desirable due to (A) the age-dependent incidence and prevalence of epilepsy, (B) a dose regimen depending on the clearance capacity and the body weight of the patient, (C) considerable inter-patient variability for effective seizure control, and (D) need of dose adaption during the treatment.

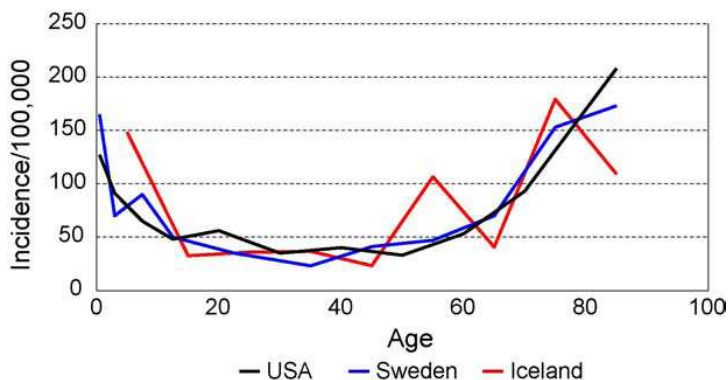


Figure 2: Incidence of unprovoked seizures per 100,000 inhabitants in industrialised countries according to Cloyd et al., 2006

The CBZ molecule (Figure 3) is a small molecule (236.3 g/mol) and has lipophilic properties, represented by a logarithmic octanol/water partition coefficient ($\log P$) of 1.51 (Scheytt et al., 2005).

CBZ exists in at least four anhydrous polymorphic modifications (Grzesiak et al., 2003). Polymorphic modifications are different crystalline forms of the same pure substance. These different crystalline forms result of different arrangements and/or different conformations of the molecules and have different chemical and physical properties, like melting temperatures, dissolution rates or bioavailability (Brittain, 1999). For CBZ, modification III is required by the European Pharmacopoeia (Ph. Eur.) for medicinal products. Nevertheless, in the past, commercial medicinal products did not only contain CBZ III, but also other modifications and mixtures of modifications (Auer et al., 2003) and notable differences in the bioavailability were observed regarding generic CBZ formulations (Meyer et al., 1992).

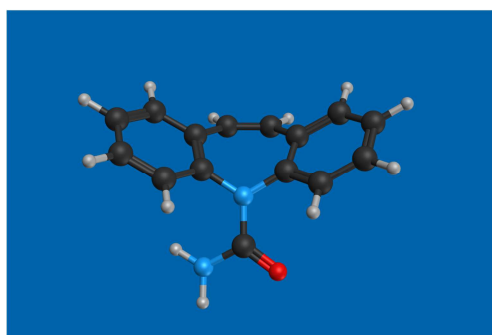


Figure 3: CBZ molecule in minimised geometry, Merck molecular force field, colour decoding of the atoms: carbon in black, hydrogen in light grey, nitrogen in blue, and oxygen in red (Molecular Operating Environment, Chemical Computing Group)

Within pharmaceutical production processes polymorphic transitions may occur due to the employment of pressure, heat, or humidity in hot-melt extrusion or granulation, for example (Zhang et al., 2004). Whereas no polymorphic transitions of CBZ have been detected during grinding and compression (Grzesiak et al., 2003; Lefebvre et al., 1986), it

has been stated that the polymorphic transition of CBZ was influenced by the melting temperature in a HME-process and the molecular weight of utilised PEGs (Pajander et al., 2012). Moreover, a polymorphic transition of CBZ III to CBZ I was found to occur when solid dispersions with PEGs were prepared by the solvent method (Nair et al., 2002).

CBZ III has a pH-independent aqueous solubility of 379 mg/L at 25 °C (Murphy et al., 2002), which is rated by Ph. Eur. as a very slightly soluble substance. Furthermore, in aqueous medium it transforms into CBZ dihydrate (CBZ DH) with an even lower solubility of 125 mg/L at 25 °C (Murphy et al., 2002) and 311 mg/L at 37 °C (Kobayashi et al., 2000). The therapeutic dose of 200 - 400 mg for adults may not be solved in the adult's stomachs liquid volume of 250 ml. Due to this solubility issue and the high permeability for membranes of the gastrointestinal tract, CBZ has been classified within the Biopharmaceutics Classification System (BCS) as class II drug (Lindenberg et al., 2004). As CBZ is a BCS class II drug and a high correlation between *in-vivo* parameters and *in-vitro* dissolution results was found (Meyer et al., 1992), the pharmaceutical formulation may be decisive for the bioavailability of the drug.

Already since 1985, physical mixtures and solid dispersions of CBZ and various excipients like sugars, sugar alcohols, PEGs, saturated polyglycolised glycerides, or polyvinyl pyrrolidone (PVP) have been investigated regarding the CBZ release rate (Attia and Habib, 1985; Doshi et al., 1997; El-Zein et al., 1998; Langer, 2003; Law et al., 2004; Perissutti et al., 2002; Perissutti et al., 2000; Zerrouk et al., 2001).

1.5. Excipients for the Formulation Development

In order to choose suitable excipients for the formulation development of CBZ-loaded rods for the SDP several aspects have to be taken into account:

For melt-extrusion as production technique, the selection of appropriate excipients is crucial, as glassy polymers, which are commonly used for melt-extrusion (Crowley et al., 2007; Repka et al., 2007), may produce sharp and brittle edges of the tablet-like slices. To allow for a safe swallowing, especially for children and the elderly, these sharp edges must be avoided. Regarding the cutting mechanism of the device, very soft or sticky formulations may show deformation or adhesion to the cutting blade and are therefore inappropriate for cutting via the SDP.

Furthermore, different dissolution profiles may be obtained depending on the excipients used for the rods: With hydrophilic binders immediate release behaviour may be achieved. In contrast, sustained release characteristics may be realised by employing a matrix-system with hydrophobic binders.

For the extrusion of cylindrical dosage forms hydrophilic binders like PEGs have already been investigated (Grassi et al., 2003; Perissutti et al., 2002; Schilling and McGinity, 2010). Due to their capability to improve the wettability and solubility of poorly soluble drugs, PEGs have been extensively utilised as drug carrier (Attia and Habib, 1985; Doshi

et al., 1997; Law et al., 2004; Moneghini et al., 2001) and drug release modifier (Güres and Kleinebudde, 2011; Windbergs et al., 2009).

Furthermore, melt-extrudates made from PEO with different molecular weights as well as Poloxamer (POL) have been successfully developed (Dierickx et al., 2013; Schilling and McGinity, 2010; Thommes et al., 2011). Wening et al. (2012) manufactured melt-extruded rods based on POL with immediate release characteristics for individual oral therapy by the SDP. Moreover, some workgroups involved hydrophilic fillers like lactose (Grassi et al., 2003; Perissutti et al., 2002) or mannitol (Thommes et al., 2011; Wening et al., 2012) for the production of rod-shaped dosage forms to optimise the viscosity of the melt and to modify the drug release characteristics.

The use of hydrophobic binders like stearic acid (SA) has already been described for extruded sustained release dosage forms (Grassi et al., 2003). Beneath SA also poly(ϵ -caprolactone), abbreviated as PCL, could serve as a low melting binder. PCL as semi-crystalline, biocompatible, and biodegradable polymer has been approved by the United States Food and Drug Administration (FDA) as biomedical material. It has been applied for the development of porous scaffolds for tissue engineering (Washburn et al., 2002), implants (Cheng et al., 2010) as well as peroral medicinal products (Dierickx et al., 2013; Dierickx et al., 2012; Douglas et al., 2010; Lyons et al., 2008). Highly hydrophobic PCL has often been blended with hydrophilic PEG (Cheng et al., 2010; Douglas et al., 2010) or PEO (Dierickx et al., 2013; Dierickx et al., 2012; Lyons et al., 2008) to tailor drug dissolution.

In order to study the *in-vitro* drug release from defined extrudates surfaces, Reitz and Kleinebudde (2008) dipped extrudate pieces into a molten lipid preventing the dissolution from those parts. Thus, lipid or wax coatings may be applied to tailor drug dissolution via a distinct surface. Low melting binders like SA, carnauba wax, or (white) bees wax, for instance, have already been described in literature for spray-congealing techniques or melt coatings: SA and carnauba wax have been utilised to produce delayed release microcapsules for the paediatric population (Balducci et al., 2011) and bees wax has been described both for the purpose of taste-masking (Patil et al., 2011) as well as for the production of controlled release dosage forms (Kennedy and Niebergall, 1998; Racz et al., 1997).

For the coating of multiparticulates, which may be incorporated into monolithic dosage forms, polymers like hypromellose (hydroxypropyl methylcellulose, HPMC) or polyvinyl alcohol-polyethylene glycol graft polymer (PVA-PEG, Kollicoat® IR) are known for drug-layering (Bühler, 2007; Schilling and McGinity, 2010; Suhrenbrock et al., 2011). For the sustained release coating of pellets, ammonio methacrylate copolymer (Eudragit® RL/RS) or polyvinyl acetate (PVAc, Kollicoat® SR 30 D) have been utilised (Dashevsky et al., 2004; Sawicki and Lunio, 2005; Schmidt and Bodmeier, 2001). To tailor drug dissolution of PVAc-coated pellets PVA-PEG as a pore-forming agent has been included into the coating (Ensslin et al., 2008; Strübing et al., 2007).

2. Aims and Outline

This work focuses on the development, the manufacturing, and the characterisation of peroral dosage forms intended for implementation by the SDP.

For this purpose, CBZ is chosen as model drug, as it would be reasonable for individual dosing. To open the concept of the SDP to drug substances with higher doses, like the model drug CBZ, rods with a larger diameter shall be manufactured. The existing prototype of the SDP will have to be adapted to be compatible with the new dimensions of the dosage forms. The applicability of the concept of the SDP for these rods - with probably different mechanical properties - shall be examined.

The first aim is to elaborate a small-scale production technique to conduct an excipient screening for the formulation development of melt-extruded rods.

Then, the rods shall be produced via melt-extrusion. Apart from the classic twin-screw melt-extrusion, new and more sophisticated techniques shall be examined for their usability: First, co-extrusion via two twin-screw extruders may produce co-extrudates combining a core- and a coat-layer. Second, ram-extrusion may allow for the embedding of multiparticulates into a matrix. Regarding the sustained release formulations, the dose-, geometry-, and size-dependent dissolution characteristics of the cut slices may be minimised or even overcome by these techniques. Additionally, further drug release profiles like biphasic drug release or zero order kinetics may be accessible.

Another objective is the extensive examination of the dissolution characteristics of the model drug CBZ with regard to the different utilised matrices, the CBZ-loading and other excipients, like pore formers or solubilizers, for example.

Furthermore, this work shall systematically evaluate the mechanical properties of CBZ-loaded rods by finding and assessing appropriate methods to this purpose. Moreover, it shall be clarified, in which way dosing by the SDP and the mass uniformity of sliced doses are influenced by the mechanical properties of the drug-loaded rods. It shall be elucidated whether the mechanical properties may be modulated by suitable excipients and whether the formulations together with the device will be suitable for patient-centred treatment.

As CBZ exists in at least four modifications and pharmaceutical production processes may induce polymorphic transitions, a thorough understanding and surveillance of the solid state properties of CBZ within the formulations has to be built up. Furthermore, it is intended to study whether storage affects the mechanical properties and the dissolution behaviour of the CBZ-loaded rods.

3. Results and Discussion

3.1. Small-Scale Production Techniques

3.1.1. Introduction and Objectives

Hot-melt extrusion (HME) has already been utilised to produce immediate release formulations for the SDP (Wening et al., 2012). These formulations contained so far poloxamer and mannitol as excipients. The first aim of this work was to conduct an excipient screening for the manufacturing of hot-melt extruded rods for the SDP. To this purpose, extrusion with a laboratory twin-screw extruder was considered. Due to an adequate filling of the screws and an appropriate dosing via a lab-scale powder feeder a minimum batch size of approximately 300 g would therefore be needed. But as only a limited amount of CBZ was available due to its high cost, a production technique requiring only small quantities of material was searched for.

Miniaturisation in pharmaceutical extrusion technology with the purpose of feasibility studies and formulation development at an early stage has been of interest to reduce drug and excipient quantities and to save costs and time (Covas and Costa, 2004; Mühlenfeld and Thommes, 2012; Sakai and Thommes, 2014; Zecevic and Wagner, 2013). Mühlenfeld and Thommes (2012) give a valuable overview over different types of miniature extruders.

As no micro-extruder was available for this work, the following chapter will focus on the development of other small-scale production techniques in order to conduct an excipient-screening for formulations intended for the SDP. By moulding and ram-extrusion preliminary formulations including CBZ and various excipients should be manufactured with a small quantity of material in order to obtain controlled release, matrix type dosage forms.

Another objective of this part of the thesis was to find and assess methods to investigate the mechanical properties of the rod-shaped dosage-forms. Moreover, the aim was to determine to which extent different matrices and the CBZ content influence the mechanical properties of the formulations.

It was intended to examine the dissolution characteristics of CBZ from the formulations in relation to their different matrices and their CBZ-loading. Furthermore, the effect of pore-forming agents on the dissolution profiles was investigated.

Finally, the solid state properties of the produced dosage forms were to be investigated with appropriate methods with regard to the CBZ modification.

3.1.2. Mini-Moulds

As a first small-scale screening set-up mini-moulds (Haupt et al., 2013) and longitudinal moulds have been produced via a melting and moulding technique (section 6.2.1.2) and are depicted in Figure 4.

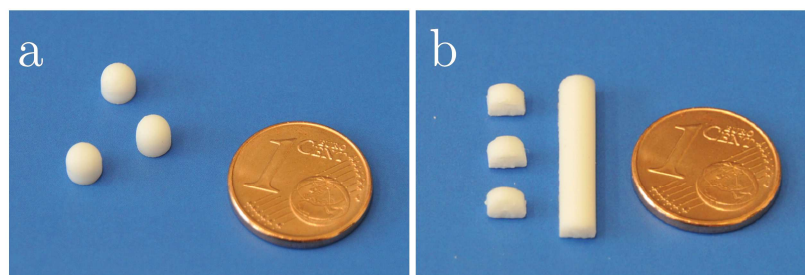


Figure 4: Mini-moulds (a) and longitudinal moulds (b); exemplarily made from 10 % CBZ and 90 % PEG 2,000 next to a one Euro cent coin

The moulding technique allowed for the processing of excipients with a low melting temperature and a low viscous melt like PEG of various grades, stearyl macrogols-32 glycerides (Gelucire[®] 50/13), or sugar alcohols like xylitol, mannitol, or isomalt. The mini-moulds ($\varnothing = 4$ mm) were intended to be utilised for dissolution studies and the longitudinal moulds (4 x 50 mm) for cutting experiments.

This first small-scale production technique comprised a lot of limitations: The main disadvantage of this screening set-up was that moulds could not be prepared for highly viscous melts. Only formulations that could be grouted into the moulds were manageable. This restricted the CBZ-loading to 30 %, as melts with solid contents above this percentage were not castable as being previously discovered for other drugs and excipients by Haupt et al. (2013). Furthermore, the CBZ may sink down in the melt during cooling of the moulds to room temperature which may lead to inhomogeneous distribution of the API. Nevertheless, first insights into the dissolution characteristics, the mechanical properties and the solid state characteristics were gained (section 3.1.4). Due to the restrictions mentioned above another small-scale production technique was assessed.

3.1.3. Ram-Extrudates

3.1.3.1. Ram-Extrusion via a High Pressure Capillary Rheometer

As a second approach, a high pressure capillary rheometer (HPCR) – generally used as an analytical tool – has been implemented for the small-scale production of hot-melt ram-extrudates (section 6.2.1.3). Figure 5 presents a scheme of the ram-extrusion via the HPCR.

For ram-extrusion (Crowley et al., 2002), the binder and - if applicable - the API and/or further excipients are mixed first. Secondly, the mixture is introduced into the pre-heated barrel and pre-compressed. After an appropriate equilibration time, the plasticised mass is forced through a die by a piston, which is moving at a certain velocity. After exiting the die, the binder solidifies and the ram-extrudate may be transported on a conveyor belt during cooling down to room temperature.

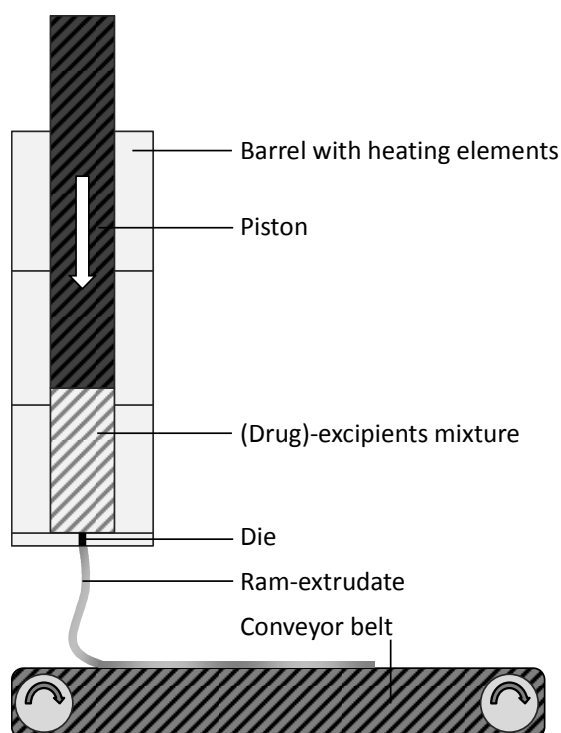


Figure 5: Scheme of the ram-extrusion via the high pressure capillary rheometer

As introduced in section 1.5, various excipients are known from literature to be utilised as binders for melt-extrusion. Table 1 gives an overview of the excipients, which were screened by utilising the small-scale ram-extrusion. Besides amorphous polymers, (semi-)crystalline binders for immediate and sustained drug release behaviour were investigated. As hydrophilic binders PEG and PEO with different molecular weights as well as POL were examined. Furthermore, PCL and SA were utilised as hydrophobic binders. Moreover, the sugar ester sucrose palmitate and sugar alcohols like isomalt, xylitol, or mannitol were examined as eroding matrices and hydrophilic fillers.

Table 1: Excipients, screened for the manufacturing of small-scale ram-extrudates with the HPCR, M_w = molecular weight, for explanation of the polymer abbreviations see text below

“HME-polymers”	HPC, HPMC, HPMC AS, PVP, PVP-PVA copolymer, PVA-PEG copolymer, aPMMA
hydrophilic binders	PEG ($M_w = 2,000, 10,000, \text{ and } 20,000 \text{ g/mol}$), PEO ($M_w = 100,000, 200,000, \text{ and } 1,000,000 \text{ g/mol}$), POL
hydrophobic binders	PCL, SA
eroding matrices and hydrophilic fillers	sucrose palmitate, mannitol, isomalt, xylitol

Dependent on each binder, the extrusion temperature (T_{extr} [°C]) was adjusted to obtain a viscosity of the material which facilitated plastic deformation and extrusion through the die ($\varnothing = 2$ mm). The conveyor belt velocity was adapted to generate a straight strand (Figure 6 a).

For protection of the die the ram does not move over the whole distance within the barrel of the HPCR which generates a dead volume of 6 mL. To consume less CBZ in the development process, the small-scale production was optimised by minimising this dead volume inside the barrel. Therefore, a hollow cylinder made from polytetrafluoroethylene (PTFE, Figure 6 b and c) was employed. By this, small-scale ram-extrusion was feasible with only 10 g material input and a product yield of 3.0 to 6.5 g per batch.

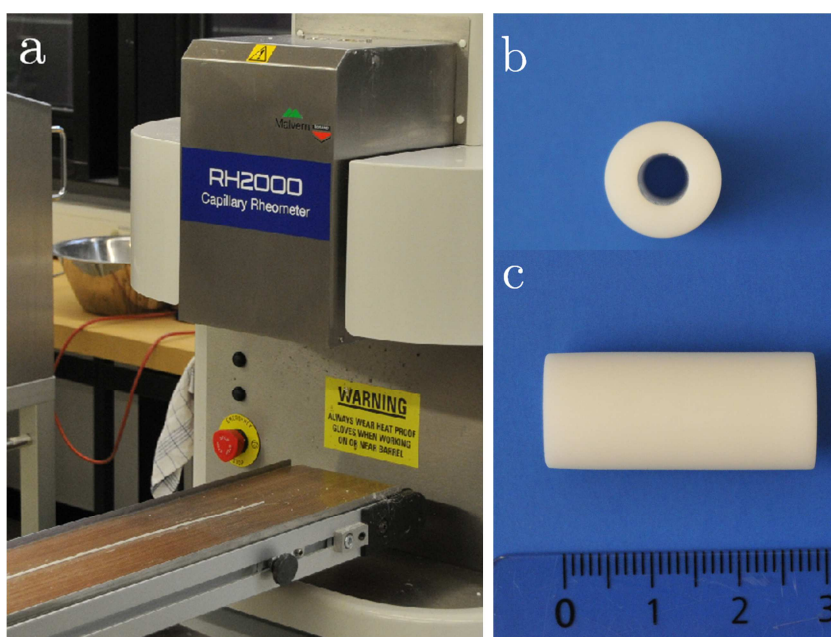


Figure 6: Production of the small-scale ram-extrudates; high pressure capillary rheometer (HPCR) and conveyor belt (a), hollow cylinder made of PTFE minimising the dead volume inside the barrel of the HPCR; top view (b) and lateral view (c), displayed scale in cm

Small-scale ram-extrusion was possible with PEGs 2,000, 10,000 and 20,000, poloxamer, sucrose palmitate, xylitol, PCL, and SA as binders resulting in ram-extrudates with a diameter of approximately 2 mm depending on the die swell. The incorporation of up to 50 % CBZ resulted in ram-extrudates with a smooth and homogeneous surface structure. For small CBZ-loadings (e.g. 10 % CBZ) the addition of 15 - 30 % mannitol as hydrophilic filler facilitated the processability by increasing the viscosity of the plasticised mass.

As a drawback of this technique, typical “HME-polymers” like polyvinyl pyrrolidone (PVP), polyvinyl pyrrolidone/polyvinyl acetate copolymer (PVP-PVA copolymer), polyvinyl alcohol-polyethylene glycol copolymer (PVA-PEG copolymer), hydroxypropyl cellulose (HPC), hydroxypropyl methylcellulose (HPMC), and hydroxypropyl methylcellulose acetate succinate (HPMC AS) as well as PEO were not processible for

various extrusion temperatures and piston velocities. Either, they showed clogging or blockage of the die due to a sticky behaviour or due to a too high viscosity for the chosen set-up. Amino-polymethylmethacrylat (aPMMA), for example, was not sufficiently plasticised in order to pass the die under the temperature conditions in the barrel, the pressure applied by the ram and the shear forces within the die. For some polymers, strands could be manufactured, but severe entrapment of air made the rod unsuitable for the intended application.

As no small-scale production technique was available for these polymers, in the course of the work they were processed on a lab-scale twin-screw extruder to perform further investigations for suitability for the SDP. Cutting experiments revealed very high maximum cutting forces of 90 and 130 N for extrudates of HPC and HPMC AS, for instance, in comparison to numbered values of below 10 N for melt-extruded drug-loaded rods by Wening et al. (2012). Extrudates made from PEO were not cuttable at all due to their toughness. Besides, brittle behaviour and to get worse, even sharply edged splinters were observed for extrudates from polymers like aPMMA or PVP-PVA copolymer. Therefore, these excipients were not evaluated further.

Coming back to the small-scale ram-extrusion, sucrose palmitate as a binder showed a rough surface and the manufactured ram-extrudates were very brittle. The sugar alcohols revealed a sticky behaviour during production and the extrudates were extremely fragile, too. Therefore, these excipients were excluded from further investigations as well.

In Table 2 the final 20 formulations produced by the HPCR and including 0, 10, 30, or 50 % CBZ are listed with the extrusion temperature in comparison to the melting temperature of the pure binders. The process of small-scale ram-extrusion was optimised by varying the process parameters, namely extrusion temperature (T_{extr}), equilibration time (t_{equil}), piston velocity (v_{piston}), and velocity of the conveyor belt. For the ram-extrusion of soft and waxy excipients extrusion rates from 20 to 500 mm/min have already been applied by other workgroups (Oliveira et al., 2013; Perissutti et al., 2002; Pinto and Silverio, 2001). Perissutti et al. applied an equilibration time of 25 min.

Table 2: Melting temperature (T_m) of the pure binders as determined by DSC measurements and extrusion temperature (T_{extr}) of the formulations of the small-scale ram-extrudates including 0, 10, 30, or 50 % CBZ

	PEG 2,000	PEG 10,000	PEG 20,000	PCL	SA
T_m [°C] pure binder	54.0	62.1	64.3	51.8	63.9
T_{extr} [°C] formulations (with 10, 30, or 50 % CBZ)	50.0*	60.5	62.0	39.0	58.0

* for the formulation 50 % CBZ, 50 % PEG 2,000: $T_{\text{extr}} = 48.5$ °C

Finally, the small-scale ram-extrudates were manufactured utilising a piston velocity of 150 mm/min, an equilibration time of 23 min, and a velocity of the conveyor belt of 0.15 m/s. In all cases T_{extr} was below the melting temperature of the pure excipients (Table 2). The plastic mouldability is known of PEG (Perissutti et al., 2002) and other soft and waxy excipients like saturated polyglycolised glycerides (Pinto and Silverio, 2001) as well as from the field of solid lipid extrusion (Reitz and Kleinebudde, 2007). Due to the crystallinity of the binders and their rapid recrystallisation at room temperature, the extrudates did not show any die swell and thus all of them have a diameter of 2.0 mm.

3.1.3.2. Mechanical Properties

To assess the mechanical properties of the produced ram-extrudates intended for the usage of the SDP, appropriate methods should be evaluated. So far, no systematic evaluation of the mechanical properties of the drug-loaded rods has been conducted. Only the maximum cutting force has been analysed with a 1,000 N load cell and a specifically developed cutting tool (Wening and Breitzkreutz, 2010; Wening et al., 2012). The tensile strength and the E-modulus (Young's modulus) of ram-extrudates have been determined by a three-point bending test (Perissutti et al., 2002). Oliveira et al. (2013, 2014) analysed the bending strength, the stiffness, the deformation, and the E-modulus with a Texture Analyser at both axial and radial directions of laminar ram-extrudates, but no further information was given about the specific execution, like the support span of the rig, the pre-testing and testing velocity [mm/s] or the equations for the determination of the parameters, for example.

For the evaluation of the mechanical properties of the small-scale ram-extrudates in this work, initially three parameters were considered: the maximum cutting force (F_{max}), the tensile strength, and the E-modulus. First, F_{max} pictured the maximum forces to cut the rods into tablet-like slices. Second, the tensile strength was mapped on the practical handling, for instance, the insertion of the rods into the device. Third, the E-modulus reproduced the material characteristics of the sample, like its stiffness.

F_{max} of the ram-extrudates was determined by Test Apparatus H10KM equipped with a newly developed cutting test set-up (section 6.2.3.1). In Figure 7 F_{max} of the ram-extrudates is plotted over the incorporated CBZ content. The maximum cutting forces for the extrudates were determined as 0.8 ± 0.4 to 7.6 ± 1.0 N. These results were in good agreement with the values obtained so far for immediate release melt-extrudates (Wening et al., 2012). The cuttability was predominantly influenced by the binder and less by the CBZ content (e.g. ≈ 6 N for PEG 2,000; ≈ 1 N for PCL, Figure 7).

It is notable that F_{max} of the PEG-formulations was not in line with their molecular weights: The values of extrudates made from PEG 10,000 did not lie between those of PEG 2,000 and 20,000 as expected, but were below F_{max} of the formulations including PEG 2,000 and PEG 20,000. These findings will be discussed further in the following paragraphs.

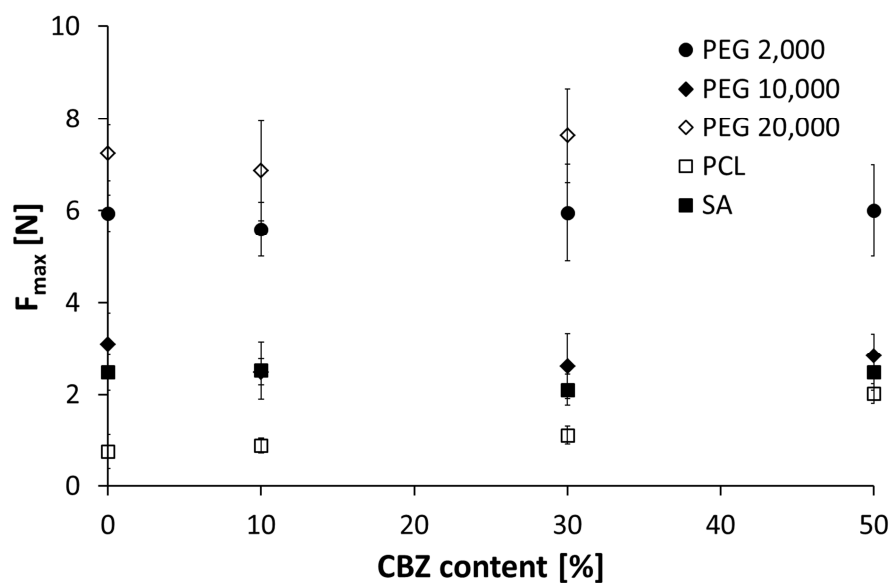


Figure 7: Maximum cutting force (F_{\max}) of the small-scale ram-extrudates determined by Test Apparatus H10KM equipped with a cutting test set-up, plotted over the CBZ content in different matrices ($n = 10$, mean \pm SD)

For the determination of the tensile strength and the E-modulus a three-point bending test was performed using a Texture Analyser equipped with a three-point bending rig (section 6.2.3.2). In Figure 8 representative force-displacement curves of the three-point bending test are exemplarily illustrated for ram-extrudates containing SA (Figure 8 a) and PEG 20,000 (Figure 8 b).

The two different binders behaved contrarily with regard to the CBZ content affecting the mechanical properties: While the addition of CBZ increased the bending force of formulations based on SA, the incorporation of the model drug into PEG 20,000 resulted in a pronounced decrease in bending strength of the small-scale ram-extrudates.

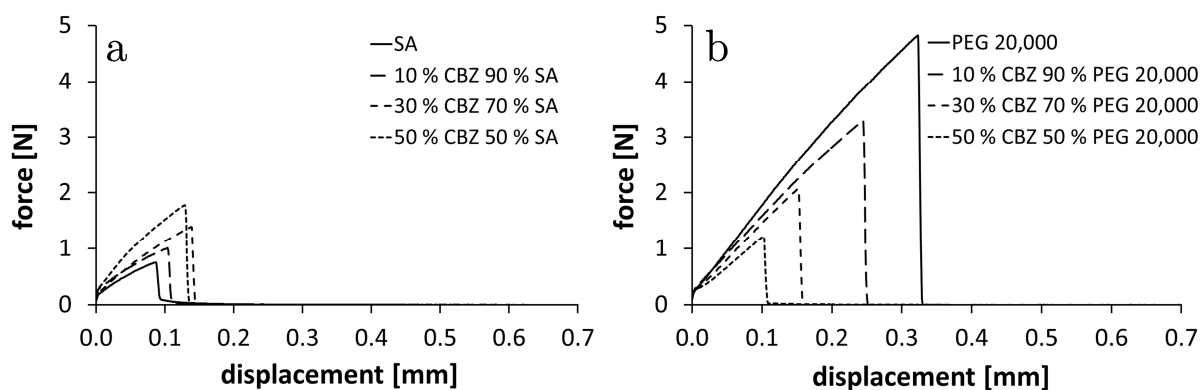


Figure 8: Representative force-displacement curves for the small-scale ram-extrudates; exemplarily for formulations based on SA (a) and PEG 20,000 (b) determined by a Texture Analyser equipped with a three-point bending rig

The tensile strength and the E-modulus of all formulations are presented in Figure 9 and Figure 10.

Measured values of the tensile strength ranged from 3.1 to 30.9 MPa (coefficient of variation from 5.2 - 20.2 %, Figure 9). Both the measured values and the coefficients of variation were in the same magnitude as described for a similar set-up (Perissutti et al., 2002).

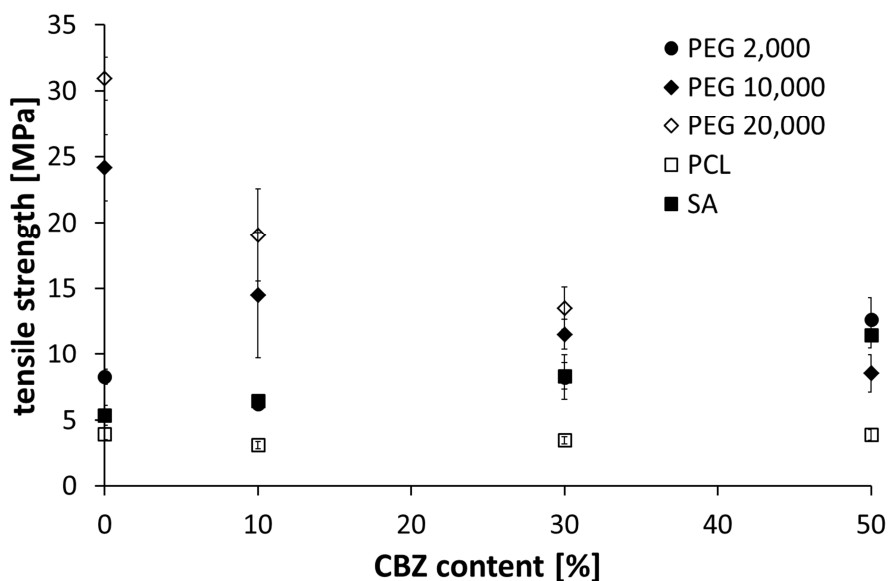


Figure 9: Tensile strength of the small-scale ram-extrudates plotted over the CBZ content ($n = 5$, mean \pm SD)

The tensile strength of the extrudates slightly increased with an increasing CBZ content for “soft” binders like PEG 2,000 and SA. For PEG 2,000, for example, the tensile strength increased from 8.3 ± 0.6 MPa to 12.7 ± 1.6 MPa. For 10 % CBZ, the value slightly decreased.

Most of the CBZ is on hand in its crystalline form due to the rather poor solubility of CBZ in PEG. The equilibrium solubility of CBZ in PEG 2,000 was determined to be 8.1 ± 0.7 % (w/w) after 136 h (section 6.2.3.12). Hence, CBZ was mostly crystalline in the extrudates and may as a solid component stabilise the “soft” binders. For 10 % CBZ in PEG 2,000 one may assume that a large part of CBZ was solubilised in the partly molten PEG, thus not acting as a stabilising solid constituent, but as a molecularly dispersed plasticiser for the polymer. In section 3.1.4 the solid state properties of the manufactured dosage forms are elaborated in more detail.

For “hard” binders like PEG 10,000 and PEG 20,000 the tensile strength decreased with an increase of CBZ content as CBZ destabilised the “hard” binder.

The tensile strength of the PCL ram-extrudates was not affected by the content of CBZ (Figure 9).

Measured E-modulus values ranged from 200 MPa to 3.2 GPa (coefficient of variation from 2.5 to 18.1 %, Figure 10). These values exceeded those of the previously mentioned study (Perissutti et al., 2002), which described values of 45 to 72 MPa for ram-extrudates with the same diameter of 2 mm, containing PEG 4,000, lactose as a hydrophilic filler, and CBZ as model drug as well. The same extrusion temperature has been utilised, and with 150 mm/min the piston velocity in this work was in the range of those in the study of Perissutti et al. (2002).

However, one major difference in the determination of the E-modulus was the installation of the three-point bending test (section 6.2.3.2): Whereas the workgroup of Perissutti et al. used a distance between the lower supports of 6.4 mm, in this study, a chunk pinch was modelled to imitate the practical handling of the rods when they are inserted into the SDP. Therefore, a support span of 17 mm has been chosen to imitate the distance between the index finger and the middle finger. This distance has been utilised by other workgroups as well (Roberts and Rowe, 1996). When the E-modulus is calculated according to Equation 3 (section 6.2.3.2) the support span of the rig is cubed in the numerator and therefore the values spurt.

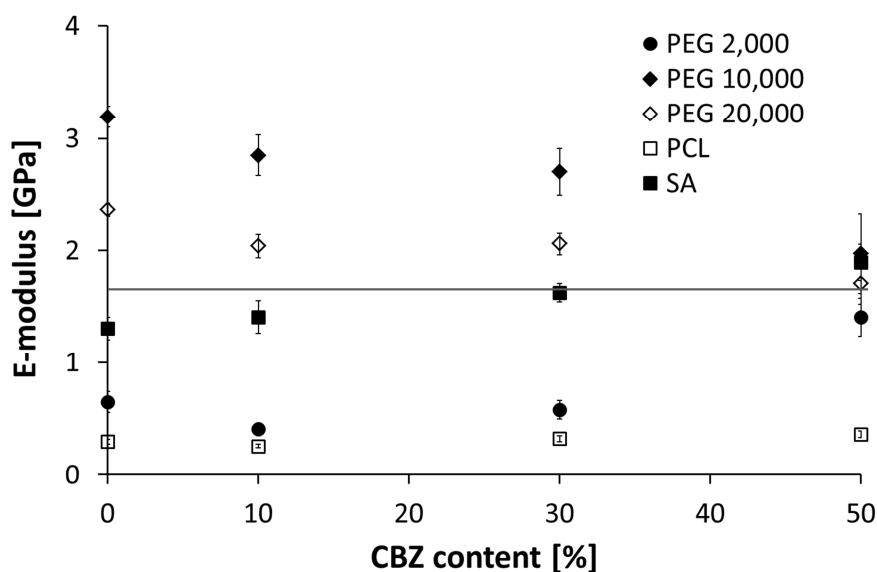


Figure 10: E-modulus of the small-scale ram-extrudates plotted over the CBZ content ($n = 5$, mean \pm SD), the horizontal line corresponds to the threshold of suitability of the ram-extrudates for the SDP (< 1.7 GPa)

Nevertheless, the observed tendencies of the tensile strength were transferable to the E-modulus (Figure 10). For PEG 2,000 and SA, calculated values of the E-modulus increased with an increasing CBZ content, exhibiting smaller values for 10 % CBZ in PEG 2,000 as well (see above). For PEG 10,000 and PEG 20,000 the E-modulus decreased with an increasing CBZ content, as observed for the tensile strength. The E-modulus of the ram-extrudates containing PCL, as observed for the tensile strength, was not influenced by the content of CBZ. This may be explained by the soft and ductile

behaviour of PCL, which was reflected by the small value of the E-modulus (0.30 ± 0.02 GPa). These material properties allowed for the incorporation of high fractions of solids (up to 50 % in this work) without any change in the matrix properties.

Formulations with PEG 10,000 as a binder showed the highest E-moduli in comparison to those with PEG 2,000 and PEG 20,000. This may explain the smaller maximum cutting forces for ram-extrudates made from PEG 10,000 (Figure 7), as more rigid substances tend to break during the cutting process, which results in an abrupt decrease in measured force. This coincidence demonstrates how valuable the combined observation of the parameters is to understand the mechanical properties of the rods. In conclusion, it has been demonstrated that the tensile strength and the E-modulus depend on the binder (“soft” against “hard” binders) and the CBZ content.

In a next step, the small-scale ram-extrudates were inserted into the SDP and exemplarily sliced in doses (section 6.2.4.1). Rods having an E-modulus below 1.7 GPa were suitable for the application while others broke inside of the device due to their rigidity (horizontal line in Figure 10).

As the temperature may affect the mechanical properties, the three-point bending test was performed with extrudates of different temperatures (17, 20, and 35 °C) to investigate the temperature dependency of tensile strength and E-modulus. The results of one formulation are exemplarily depicted in Figure 11.

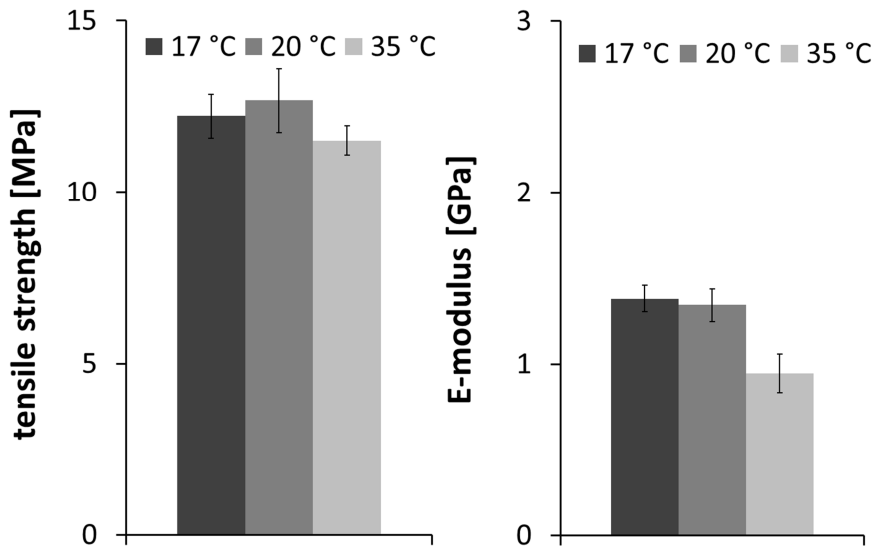


Figure 11: Tensile strength and E-modulus determined at different temperatures of the small-scale ram-extrudates composed of 50 % CBZ and 50 % PEG 2,000 (17, 20, and 35 °C), $n = 10$, mean \pm CI, $\alpha = 0.05$

As regards the tensile strength no difference was observed within the accuracy of the measurements. At 35 °C the E-modulus decreased slightly. In conclusion, the temperature

dependency of the measurements was not as high as expected. Still, the temperature was supervised and documented.

Regarding the administration of the rods via the SDP for the patients later on, the rather weak influence of the temperature on the mechanical properties can be mentioned as an advantage, as constant mechanical properties would allow for dosing from 17 to 35 °C.

3.1.3.3. Dissolution Studies

Besides the assessment of methods to investigate the mechanical properties, the dissolution of the drug CBZ from the small-scale ram-extrudates was of major interest. Therefore, dissolution testing of the ram-extrudates was conducted according to Ph. Eur. 2.9.3. As some of the ram-extrudates floated inside the media utilising the paddle-apparatus, the experiments were performed in a basket-apparatus (section 6.2.3.7). The dissolution profiles were obtained under sink-conditions with 20 mg CBZ per vessel (equalling 3 to 10 extrudate pieces per vessel).

Figure 12 exemplarily illustrates the dissolution profiles of the ram-extrudates made from PEG 10,000. Dissolution studies exhibited a drug release of 98 - 105 % with an immediate release profile for extrudates with hydrophilic binders and a low CBZ content (≤ 30 %). The release rate decreased with increasing CBZ content (50 %). These findings were in accordance with Perissutti et al. (2002), who have reported that higher fractions of PEG 4,000 increased the drug dissolution rate within their CBZ formulation. The decrease of the dissolution rate for increasing CBZ-loads may be explained by the loss of hydrophilicity of the PEG-formulation with an increase of CBZ-load (Verhoeven et al., 2009).

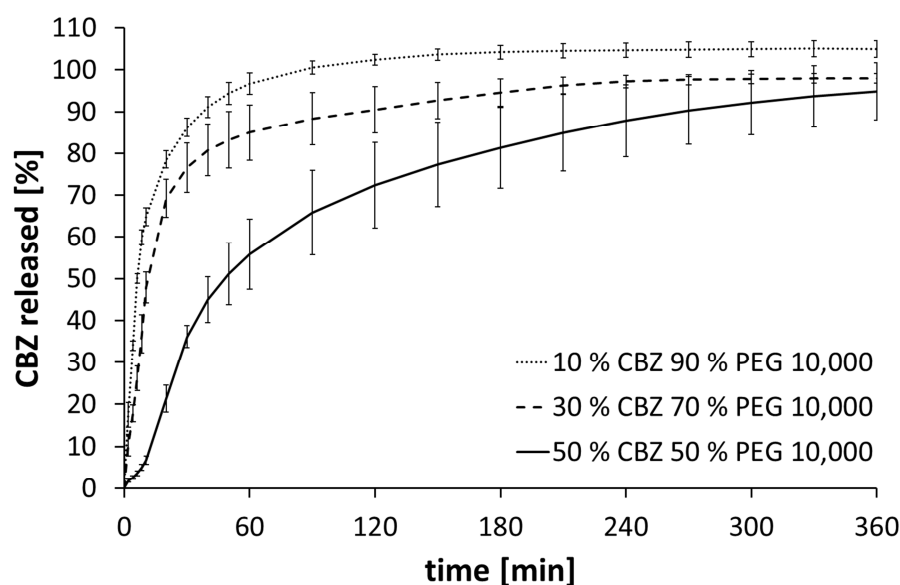


Figure 12: CBZ release of the small-scale ram-extrudates with PEG 10,000 as hydrophilic binder and 10, 30, or 50 % CBZ; 20 mg CBZ per vessel; apparatus 1, 75 rpm in 900 mL of degassed, demineralised water at 37.0 ± 0.5 °C ($n \geq 3$; mean \pm SD)

For ram-extrudates including PEG 2,000 and 20,000 similar dissolution curves were obtained (data not shown). Only in the first minutes the dissolution rate of CBZ depended on the molecular weights of the PEGs in the matrix (Figure 13): For lower molecular weights (e.g. PEG 2,000) higher dissolution rates were received, while the dissolution rate of the drug decreased in formulations including PEG with higher molecular weight (e.g. PEG 20,000). This may be due to the higher dissolution rate of lower molecular weight PEGs, due to less polymer swelling of the shorter-chained molecules and higher hydrophilicity (Corrigan et al., 1979). An increase in molecular weight also leads to an increase in viscosity of the emerging polymer gel, which tends to decrease the drug dissolution rate, as proposed by Verhoeven et al. (2009). For lower CBZ-loadings this effect was more pronounced (Figure 13), as the proportion of the matrix in the formulation was higher and the properties of PEGs became more distinct for drug release (Corrigan et al., 1979; Verhoeven et al., 2009).

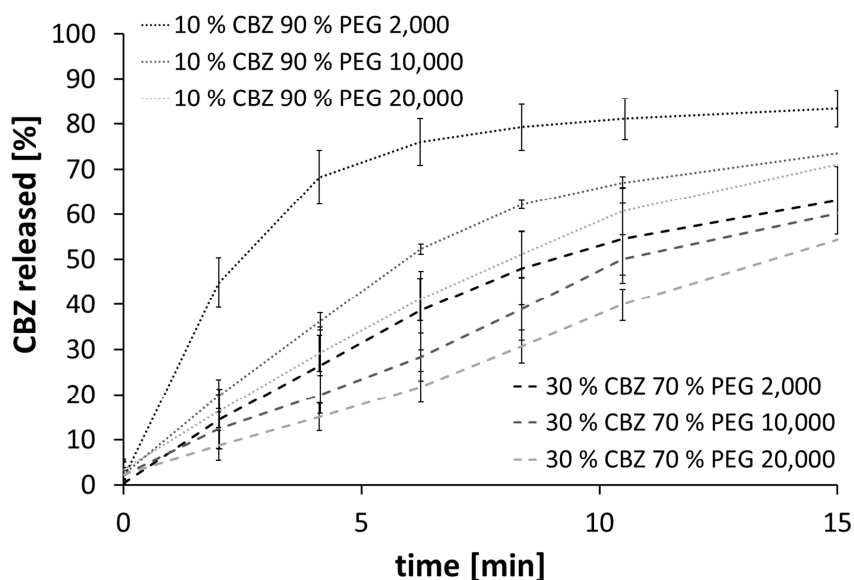


Figure 13: CBZ release of the small-scale ram-extrudates with PEG 2,000, 10,000, and 20,000 as hydrophilic binder and 10 or 30 % CBZ; 20 mg CBZ per vessel; apparatus 1, 75 rpm in 900 mL of degassed, demineralised water at 37.0 ± 0.5 °C ($n \geq 3$; mean \pm SD)

Figure 14 illustrates the CBZ release from formulations containing PCL and SA as lipophilic binders. The CBZ release was in this case normalised to the surface of the formulations, calculated as the surface of a cylinder. The formulations showed sustained release characteristics and a higher CBZ content resulted in a higher dissolution rate. This is in line with the results of several authors, working on melt-extruded hydrophobic matrix systems, including lipids, PCL or SA (Dierickx et al., 2013; Grassi et al., 2003; Güres and Kleinebudde, 2011; Lyons et al., 2008).

Regarding the relative CBZ release (data not shown) even after a period of 8 h, less than 25 % of the drug was released from the matrix for all formulations, which was regarded as a too low dissolution rate.

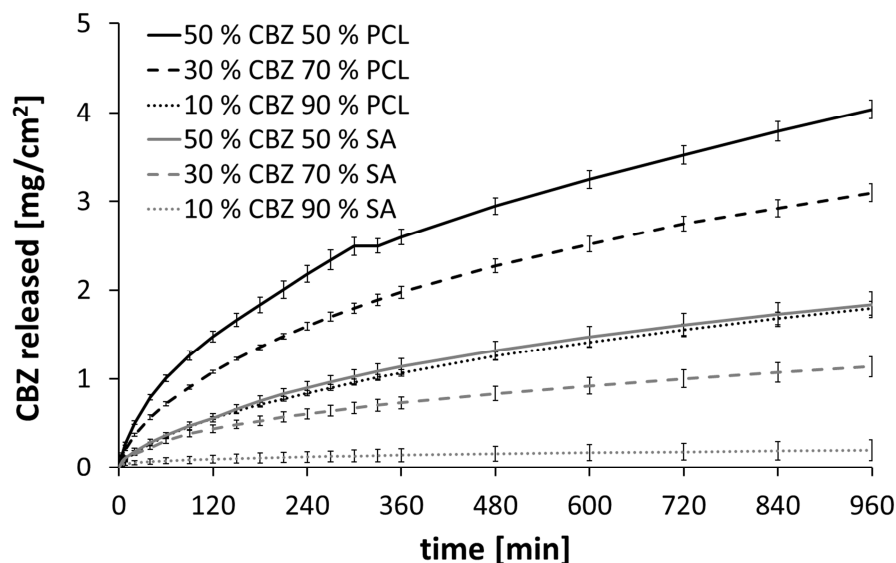


Figure 14: CBZ release of the small-scale ram-extrudates with PCL and SA as lipophilic binders and 10, 30, and 50 % CBZ; 20 mg CBZ per vessel; apparatus 1, 75 rpm in 900 mL of degassed, demineralised water at 37.0 ± 0.5 °C (n = 6; mean \pm SD)

To visualise and examine the surface of the ram-extrudates with PCL and SA as lipophilic binders, they were investigated by scanning electron microscopy (SEM, section 6.2.3.4) before and after 24 h of dissolution (Figure 15).

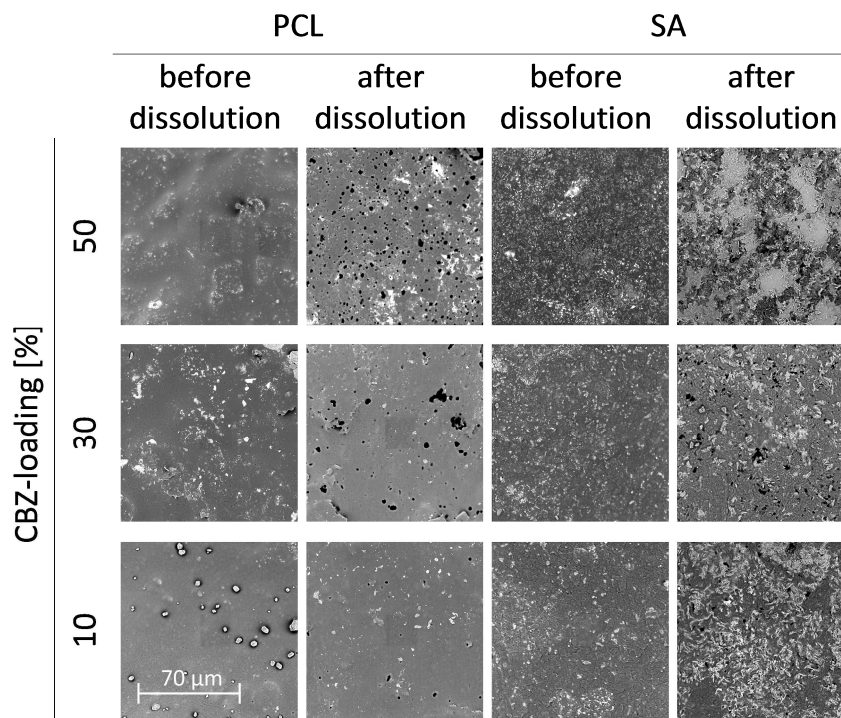


Figure 15: SEM micrographs of the ram-extrudates with PCL and SA as lipophilic binders and 10, 30, and 50 % CBZ before and after 24 h of dissolution in 900 mL of degassed, demineralised water at 37.0 ± 0.5 °C

The drug particles may clearly be distinguished from the matrix materials. The higher the drug-loading the more particles on the surface were visible. After dissolution CBZ dihydrate (CBZ DH) particles (section 1.4) were seen on the surface, which will be discussed further in section 3.1.4. Moreover, the quantity and size of pores on the examined samples after dissolution were shown by utilising SEM. It can be seen from Figure 15 that CBZ was released from the matrix via pores, which were generated by the drug itself (Windbergs et al., 2009). As described above the drug worked as a pore builder and therefore slightly increased the dissolution rate with increasing drug content.

3.1.3.4. Addition of Pore Formers

As the dissolution of CBZ from the lipophilic formulations was very slow (section 3.1.3.3), and the pore-forming characteristic of CBZ enhanced the dissolution, the effect of pore-forming agents was examined to increase the dissolution rate. The dissolution from solid lipid extrudates and implants containing release modifiers, as, for instance, pore formers like mannitol or PEG has already been investigated (Güres and Kleinebudde, 2011; Herrmann et al., 2007; Windbergs et al., 2009). PEG has furthermore been utilised as pore former for a higher release rate of PCL-melt extrudates (Douglas et al., 2010).

In this work, 5 % Mannitol and PEG 4,000 were utilised as pore formers in the lipophilic matrices. Both were processed below their melting temperatures of 166.7 °C and 61.4 °C (determined by DSC measurements, section 6.2.3.10). Therefore, they acted as solid pore formers for both PCL and SA (Table 2, section 3.1.3.1).

For formulations including pore formers, dissolution testing was conducted and SEM was applied before and after dissolution. Figure 16 exemplarily presents formulations based on PCL including 30 % CBZ with and without pore formers.

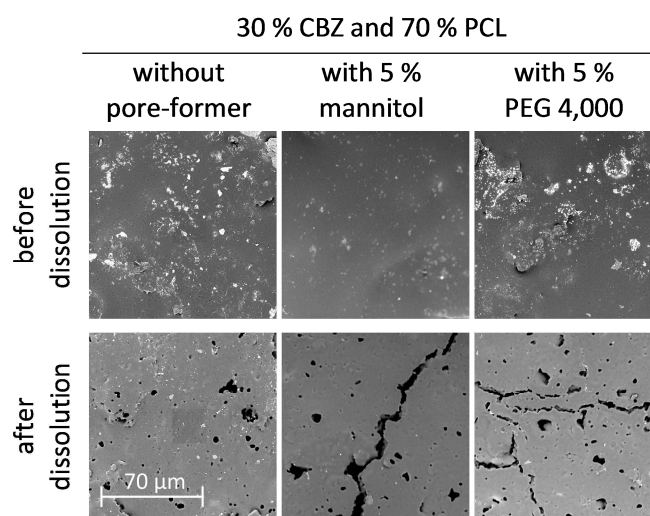


Figure 16: SEM-micrographs of the ram-extrudates with 30 % CBZ and PCL as lipophilic binder, without pore formers and with 5 % mannitol or PEG 4,000, before and after 24 h of dissolution

The figure illustrates that the pore-structure after dissolution was more pronounced with the inclusion of pore formers. Furthermore, fractures in the structure appeared and the ram-extrudates partially cracked. This destruction of the matrix may be due to the hydrodynamic pressure provoked by the osmotic active excipients.

In Figure 17 the dissolution profiles of ram-extrudates with and without pore formers are compared. It was described that the addition of only 5 % PEG 6,000 and 10,000 resulted in a significant increase of drug dissolution rate from a lipid binder (Herrmann et al., 2007; Windbergs et al., 2009). Still, the dissolution studies revealed that the dissolution rate in this work was only slightly increased by 5 % PEG 4,000. Mannitol only moderately accelerated the dissolution for extrudates based on PCL.

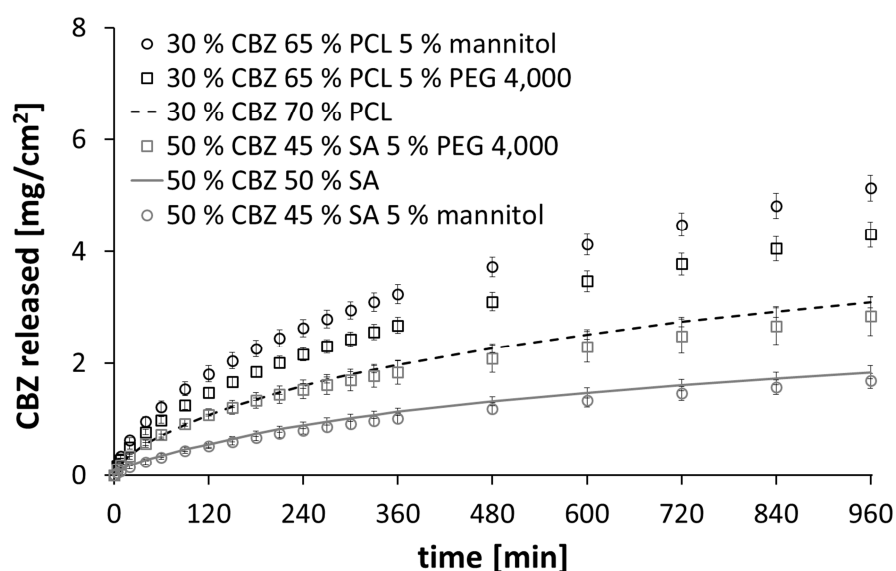


Figure 17: CBZ release of ram-extrudates with 30 % CBZ and PCL and 50 % CBZ and SA, and 5 % mannitol or PEG 4,000 as pore formers; 20 mg CBZ per vessel; apparatus 1, 75 rpm in 900 mL of degassed, demineralised water at 37.0 ± 0.5 °C ($n = 6$; mean \pm SD)

The addition of 15 % pore formers to the lipophilic binders hardly increased the dissolution rate. Even a decrease of the lipophilic binder SA to 10 % within the formulation resulted in a strong prolongation of the release of the model drug (35 % released drug in 8 h).

Wetting behaviour is particularly important for the dissolution characteristics of a hydrophobic dosage form, as the dissolution rate depends on the release surface (Brunner, 1904; Nernst, 1904). To investigate whether the dissolution rate was predominantly limited by a lack of wettability of the lipophilic excipients, dissolution studies were conducted with the addition of 0.001 % polysorbate 20 as a detergent in dissolution media. As no remarkable changes were observed, the ram-extrudates were assessed as sufficiently wettable and for further experiments no detergent was utilised.

In conclusion, the utilisation of PCL and SA as lipophilic binders in a matrix-formulation with CBZ as BCS class II drug was not investigated further due to the low dissolution rate. For drugs with a higher solubility, matrix formulations based on PCL or SA could be valuable.

3.1.4. Solid State Properties

For medicinal products, according to Ph. Eur. CBZ modification III is mandatory. For instance, dissolution properties and bioavailability vary amongst the CBZ modifications (Auer et al., 2003; Kobayashi et al., 2000). But due to the employment of heat, for example, within pharmaceutical production processes polymorphic transitions may occur (Zhang et al., 2004). For pure CBZ III a transition temperature of 71 °C was reported (Behme and Brooke, 1991). Within a HME-process high temperatures and a lower molecular weight of the utilised excipient PEG exhibited the greatest risk for the transition of CBZ (Pajander et al., 2012). A polymorphic transition of CBZ III to CBZ I was stated to depend on the CBZ/PEG-ratio for solid dispersions (Nair et al., 2002).

As, ICH Guideline Q6A demands full understanding of polymorphism in medicinal products, the control of CBZ modifications is essential for the development of CBZ-loaded dosage forms for the SDP. Consequently, in this section analytic methods are assessed to identify the different modifications of CBZ within the produced dosage forms and to examine whether undesirable polymorphic transitions of CBZ took place during the manufacturing.

For this purpose, mini-moulds (MM) as described in section 3.1.2 containing 10 % CBZ III, 15 % mannitol and 75 % PEG 2,000 were investigated. For comparison, CBZ I was produced (section 6.2.1.1) according to Lefebvre et al. (1986). Then, the mini-moulds were prepared with CBZ I as well. They are abbreviated as MM CBZ I in the following paragraphs. A physical mixture (PM) of 10 % CBZ III, 15 % mannitol and 75 % PEG 2,000 served as reference, too.

The pure drug substances, namely CBZ III and CBZ I, could be distinguished by several structure-sensitive analytical methods in this work: On the particulate level techniques like X-ray powder diffraction (XRPD), polarised light microscopy, SEM, and differential scanning calorimetry (DSC) were successfully applied according to literature data (Grzesiak et al., 2003; McMahan et al., 1996; Roberts et al., 2000; Rustichelli et al., 2000). Furthermore, Fourier transform-infrared spectroscopy (FT-IR) and Raman spectroscopy allowed for the analysis on the molecular level in comparison to published data (Auer et al., 2003; Grzesiak et al., 2003; Kogermann et al., 2007; Lowes et al., 1987; O'Brien et al., 2004; Rustichelli et al., 2000; Strachan et al., 2004a).

In the following, three examples of analytical methods for the determination of the CBZ modification will be presented:

First, XRPD was performed from 10 to 50° 2 Θ in transmission mode by preparing the samples in a holder between two polyimide films (section 6.2.3.8). As in angles from 30 to 50° 2 Θ no relevant information was displayed, the resulting diffractograms of CBZ I and CBZ III were depicted from 10 to 30° 2 Θ (Figure 18).

Characteristic peaks for CBZ I were detected at 12.3, 13.1, 14.0, 18.3, and 19.9° 2 Θ and for CBZ III at 13.0, 15.3, 15.8, 18.7, 19.4, and 24.9° 2 Θ according to literature data (Grzesiak et al., 2003; Rustichelli et al., 2000).

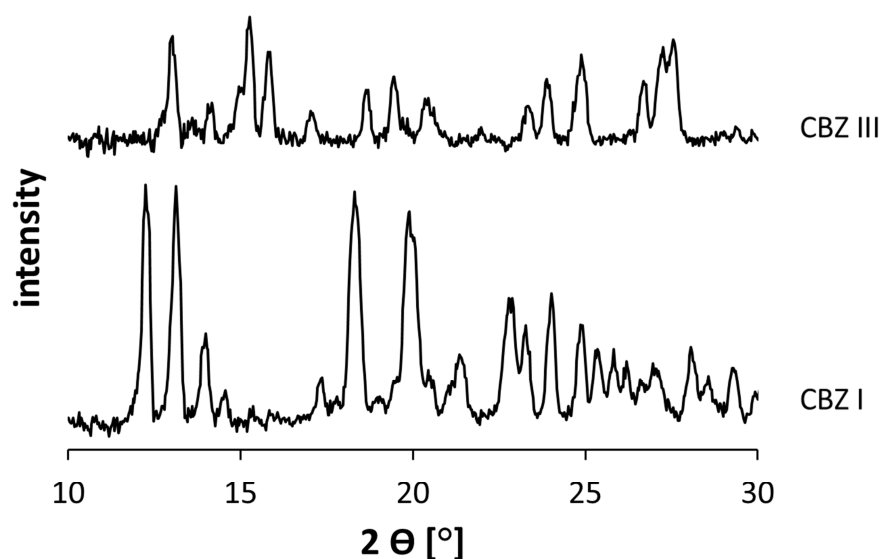


Figure 18: X-ray diffractograms of CBZ I and CBZ III depicted from 10 to 30° 2 Θ , measured in transmission mode; measured values of the polyimide films were subtracted from the sample values

Second, Figure 19 presents FT-IR spectra of CBZ I and CBZ III. The spectra were recorded from 4000 to 600 cm^{-1} with a resolution of 1 cm^{-1} and by using eight scans per spectrum (section 6.2.3.9). Three peaks for each CBZ modification are depicted in detail to demonstrate the modification sensitivity of the method: For instance, peaks at 3484, 1683, and 1389 cm^{-1} were characteristic of CBZ I and peaks at 3464, 1673, and 1380 cm^{-1} of CBZ III (Grzesiak et al., 2003; Lowes et al., 1987; Rustichelli et al., 2000; Strachan et al., 2004a).

Third, DSC measurements were conducted in the temperature range from 20 °C to 220 °C with a heating rate of 10 °C/min (section 6.2.3.10). Figure 20 illustrates the thermogram of CBZ with a first fusion peak at 176 °C for CBZ III, followed by a recrystallisation to form I, which showed a melting peak at 191 °C like the pure CBZ I.

Although the detection of the CBZ modifications of the pure drug was feasible by various methods, the discrimination of the CBZ modifications in the physical mixture and the mini-moulds was more challenging.

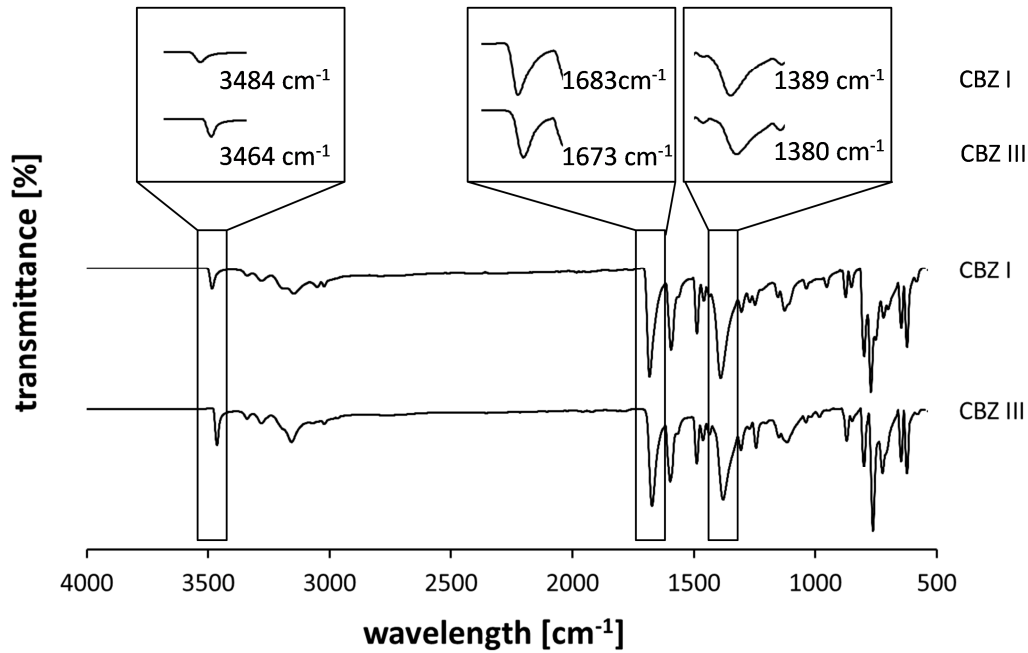


Figure 19: FT-IR spectra of CBZ III and CBZ I, with three characteristic peaks of the drug modifications in detail

X-ray diffractograms were ambiguous due to the low CBZ concentration within the formulation (10 % (w/w)) and the crystalline carriers PEG 2,000 and mannitol, which overlay some CBZ peaks (data not shown). With FT-IR, characteristic peaks of CBZ III were identified in PM, but no distinguishing peaks could be found in MM (data not shown). Moreover, in DSC thermograms there was no CBZ fusion peak for PM and MM (Figure 20) since PEG melted at lower temperatures than the drug and CBZ dissolved in the molten PEG (Nair et al., 2002).

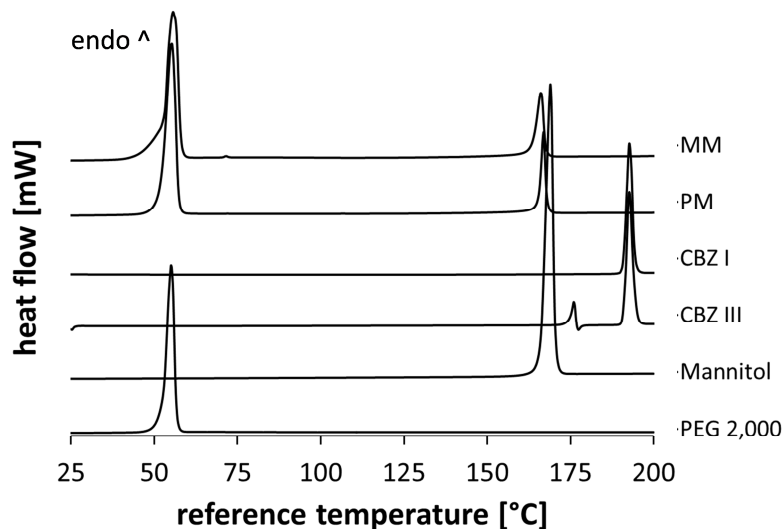


Figure 20: DSC thermograms of PEG 2,000, mannitol, CBZ III and I, the physical mixture (PM), and the mini-moulds (MM)

These findings were also observed by hot stage microscopy (HSM) using polarised light (section 6.2.3.4): A physical mixture of CBZ and PEG 2,000 was therefore prepared on a temperature controlled microscopy stage and was heated at a heating rate of 10 °C/min. The microscopy images of CBZ dissolving in PEG 2,000 are illustrated in Figure 21 in a chronological sequence.

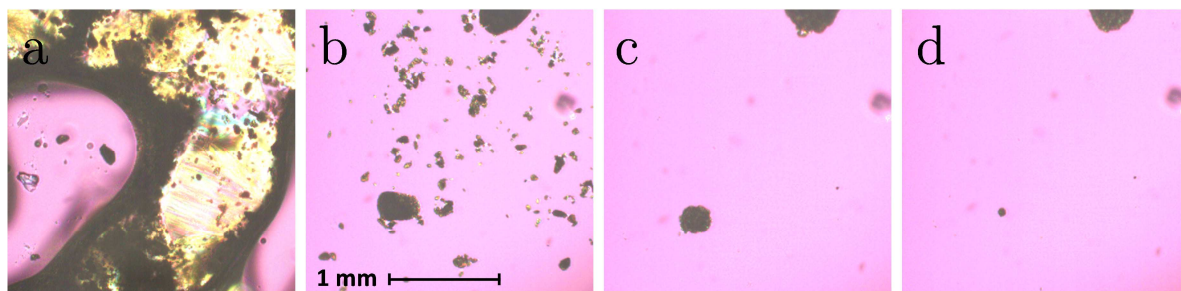


Figure 21: Hot stage microscopy images of CBZ dissolving in PEG 2,000, chronological sequence with a heating rate of 10 °C/min: 50 °C, at time point 3 min (a); 80 °C, at time points 6 to 7 min (b - d)

SEM has already been utilised for the observation of the solid state of CBZ for low CBZ-loadings in PEG solid dispersions (Moneghini et al., 2001). In this work, morphological differences of the surfaces of the MM versus those of the MM CBZ I (prepared with CBZ I) were observed via SEM as well. Figure 22 presents micrographs of CBZ III and CBZ I powders as well as the surfaces of the casted MM and MM CBZ I.

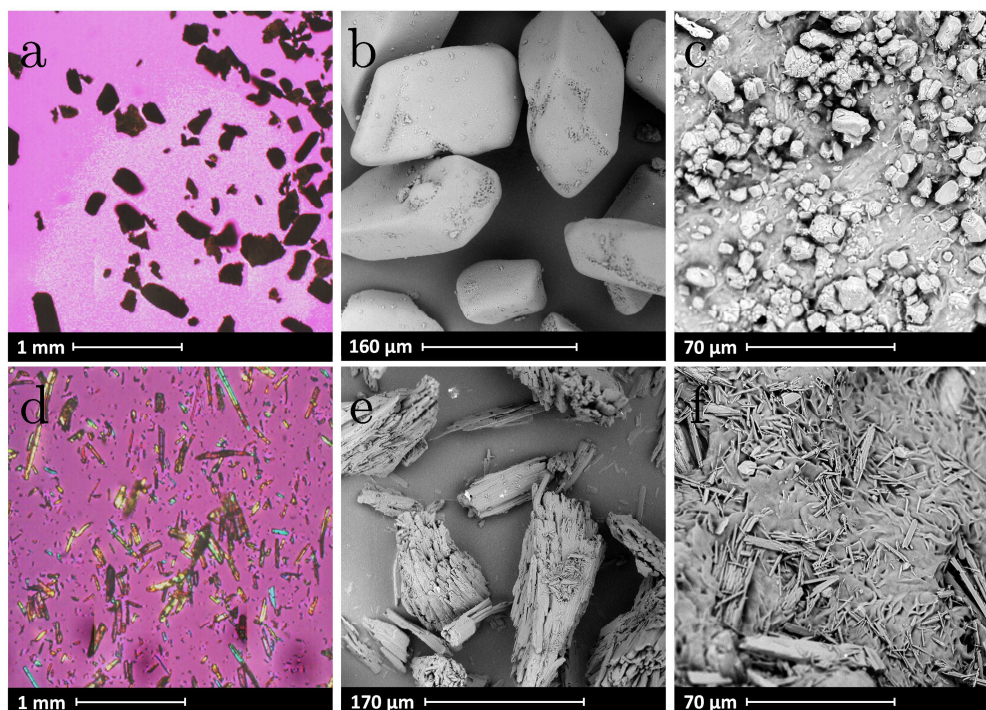


Figure 22: Micrographs of CBZ powder (a, b, d, and e) and the mini-moulds (c and f); micrographs with a polarising filter (a, d) and SEM micrographs (b, c, e, and f); prismatic CBZ III (a - c) and needle shaped CBZ I (d - f)

The MM exhibited mainly prismatic crystals on their surface, similar to CBZ form III, whereas the MM CBZ I showed fine, needle shaped crystals corresponding to CBZ I. In conclusion, according to SEM it was likely that CBZ III was not transformed to CBZ I within the melting and casting method of producing the mini-moulds.

Raman spectroscopy has already been utilised to analyse the different CBZ modifications in polymorphic mixtures of CBZ (Kogermann et al., 2007; O'Brien et al., 2004; Strachan et al., 2004b) as well as in commercially available CBZ drug formulations with a yield of around 70 % (Auer et al., 2003).

In this work, Raman spectra of the pure substances and the drug formulations were recorded as described in section 6.2.3.11. Analysis was carried out in a spectral range of 1890 to 150 cm^{-1} with a PhAT probe as a non-contact optic sampling device. Raman spectra were pre-treated by selecting a CBZ characteristic spectral region, accomplishing a baseline correction via standard normalised variation (SNV) transformation and mean centring the data (Kogermann et al., 2007).

Figure 23 presents the treated spectra in the region of interest in detail. The excipients mannitol and PEG 2,000 did not show any peak in the named region and thus did not disturb the analysis.

The Raman spectra showed bands at 1622, 1598, 1562, 719 cm^{-1} for CBZ I and bands at 1624, 1600, 1566, and 724 cm^{-1} for CBZ III. These values were in line with values described in literature (Kogermann et al., 2007; O'Brien et al., 2004; Strachan et al., 2004a).

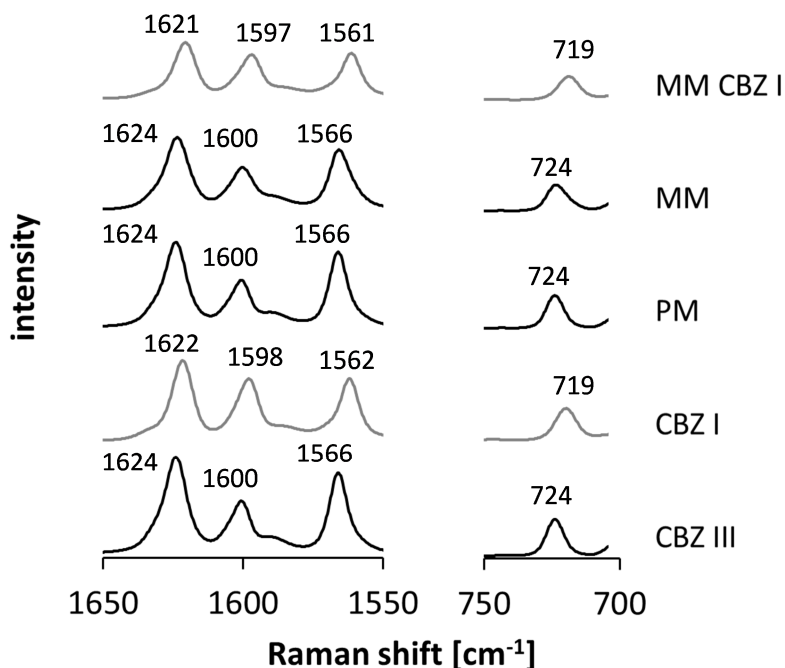


Figure 23: Raman spectra of CBZ III, CBZ I, the physical mixture (PM), and the mini-moulds (MM and MM CBZ I), spectra were corrected via SNV transformation and mean centred

However, spectral differences in the samples were small: the peaks of CBZ III and CBZ I, for example, only differ for 2 wavelengths per cm. According to Auer et al. (2003) the significance of subtle differences between the characteristic bands has to be judged depending on the repeatability and wavenumber accuracy of the Raman measurement. Therefore, the instrument wavenumber accuracy was determined according to Ph. Eur. 2.2.48 (section 6.2.3.11). All five evaluated distinctive peaks of cyclohexane matched the required tolerances of shift ($\pm 1.0 \text{ cm}^{-1}$). The repeatability of the method was satisfying as well, as the repetitions of the measurement were widely overlapping ($n = 3$).

To sum it up, the discrimination between CBZ III and CBZ I was feasible although differences in Raman shifts were found to be small. Moreover, CBZ III was detected in the PM and the MM. MM prepared with CBZ I (MM CBZ I) exhibited peaks at 1621, 1597, 1561, and 917 cm^{-1} , representative for CBZ I. Hence, these findings confirmed the results of SEM.

In a next step it was examined using the discussed solid state characterisation methods whether small-scale ram-extrusion influenced the modification of CBZ within the formulations. Thus, Raman spectra of the small-scale ram-extrudates were recorded, normalised via SNV, and mean centred as described above. The resulting Raman spectra are illustrated in Figure 24.

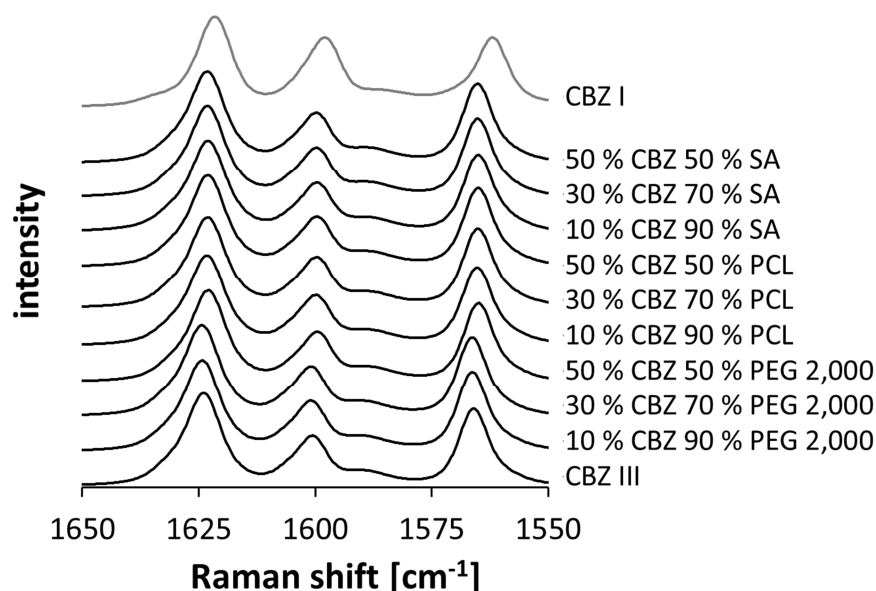


Figure 24: Raman spectra of the small-scale ram-extrudates made from SA, PCL, and PEG 2,000 including 10, 30 or 50 % CBZ, in comparison to spectra from CBZ III (all depicted in black lines) and CBZ I (grey line); spectra were corrected via SNV transformation and mean centred

The excipients SA and PCL did not show any peaks in the region sensitive to CBZ modification. It was ensured that all formulations contained CBZ III, which meant that no undesired change of CBZ modification had happened under the manufacturing process.

As XRPD was described as the “gold-standard” for phase identification (Zhang et al., 2004), the results obtained by the Raman measurements should be verified by XRPD. Due to the higher drug content in the small-scale ram-extrudates X-ray diffractograms were meaningful in contrast to those of the MMs, which included only a low drug-loading (see above). The diffractograms of the small-scale ram-extrudates with a CBZ content of 50 % affirmed that CBZ III was incorporated (Figure 25).

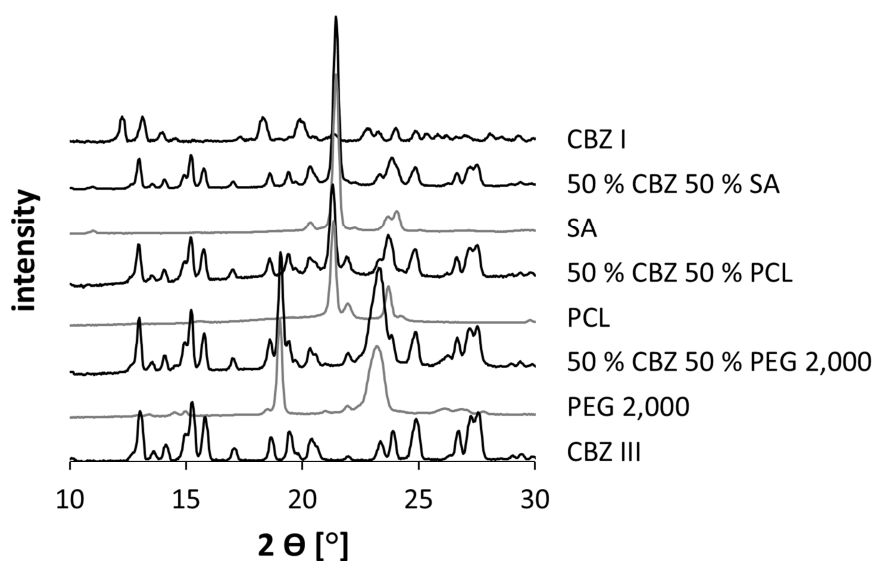


Figure 25: X-ray diffractograms of CBZ I and CBZ III and of the ram-extrudates containing 50 % CBZ and either SA, PCL or PEG 2,000 as binders depicted from 10 to 30° 2θ ; measured values of the polyimide films were subtracted from the sample values and diffractograms of the excipients were normalised to the peak intensities within the formulations

In conclusion, the solid state analysis revealed that both the mini-moulds and the small-scale ram-extrudates contained the required modification of CBZ and that the manufacturing methods did not alter the modification of the drug. Whereas XRPD, DSC, and FT-IR exposed restrictions for low-loaded CBZ formulations, Raman was successfully proven to be a suitable analytical method, allowing for the solid state analysis of CBZ even for those dosage forms.

3.1.5. Summary

As twin-screw extrusion in the utilised experimental set-up needs a minimum batch size of 300 g and only a limited amount of CBZ was available due to its high cost, in this part of the thesis moulding and ram-extrusion were investigated as small-scale production techniques (Figure 26).

While moulding involved some disadvantages, small-scale ram-extrusion with a high pressure capillary rheometer made an excipient screening and the production of extrudates containing 10 to 50 % CBZ feasible. With batches of only 10 g the exploration of the mechanical properties and dissolution testing was possible. Still, for the ram-extrusion as small-scale production technique one disadvantage may be a lack of homogeneity, as less dispersive and distributive mixing is inherent in the process compared to screw extrusion. Nevertheless, according to the low standard deviations in dissolution studies one may assume that the drug was homogeneously dispersed within the matrix by the manual mixing by mortar and pestle.

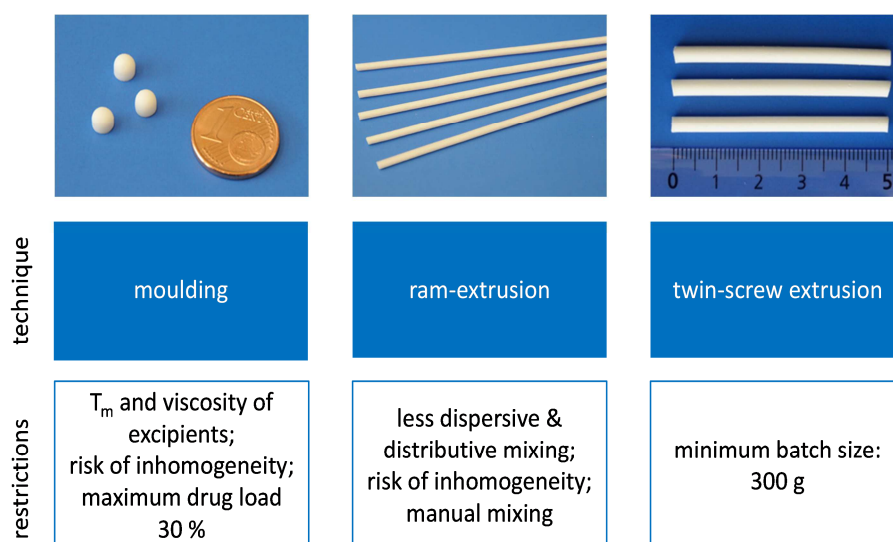


Figure 26: Overview of the small-scale production techniques and their restrictions, displayed scale in cm

With the examination of F_{max} , the tensile strength and the E-modulus, methods for the investigation of the mechanical properties of the formulations were found and assessed. Moreover, it has been shown that the applicability of the SDP depended for the tested ram-extrudates with 2 mm diameter on the rigidity of the extrudates, which is represented by the E-modulus. While the cuttability was mainly influenced by the binder, the tensile strength and the E-modulus were affected by the CBZ content as well.

PEG 2,000 demonstrated superior properties as hydrophilic binder to PEG 10,000 and PEG 20,000: Formulations based on the lower molecular weight PEG required medium F_{max} . Moreover a similar tensile strength as formulations including PEG 10,000 or PEG 20,000 was achieved with a drug-loading of 30 to 50 %. Moreover, rods made from

PEG 2,000 had comparatively low E-moduli and were therefore suitable for the application of the SDP.

Depending on the drug-load and the matrix immediate release and sustained release dissolution profiles were obtained. For hydrophilic binders, a higher CBZ-loading resulted in lower dissolution rates. For lipophilic binders the dissolution rate was very low and only slightly increased by the increase of CBZ-loading or the addition of pore-forming agents. Therefore, only hydrophilic matrices will be examined further for the poorly soluble model drug CBZ.

Solid state analysis via XRPD or Raman revealed that the small-scale production techniques did not change the modification of the drug and all formulations enclosed CBZ III.

In the following chapters it will be investigated, whether the results of the small scale are transferable to a larger scale, for example to drug-loaded rods manufactured by twin-screw extrusion.

3.2. Drug-Loaded Rods

3.2.1. Introduction and Objectives

On the basis of the experiences in the small scale (section 3.1) the pursued objective in this chapter is the development of drug-loaded rods by hot-melt twin-screw extrusion for the implementation of the SDP.

Based on extrudates offering immediate and sustained release characteristics, co-extrudates shall be established, manufactured, and characterised. Co-extrudates consisting of a core- and a coat-layer give access to biphasic drug release (Dierickx et al., 2013). The dissolution of sustained release formulations by Wening (2011) showed an undesired dependency on the length of the sliced tablet-like dose-carriers. This drawback may be minimised by wax-coated formulations manufactured via co-extrusion.

The selection of appropriate coat and core formulations should be conducted by matching the pre-defined dissolution behaviour, the mechanical properties, and the process parameters of extrudates.

Apart from the well-known challenges of co-extrusion (Dierickx et al., 2013; Dierickx et al., 2012; Vynckier et al., 2014a; Vynckier et al., 2014b), in this study, individual dosing via cutting the co-extrudates at ambient temperature was considered. For proper cuttability via the SDP, similar mechanical properties of both layers are needed in order to maintain the integrity of the cut co-extrudate doses later on.

The increase of the diameter of the drug-loaded rods, and thus, the higher maximum cutting forces require a new design of the prototype of the SDP.

Furthermore, this chapter will focus on the systematic evaluation of the mechanical properties of CBZ-loaded rods and their modulation by suitable excipients. The aim is to clarify how dosing by the SDP and mass uniformity of sliced doses depend on the mechanical properties of the drug-loaded rods. To examine the practicability of the device and the formulations for patient-centred treatment, the needed maximum cutting forces have been compared to literature data of the manual forces of different age groups of the population.

Moreover, in this part of the thesis it is also intended to study to which extent the mechanical properties and the dissolution behaviour of the CBZ-loaded rods are affected by storage.

3.2.2. Extrudates

3.2.2.1. Hot-Melt Extrusion via a Twin-Screw Extruder

Seven batches of hot-melt extrudates were produced on a 16 mm twin-screw extruder as described in detail in section 6.2.1.4. It was shown that the drug content affects the dissolution profiles (section 3.1.3.3). Therefore, in this section, a drug-load of 30 % (w/w) CBZ was selected for formulations F1 - F3 to obtain immediate release properties, whereas formulations F4 - F7 contained 45 % or 50 % (w/w) CBZ to achieve sustained release behaviour. Additionally, they enclosed PEG 2,000, and either an addition of PEG 1,500 or Poloxamer 188 (POL, Table 3).

Table 3: Extrudate formulations, fraction of drug and excipients (% w/w), melting temperature (T_m) of the excipients as determined by DSC measurements (section 6.2.3.10), and extrusion temperature (T_{extr})

	CBZ	PEG 2,000	PEG 1,500	POL	
T_m [°C]	175.9/191.4*	54.0	49.2	54.7	
Formulation no.					T_{extr} [°C]
F1	30	70	-	-	46
F2	30	60	10	-	45
F3	30	60	-	10	47
F4	45	55	-	-	46
F5	45	40	15	-	42
F6	45	40	-	15	47
F7	50	50	-	-	46

* referring to CBZ III and CBZ I (section 3.1.4)

PEG 2,000 was investigated further as a hydrophilic binder, since more appropriate mechanical properties than those for higher molecular weight PEGs have been proved (section 3.1.3.2).

In this chapter, the added excipients POL and PEG 1,500 were used to modulate the mechanical properties and simultaneously the dissolution behaviour of the extrudates. A higher dissolution rate was anticipated by the addition of the surface-active POL due to a better wetting of the lipophilic CBZ molecule. A standard grade of poloxamer resulted in incomplete drug release in a previous study, which was overcome by the usage of a micronized quality (Wening et al., 2012). Therefore, in this work, the micronized quality was utilised, too. As PEG 1,500 consists of shorter-chained molecules than PEG 2,000, an increase in the drug dissolution rate was expected due to a higher dissolution rate of PEG 1,500 itself as discussed in detail in section 3.1.3.3. As seen for the small-scale ram-extrudates made from PEG 2,000 in section 3.1.3.2, F_{max} was predominantly

influenced by the binder, whereas the tensile strength of extrudates increased with an increase of CBZ content. Thus, the proportion of the added excipients was chosen in relation to the CBZ percentage (1:3, Table 3).

In accordance with the ram-extrusion (section 3.1.3.1), all batches were extruded below the melting temperatures (T_m) of the pure excipients (Table 3). The barrel length of 400 mm, the screw speed of 60 rpm, and the feeding rate of 600 g/h resulted in a material residence time of 3.5 to 4 min. Within this period of time the material was softened and then formed into cylindrical rods through the die (diameter of 4 mm).

For the adjustment of the barrel temperature a systematical examination was conducted in a preliminary study. In this study, the temperature of the whole barrel was varied in intervals of 1 °C. The aim was to obtain extrudates, which have an appropriate viscosity for transport on the conveyor belt directly after the die without losing their cylindrical shape. Further, the extrudates must not show any surface defects, which predominantly occur at too low temperatures.

Adjusting the velocity of the conveyor belt made it possible to manufacture straight extrudates with a smooth surface. Formulation F2 is depicted in Figure 27 as an example.

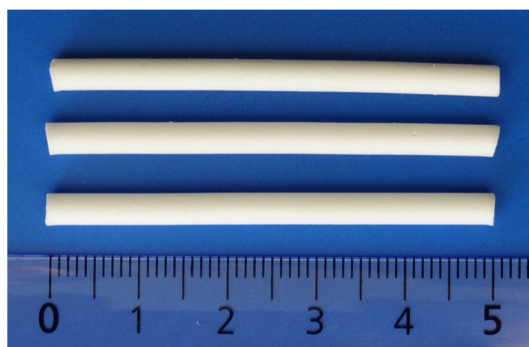


Figure 27: Manufactured extrudates, formulation F2 (30 % CBZ, 60 % PEG 2,000, 10 % PEG 1,500), $\varnothing = 4$ mm, displayed scale in cm

As the hydrophilic binder recrystallised rapidly at room temperature, the extrudates exhibited no die swell (diameter 4 mm). For the production of rod-shaped melt-extrudates this has already been mentioned as an advantage of (semi-)crystalline polymers with low melting temperatures (Schilling and McGinity, 2010).

3.2.2.2. Mechanical Properties

As described in 3.1.3.2 for the small-scale ram-extrudates, F_{max} , the tensile strength, and the E-modulus emerged as parameters for the evaluation of the mechanical properties. In this part of the work, it was tested, if they are appropriate parameters for CBZ-loaded rods with a higher diameter as well.

In Figure 28 F_{max} of the extrudate formulations F1 - F7 is plotted. F_{max} was in this case determined by a Texture Analyser as well as by Test Apparatus H10KM, both equipped with special cutting test set-ups (section 6.2.3.1).

F_{\max} ranged from 22.2 ± 2.9 to 41.9 ± 1.7 N for measurements with the Texture Analyser and from 13.3 ± 0.7 to 30.5 ± 3.3 N for the Test Apparatus H10KM. Thus, results recorded with the Texture Analyser were in the mean 10.6 N higher than those measured with the Test Apparatus H10KM, but exhibited the same tendencies. These differences in accuracy may be due to the different cutting test set-ups and utilised devices (section 6.2.3.1).

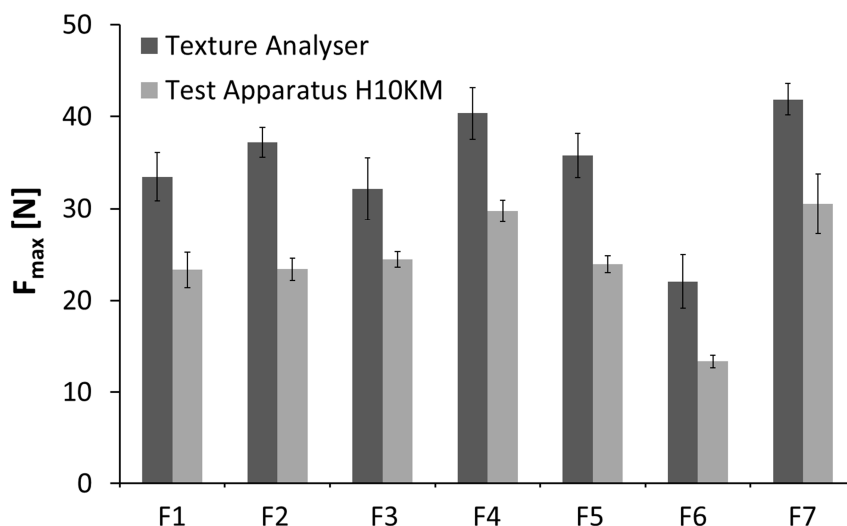


Figure 28: Maximum cutting force (F_{\max}) of the extrudates (F1 - F7), determined by the Texture Analyser and the Test Apparatus H10KM ($n = 10$, mean \pm SD)

The coefficients of variation for measurements with the Texture Analyser ranged from 4.1 to 13.1 % and were therefore slightly larger than those resulting from the Test Apparatus H10KM (3.5 to 10.7 %).

With the cutting test set-up designed for the Test Apparatus (section 6.2.3.1, Figure 74 b) more measuring errors like inexplicable outliers occurred which were leading to not usable measurements. To obtain force-displacement profiles of the cutting experiments with accuracy in the μm -scale, further measurements were conducted with the Texture Analyser.

Regarding the results of the test, the added excipients PEG 1,500 and POL were added with respect to the API content to modulate F_{\max} and to optimise the mechanical properties. But for formulations with 30 % CBZ the added excipients did not alter F_{\max} within the measurement accuracy. But PEG 1,500 slightly decreased F_{\max} at the 15 %-level (F5) and the addition of 15 % POL (F6) decreased F_{\max} from 40.4 ± 2.9 to 22.9 ± 2.9 N. The tensile strength and the E-modulus of the extrudates, which were obtained from the three-point bending test (section 6.2.3.2) are depicted in Figure 29.

For formulations F1 - F7 the CBZ-loading varied less than for the small-scale ram-extrudates (section 3.1.3). Therefore, the tensile strength of formulations without added excipients (F1, F4 and F7) increased only slightly with increasing CBZ content from 9.0 ± 0.9 MPa (30 % CBZ) to 10.6 ± 1.3 MPa (50 % CBZ).

Regarding the data in Figure 29 one can assume that the tensile strength did not predominantly depend on the CBZ content, but on the nature of the added excipients: PEG 1,500 reduced the tensile strength, whereas POL raised the tensile strength. For formulations including 45 % CBZ, the tensile strength was reduced from 10.0 ± 0.3 MPa (without added excipient) to 7.4 ± 0.2 MPa when 15 % PEG 1,500 was added, for instance. By the addition of 15 % POL it raised to 11.6 ± 0.6 MPa.

For formulations of Perissutti et al. (2002) the tensile strength depended on the extrudate compositions, while the E-moduli were less affected by the compositions. However, the E-moduli were strongly linked to the composition of the formulations examined in this study: PEG 1,500 as a soft excipient with waxy appearance (Ph. Eur.) led to smaller E-moduli, whereas formulations including POL as an excipient showed higher values (Figure 29).

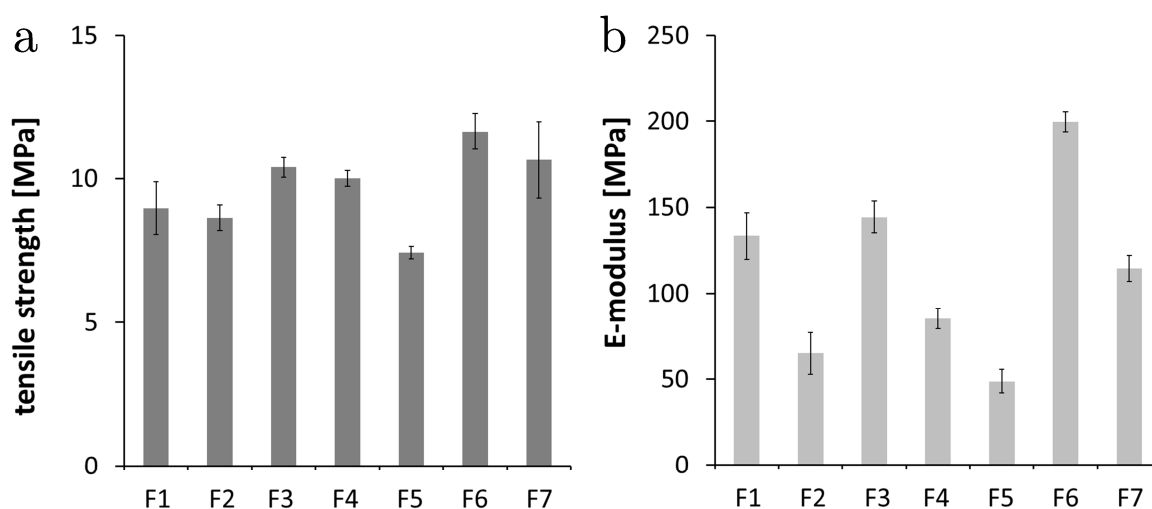


Figure 29: Tensile strength (a) and E-modulus (b) of the extrudates (F1 - F7) determined by a Texture Analyser equipped with a three-point bending rig ($n = 5$, mean \pm SD)

A high E-modulus may cause problems in practical handling of the drug-loaded rods and the insertion into the SDP: As discussed in section 3.1.3.2 the small-scale ram-extrudates were suitable for application up to a threshold of 1.7 GPa for the E-modulus, but broke inside of the device due to their rigidity when exceeding this value. As the E-modulus of the extrudates in this study did not exceed 200 MPa, all formulations were assured to be appropriate for the application via the SDP.

3.2.2.3. Interindividual Manual Forces

In patient-centred treatment, usability of delivery devices (as well as accuracy and precision) is important, as, for example, the manual forces depend on gender, age, and state of health of the patients (Ager et al., 1984; Kircher, 2007; Lowe, 2001; Mathiowetz et al., 1986). The required F_{\max} of the drug-loaded rods is therefore crucial, as the SDP is also intended to be used for individual dosing by children and elderly people, who may have limited manual forces and dexterity. Consequently, required forces for cutting the drug-loaded rods should be evaluated with regard to published data for grip forces of different age groups including school children (5 - 19 years: Ager et al., 1984; Mathiowetz et al., 1986) and elderly people (66 - 82 years: Lowe, 2001).

For 20- to 60-year-old healthy individuals, average manual forces were described to depend on gender and pinch type (e.g. tip-, key-, or chunk-pinch) and to be between 55 and 115 N (Kircher, 2007). The cutting mechanism of the SDP is triggered by employing a tip (one-point) pinch grip between thumb and forefinger (Figure 30).



Figure 30: Trigger mechanism of the SDP (a), one-point pinch grip (b), and triggering of the SDP (c)

Lowe (2001) examined the dynamic force of a one-point pinch grip with a simulated hand tool device. The younger participants (39.4 ± 11.8 years, $n = 9$) had a maximal pinch strength of 60.1 ± 15.5 N, while the older age group (73.9 ± 4.9 years, $n = 9$) reached only 45.9 ± 12.1 N. Ager et al. (1984) tested 474 children aged 5 to 12 for their pinch strength utilising a pinch gauge and finding a steady increase in pinch strength with increasing age. While hand dominance was not an important factor, males were found to be consistently stronger than females across the age ranges. These observations were confirmed by investigations by Mathiowetz et al. (1986) on 471 6- to 19-year-olds.

Formulations F4 and F7 containing 45 and 50 % CBZ (w/w) and no added excipients required the highest maximum cutting forces (40.0 ± 0.9 and 41.9 ± 1.7 N for measurements with the Texture Analyser, Figure 28). Still, these values were below those published by Lowe (2001) and Kircher (2007). However, if one applies a surgery knife to cut manually, F4 and F7 could only be sliced with difficulty. Formulations F1 - F3, F5, and F6, which include a lower CBZ content and added excipients, were manually sliceable by a surgery knife. They required a maximum cutting force between 22.1 ± 2.9 and 37.2 ± 1.6 N, respectively (Figure 28) and were presumed to be applicable via the SDP. In

conclusion, the data demonstrated that the added excipients decreased F_{\max} of the CBZ-loaded rods.

Figure 31 illustrates the right hand finger-tip pinch strength of school children across the age groups according to literature in comparison with the range of measured F_{\max} of the extrudates. Definitely, the measured values of F_{\max} do not completely represent the values from literature, as different set-ups, devices, and methods were utilised; but it was assessed that a comparison of the data was still feasible to see whether an application of the SDP could be possible in general.

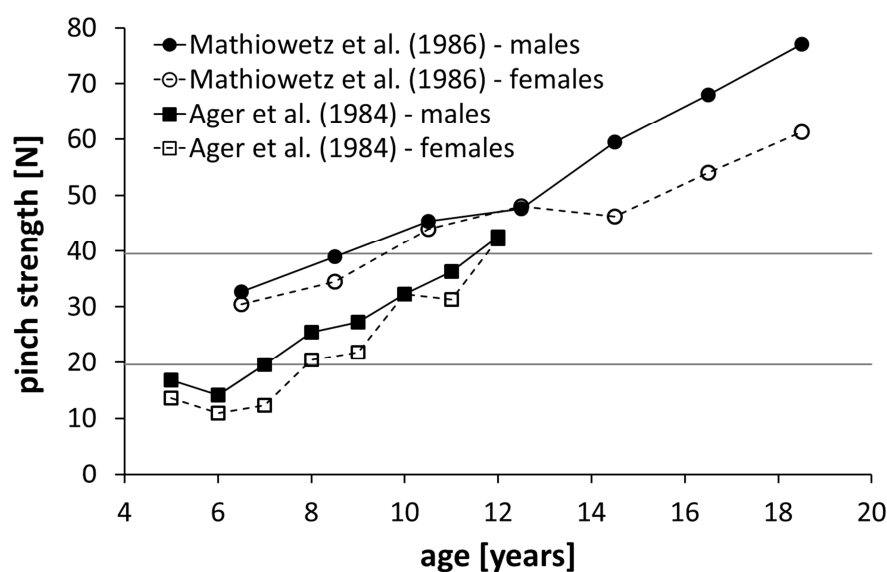


Figure 31: Right hand finger-tip pinch strength of males and females across the age according to Mathiowetz et al. (1986) with 471 participants and Ager et al. (1984) with 474 participants; the two horizontal lines represent the range of F_{\max} for the extrudates F1 - F7

Concerning the deployment of the SDP within the paediatric population, the pinch strength of children older than 12 years (42.2 N (Ager et al., 1984) and 48.1 N (Mathiowetz et al., 1986)) would be sufficient to trigger the cutting mechanism of the SDP for all formulations. According to Mathiowetz et al. (1986) some formulations could already be handled by 8-year-olds not taking into account the intellectual capability (fingertip pinch strength of 39.0 and 34.5 N for males and females). For younger children, drug dosing action is usually not made by the children, but the parents act as caregivers.

3.2.2.4. Dissolution Studies

Dissolution testing for the extrudates was performed with apparatus 1 under sink conditions (section 6.2.3.7). Depending on the CBZ-loading and the added excipients immediate and sustained release characteristics were achieved (Figure 32). Like in the case of the ram-extrudates made from PEG (section 3.1.3.3), for the extrudates higher CBZ-loads led to slower drug release and higher fractions of PEG resulted in faster drug release (Figure 32).

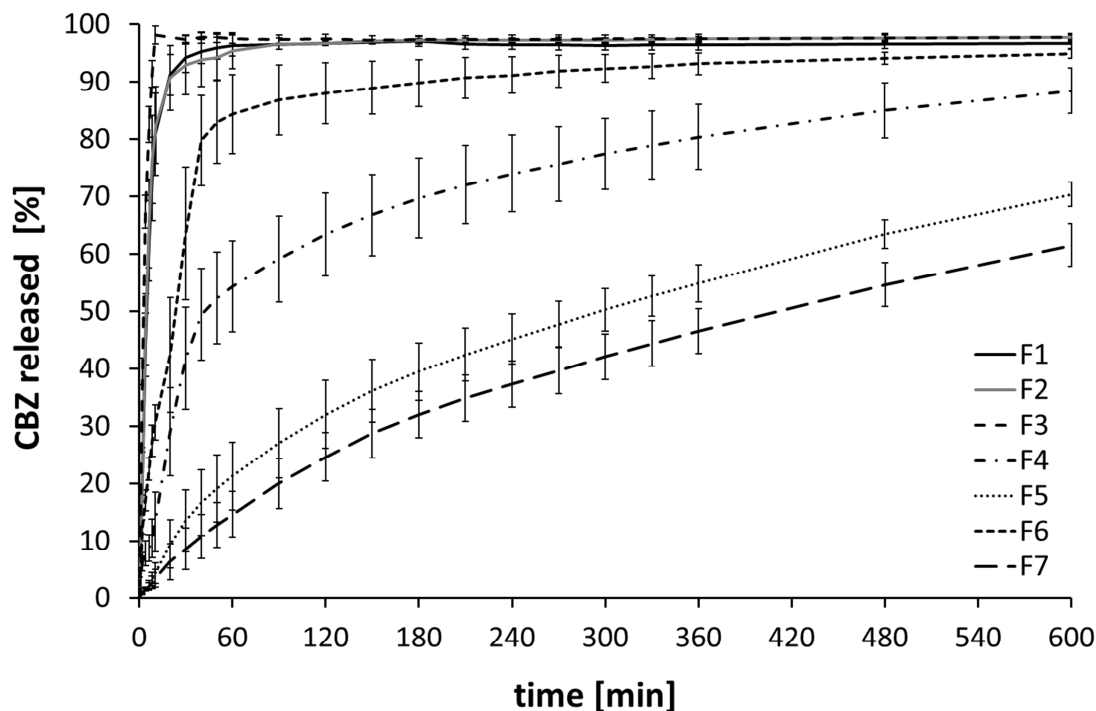


Figure 32: CBZ release of extrudates (formulation F1 - F7), one extrudate piece per vessel (40 mg extrudate mass, corresponding to 12 - 18 mg CBZ); apparatus 1, 75 rpm in 900 mL of degassed, demineralised water at 37.0 ± 0.5 °C ($n = 6$; mean \pm CI; $\alpha = 0.05$)

The addition of the surface active agent POL increased the dissolution rate both for formulations with 30 and 45 % CBZ (F3 and F6). For the lower drug-load PEG 1,500 as an added excipient did not change the dissolution profile (F2), but for the higher drug-load a decrease in dissolution rate was observed (F5). This finding was unexpected, as PEG with lower M_w were described to lead to higher drug release (section 3.1.3.3). In this case, the different production temperatures of the extrudates may have to be considered as well: F5 was extruded at 42 °C whereas F4 was extruded at 46 °C. Therefore, the included PEG 2,000 melted to a dissimilar degree, which may result in different dissolution characteristics.

3.2.2.5. Application of the Solid Dosage Pen

So far, the SDP has only been used for low drug masses and extrudate diameters up to 2.7 mm (Wening and Breitzkreutz, 2010; Wening et al., 2012). The maximum cutting forces for melt-extruded drug-loaded rods did not exceed 10 N (Wening et al., 2012).

To incorporate higher drug doses in the rods, in this work, the diameter of the extrudates was set to 4 mm. The increase of the rods' diameter, and thus, their higher F_{max} (section 3.2.2.2) required some changes of the existing prototype of the SDP: Beneath the widening of the shaft, a novel cutting mechanism with a round cutting opening in the blade and a more rigid spring was constructed (Figure 33).

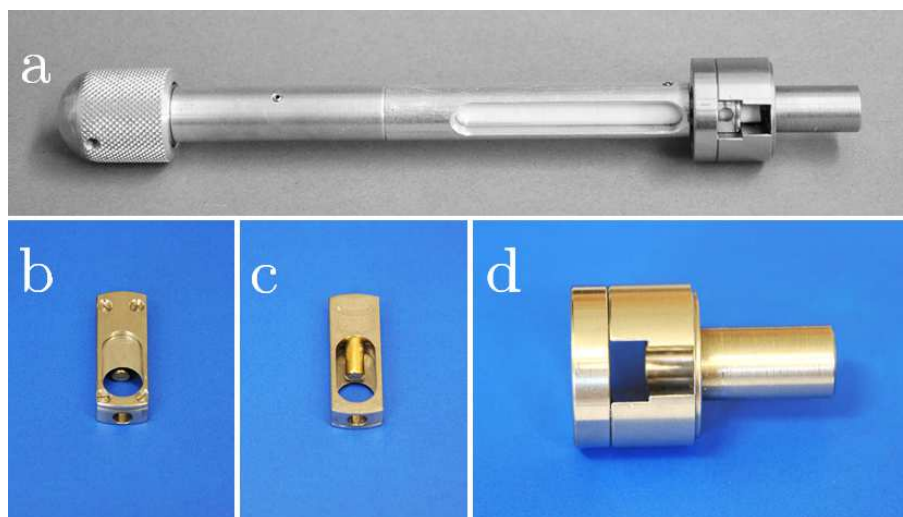


Figure 33: Newly designed SDP (a), novel cutting mechanism with a round cutting opening in the blade and a more rigid spring (b and c) and the new sample outlet with the mounting for the blade (d)

The applicability of the SDP was exemplarily investigated utilising formulations F2, F3, F5 and F6 including the added excipients PEG 1,500 or POL. The extrudates exhibited mechanical properties which allowed for a practical handling, insertion into the device, and cutting off in doses. One full revolution of the adjusting screw resulted in 0.4 mm propulsion of the drug-loaded rod and was defined as one dose unit (DU). Ten doses with 5, 10, and 15 DUs corresponding to extrudate pieces with lengths of 2, 4, and 6 mm were cut using the newly designed device (section 6.2.4.1).

So far, the optical appearance of the slices of melt-extrudates cut via the SDP was worse compared to those cut from wet-extruded rods (Wening et al., 2012). As claimed by Wening et al. the optical appearance of melt-extruded rods should be improved by the addition of plasticisers to soften the strands for more accurate cutting.

As examples, Figure 34 shows drug carriers with 2 mm length of formulation F2 (first row) and F5 (second row) sliced by the SDP next to a one Euro cent coin.

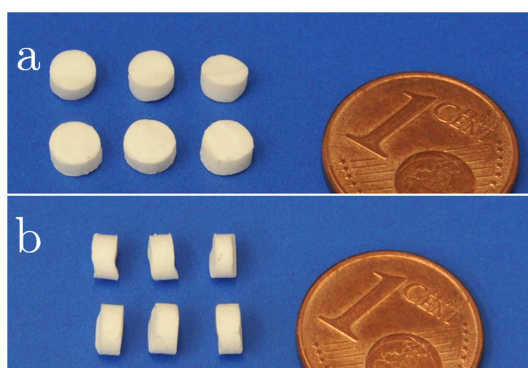


Figure 34: Drug carriers with 2 mm length, (a) top and (b) lateral view of extrudates F2 (first row) and F5 (second row) sliced by the SDP next to a one Euro cent coin

The optical appearance of the sliced doses containing PEG 1,500 was improved by smoother cross-sections and more regular edges of the tablet-like slices in comparison to Wening et al. (2012). The lateral view on the sliced doses reveals that a higher fraction of PEG 1,500 (F5) ameliorated the look of the drug carriers even more than the lower fraction of PEG 1,500 (F2). Due to the soft and ductile properties of the utilised excipients, for all formulations no hard edges or splinter were produced and therefore a safe swallowing was assumed.

3.2.2.6. Uniformity of Dosage Units

Mass and content of slices with 5, 10, and 15 DUs were determined for ten slices each as described in sections 6.2.4.2 and 6.2.4.3 and results are depicted in Table 4.

10 DUs corresponded approximately to 65 mg mass, meaning for a CBZ-loading of 45 % within the sustained release formulations F3 and F6 that two sliced pieces would result in a single dose of 60 mg CBZ. This dose would be appropriate for a 6-year-old child with 20 kg body weight as minimal dose according to literature (Kearns et al., 2003). For higher single doses, 180 mg CBZ, for instance, four pieces of 15 DUs, equalling approximately 100 mg formulation mass each could be administered.

For validated manufacturing processes of finished products in the pharmaceutical industry, acceptance values (AV) are determined according to Ph. Eur. 2.9.40 (section 6.2.4.4). During formulation development, the investigation of the mass variation and content uniformity of the cut slices may give more detailed information than the sole consideration of the AV. As the determination of an AV needs a label claim, in this work AV were exemplarily calculated based on the label claims given in Table 4 (10, 20, and 30 mg for F2 and F3; 15, 30, and 45 mg for F5 and F6).

Table 4: Masses, contents, and acceptance values based on label claims (AV, according to Ph. Eur. 2.9.40) for doses with 5, 10, and 15 DUs (corresponding to lengths of 2, 4, or 6 mm) sliced with the SDP (n = 10, mean \pm SD)

DUs	length [mm]		F2	F3	F5	F6
5	2	mass [mg]	33.4 \pm 1.9	32.8 \pm 2.8	34.1 \pm 1.4	32.9 \pm 4.8
		content [%]	99.7 \pm 6.2	97.2 \pm 8.1	100.6 \pm 3.9	98.2 \pm 13.7
		AV (label claim [mg])	15.0 (10)	22.1 (10)	11.1 (15)	34.0 (15)
10	4	mass [mg]	64.7 \pm 3.0	65.0 \pm 2.7	69.3 \pm 1.7	67.5 \pm 3.7
		content [%]	98.0 \pm 4.1	97.4 \pm 4.0	101.7 \pm 2.2	97.2 \pm 5.0
		AV (label claim [mg])	13.0 (20)	12.8 (20)	9.7 (30)	12.2 (30)
15	6	mass [mg]	98.6 \pm 1.7	97.0 \pm 2.1	101.1 \pm 2.3	95.1 \pm 3.0
		content [%]	100.6 \pm 2.8	96.9 \pm 4.6	99.7 \pm 3.8	97.9 \pm 3.3
		AV (label claim [mg])	6.6 (30)	15.2 (30)	9.3 (45)	12.8 (45)

The mass of the cut slices showed small standard deviations (SD), indicating the appropriateness of the performance of the SDP as a device and the extrudates regarding their mechanical properties for the utilisation of the device (Table 4). Nevertheless, differences in the accuracy of cutting were observed, as formulations with PEG 1,500 exhibited SDs between 1.4 and 3.0 mg and formulations with POL showed SDs between 2.1 and 4.8 mg. The SDs of the content were smaller for F2 and F5 than for F3 and F6 (2.2 to 6.2 % and 3.3 to 13.7 %).

As a result, the content uniformity of F2 and F5 was found to be in accordance with the pharmacopoeial specifications (even for the smallest examined dose of 5 DUs), whereas F3 and F6 only partially met the requirements ($AV \leq 15$ on L1). As this result could not be attributed to outliers, but to a general tendency over all ten examined samples, the investigation was not expanded on L2 ($n = 30$, $k = 2.0$, $AV \leq 25$).

3.2.2.7. Stability Studies

To examine whether the mechanical properties change over storing, stability testing was performed for formulations including PEG 1,500 and POL (F2, F3, F5, and F6). After a period of 6 months at 21.0 ± 0.2 °C and 45 % RH the corresponding tests were repeated (Table 5).

Table 5: Maximum cutting force (F_{\max} , $n = 10$), tensile strength, and E-modulus (both $n = 5$) after production and after six months of storage for F2, F3, F5, and F6; mean \pm SD

no.	after production			after 6 months of storage		
	F_{\max} [N]	tensile strength [MPa]	E-modulus [MPa]	F_{\max} [N]	tensile strength [MPa]	E-modulus [MPa]
F2	37.2 ± 1.6	8.6 ± 0.5	65.0 ± 12.2	$39.5 \pm 2.3^*$	9.1 ± 0.3	$135.9 \pm 7.2^*$
F3	32.1 ± 3.4	10.4 ± 0.3	144.2 ± 9.5	31.9 ± 5.7	$11.7 \pm 0.5^*$	$197.7 \pm 5.6^*$
F5	35.8 ± 2.4	7.4 ± 0.2	48.6 ± 7.1	$39.5 \pm 1.4^*$	$8.0 \pm 0.2^*$	$88.9 \pm 2.8^*$
F6	22.1 ± 2.9	11.6 ± 0.6	199.7 ± 5.8	19.6 ± 3.9	11.3 ± 0.5	$245.7 \pm 21.9^*$

*significant difference of measured values after production and after six months of storage ($\alpha = 0.05$)

While F_{\max} was slightly higher for formulations containing PEG 1,500, for formulations containing POL no significant effect was observed after the storing period. For three formulations the tensile strength slightly increased within the storing period, but only F3 and F5 demonstrated a significant increase.

In contrast, the E-modulus significantly increased after six months of storage for all four formulations. This was consistent with Oliveira et al. (2013, 2014) analysing the elasticity of lipid based laminar (co-)extrudates and may be explained by the higher degree of crystallinity of the PEGs over time. The higher crystallinity resulted in stronger interactions between the molecules and thus in a loss of elasticity.

As a higher E-modulus represents a less elastic behaviour, which may cause problems when it comes to dosing by the SDP, the increase of the E-modulus has to be especially monitored during formulation development and over storage. In this investigation, the extrudates were still sliceable by the SDP after several months of storage. For an approved medicinal product, specifications for the mechanical properties would be needed and the mechanical properties would have to comply with the given specifications over the whole lifespan of the product.

3.2.2.8. Influence of the Mechanical Properties on the Mass Uniformity

The parameters of the mechanical properties (F_{\max} , tensile strength, and E-modulus) were investigated as indicators for the applicability of the SDP. For this purpose, the standard deviation of the mass of single doses (Table 4) was plotted over the mechanical properties of the extrudates (Table 5) in Figure 35.

For small doses (e.g. 5 DUs), the mass uniformity depended on the tensile strength and the E-modulus of the CBZ-loaded rods. For instance, this may be due to rigid behaviour, which is indicated by a higher E-modulus and which may generate broken edges of the cut doses. Thus, an increase in SD of the mass was observed (Figure 35).

With increasing dose (10 and 15 DUs) the mechanical properties gained proportionately less importance on the SD of the mass of the cut doses (Table 4 and Table 5).

While the SDs of the mass increased with an increase of the tensile strength and the E-modulus in this study, formulations F2 and F5 with the higher F_{\max} values resulted in smaller SDs of the mass. It was then valuable to answer the question, if – against intuition – higher F_{\max} values are to be preferred in the formulation development for the SDP. An answer to this question can be found regarding the force-displacement curves for the formulations determined by the Texture Analyser equipped with the cutting test set-up (Figure 36).

Formulations including POL (F3 and F6) did not show a cut, but a break, represented by a sharp peak and a sudden decline of the recorded force. In contrast, PEG 1,500 modulated the mechanical properties of the CBZ-loaded rods leading to a cut, which is demonstrated by a rather smooth force-displacement curve. Still, a certain part of these formulations was not cut, but broken, which is revealed by the fall in the force-displacement curve at approximately 2.8 mm for the representative profiles. As the CBZ-loaded rods had a diameter of 4 mm, one can presume that 30 % of the height of the extrudates broke instead of being cut. This phenomenon may also be seen in Figure 34 b for formulation F2 (first row). However, due to their circular cross-section the area of this broken cross-section was calculated to be below 20 % of the total area.

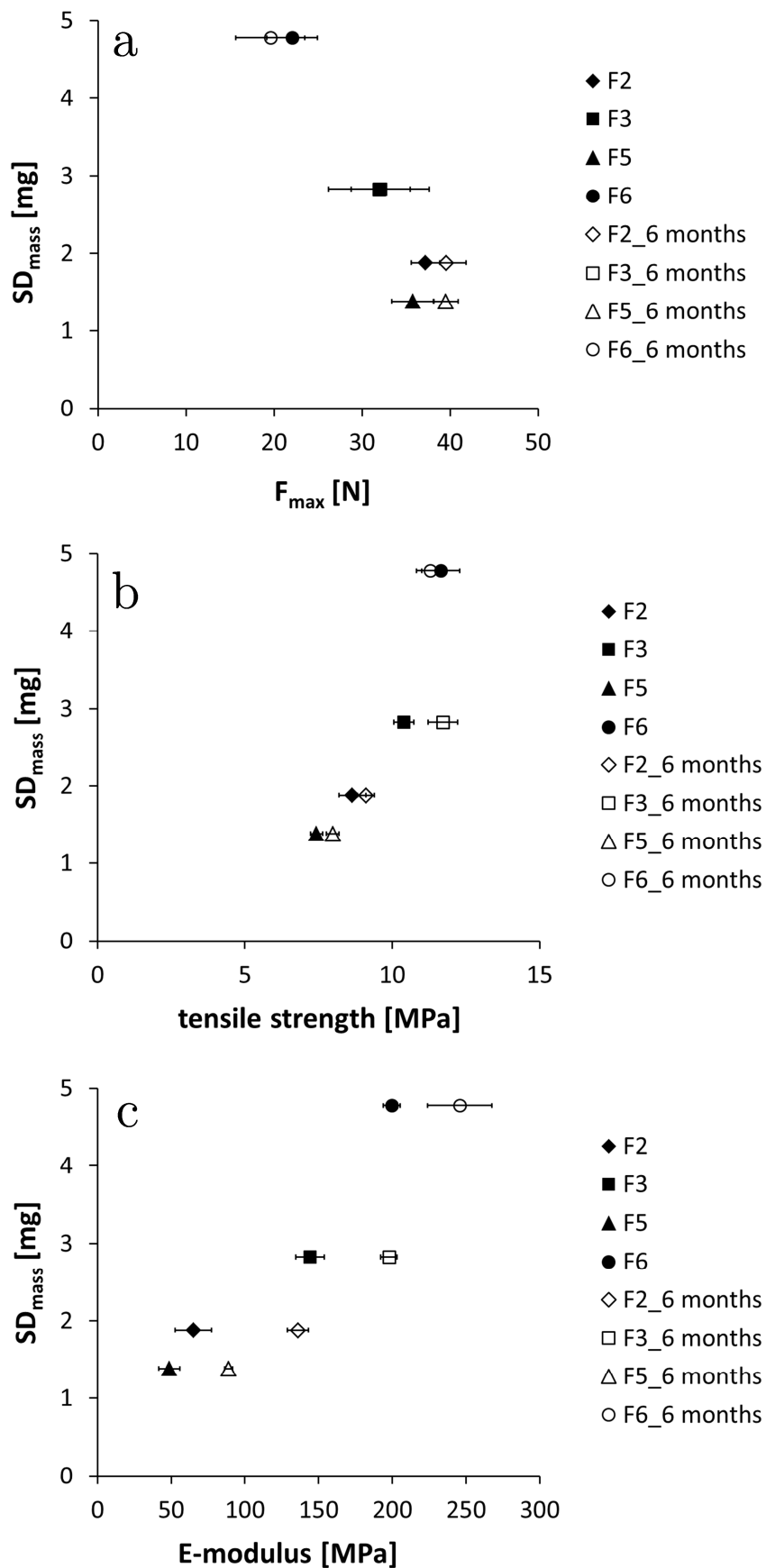


Figure 35: SD of the mass for 5 DUs in relation to (a) F_{max} ($n = 10$, mean \pm SD), (b) tensile strength, and (c) E-modulus (both $n = 5$, mean \pm SD) of formulations F2, F3, F5, and F6 after production and after 6 months of storage at 21.0 ± 0.2 °C and 45 % RH

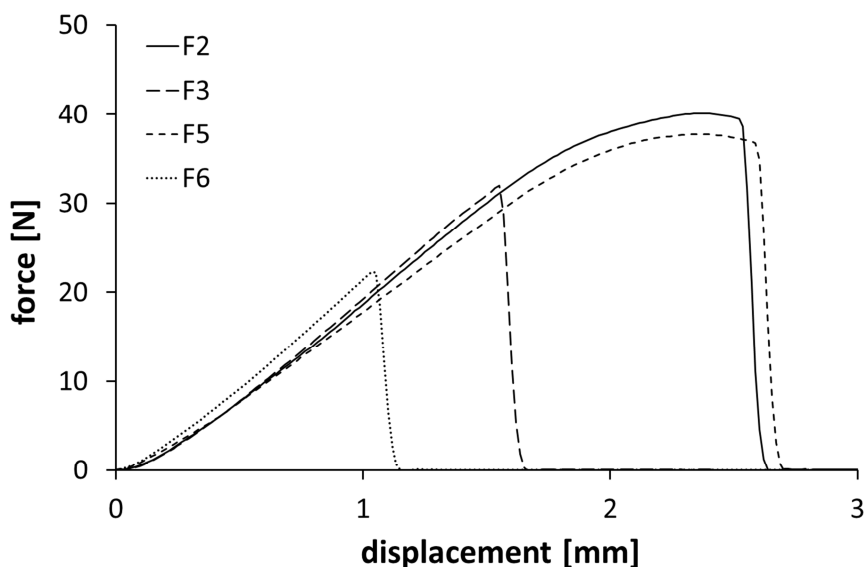


Figure 36: Representative force-displacement curves for the formulations F2, F3, F5 and F6, determined by a Texture Analyser equipped with the cutting test set-up

These findings were in line with the determined E-moduli of the formulations (Table 5), which were much higher for F3 and F6. These higher values of the E-modulus described a more rigid behaviour that caused a break instead of a cut. Thus, the value of F_{\max} may only be indirectly seen as an indicator, but it is advised to regard the cutting behaviour as well. One may assume that for the applicability of the SDP, formulations that tend to be sliced by the device (than rather be broken) are more appropriate.

In conclusion, formulations F2 and F5 with PEG 1,500 as added excipient met the pharmacopoeial requirements (Table 4). They exhibited a tensile strength $\leq 9.1 \pm 0.3$ MPa and an E-modulus $\leq 135.9 \pm 7.2$ MPa (Table 5), which may be useful thresholds for future formulation development for the SDP.

3.2.3. Co-Extrudates

3.2.3.1. Formulation Development

In this part of the thesis sustained release and dual drug release formulations for the use of the SDP were developed via hot-melt co-extrusion. “Dual drug release” as a term has been introduced in literature (Dierickx et al., 2013) and means in this context the superposition of two release kinetics as, for example, immediate and sustained release, resulting in a biphasic dissolution profile. The selection of appropriate core and coat formulations for the co-extrudates was conducted by matching the mechanical properties, the dissolution characteristics, and the process parameters of extrudates.

Extrudate formulations F1 - F7, containing different loads of CBZ (30 %, 45 %, and 50 % w/w), have been described in detail in section 3.2.2. To resume, they showed immediate or sustained release depending on the CBZ-loading and the added excipients. In order to develop a dual drug release co-extrudate (co-ex dual), F1, F2, and F3 were suitable for an immediate release coat (85 % dissolved drug within 45 min). For F7, F5, and F4 after 10 h only 62, 71, and 88 % CBZ were released, revealing a strong retardation in drug release. Nevertheless, these formulations were screened for the core of the co-extrudates, as the change in dimensions may alter the release profiles, which will be discussed in more detail in section 3.2.3.4. Formulation F6 was neither suitable for an immediate release (85 % dissolved drug only within 90 min), nor for a sustained release formulation.

For a wax-coat, additional extrudate formulations were manufactured on a 16 mm twin-screw extruder (section 6.2.1.4). These formulations, F8 - F11, are presented in Table 6. They included white bees wax as hydrophobic matrix and either SA or carnauba wax as consistency builders.

Table 6: Extrudate formulations F8 - F11 for the wax-coat, fraction of the excipients (% w/w), melting temperature (T_m) determined by DSC measurements, and extrusion temperature (T_{extr})

	bees wax	SA	carnauba wax	
T_m [°C]	61 - 66	63.9	80 - 87	
Formulation no.				T_{extr} [°C]
F8	80	-	20	48
F9	70	-	30	50
F10	33	67	-	45
F11	50	50	-	46

Like for F1 - F7, F8 - F11 were manufactured below the melting temperatures of the pure excipients, due to the applied shear forces by the twin-screws in the extruder barrel. The

diameters of formulations F8 - F11 were larger than those of the formulations based on PEG 2,000 (section 3.2.2.1) due to an occurring die-swell. This increase in diameter may be explained by the viscoelastic recovery of the materials (Oliveira et al., 2014) standing in contrast to the rapidly crystallising PEGs, which show less viscoelastic properties (Schilling and McGinity, 2010).

To achieve an appropriate cutting behaviour of the coat and the core within the co-extrudates when the SDP is used for dosing, similar mechanical properties of core- and coat-formulations are essential. The tensile strength and the E-modulus of all manufactured extrudates are presented in Figure 37.

PEG 1,500 (F2 and F5) has already been proved to be the more appropriate added excipient, with regard to smaller values of the E-modulus, smoother cross-sections and more regular edges of the tablet-like slices, and smaller standard deviations in mass of the single doses sliced by the SDP (section 3.2.2).

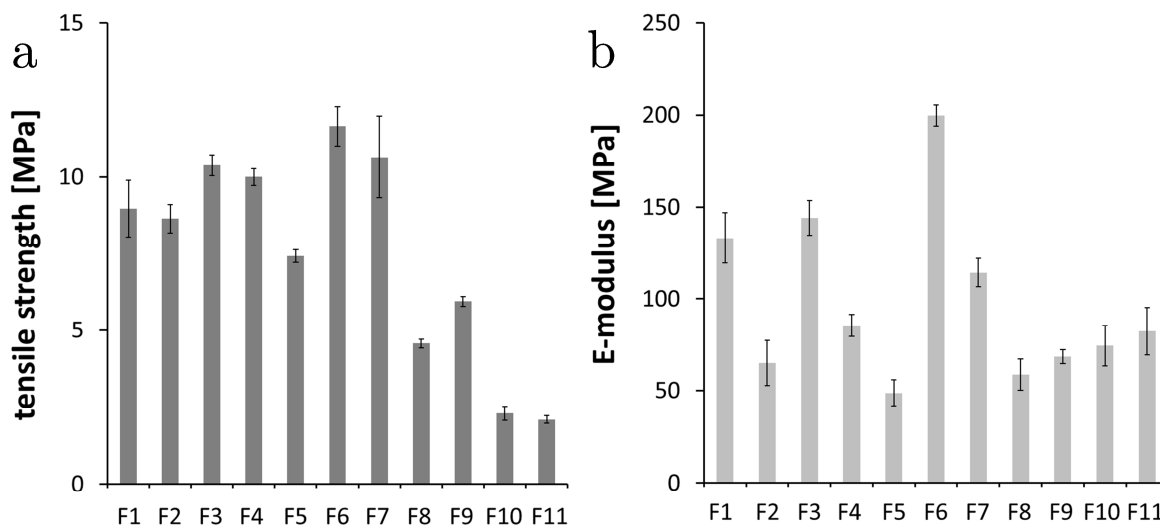


Figure 37: Tensile strength (a) and E-modulus (b) of the extrudates (F1 - F11) determined by a Texture Analyser equipped with a three-point bending rig ($n = 5$, mean \pm SD)

For a dual drug release co-extrudate (co-ex dual), the results of the tensile strength and the E-modulus were compared with the aim of including an immediate release (F1 - F3) and a sustained release formulation (F4, F5, and F7). It was concluded that F2 and F5 show the most similar properties.

The wax mixtures containing SA (F10 and F11) exhibited the lower tensile strengths, whereas carnauba wax acted as a consistency builder for F8 and F9 as anticipated. Carnauba wax raised the tensile strength of the formulation with increasing fraction (5.6 MPa for 20 % (F8) to 5.9 MPa for 30 % (F9)) making it more similar to the PEG-formulations (F1 - F7).

For the wax-coated co-extrudate (co-ex wax) F9 combined the highest investigated tensile strength of all wax mixtures and a low E-modulus. Therefore F9 was most appropriate as wax-coat to match F5 as a sustained release formulation for the core.

In Figure 38 the cutting strength of formulations F1 - F11 is plotted over the so-called optimal barrel temperature (see below).

In this case, normalisation of F_{\max} was required as the diameters of the extrudates varied between 3.9 mm and 4.4 mm. Thus, a normalisation was conducted by dividing through the cross-section of the extrudates (mm^2 , cutting strength [MPa]).

In this context, the optimal barrel temperature ($T_{\text{barrel}}^{\text{optimal}}$, Figure 38) was defined as the process temperature which induced a melt viscosity allowing for the transport of the extrudates on a conveyor belt under stability of shape and simultaneously leading to extrudates with a smooth surface. Therefore, $T_{\text{barrel}}^{\text{optimal}}$ was utilised in this study as an indicator for the matching of the viscosity of coat and core formulations. $T_{\text{barrel}}^{\text{optimal}}$ was identified by changing the temperature of the whole barrel in intervals of 1 °C in a systematic examination (section 3.2.2.1).

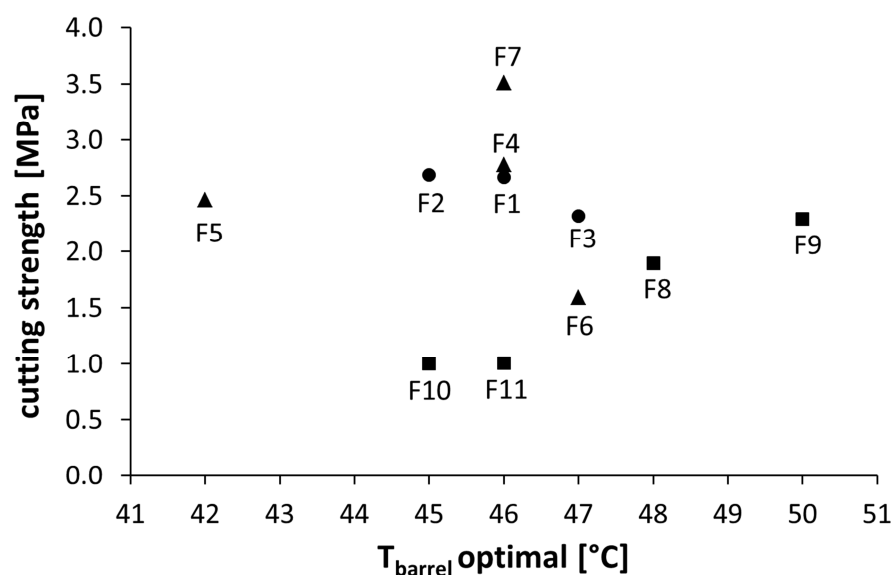


Figure 38: Cutting strength determined by a Texture Analyser equipped with a cutting test set-up ($n = 10$, mean) over the optimal barrel temperature ($T_{\text{barrel}}^{\text{optimal}}$) for the extrudate formulations F1 - F11; ●: immediate release formulations; ▲: sustained release formulations; ■: wax mixtures

Cutting forces for the coat and the core formulations needed to be adapted to each other, too. For instance, if the required cutting force of the core would be higher than the one of the coat, the core would be pressed down within the coat while being cut. This deformation may alter the uniformity of sliced doses.

Formulations containing high percentages of CBZ (e.g. 50 % (w/w) in F7) required the highest cutting forces (more than 3 MPa) and could hardly be cut by hand. Formulations

exhibiting maximum cutting forces below 1.5 MPa (F10 and F11) exhibited deformation while being cut and therefore were not suitable for dosing via the SDP.

For the development of a co-extrudate with dual drug release, two layers providing immediate release (containing 30 % CBZ) and sustained release (containing 45 % CBZ) should be combined. As the CBZ content influenced the mechanical properties of the drug-loaded rods (section 3.1.3.2) they had to be modified. PEG 1,500 (F2 and F5) and POL (F3 and F6) were added and made a modification of the tensile strength and the E-modulus possible (section 3.2.2.2). The cutting strength was not changed by the addition of PEG 1,500, but the addition of POL decreased the cutting strength (Figure 38). In line with the findings for the tensile strength and the E-modulus, formulations F2, F5, and F9 met the requirement of similar cutting forces. Moreover, the cutting of formulations F2 and F5 resulted in very similar force-displacement curves (Figure 36, section 3.2.2.8).

Furthermore, it was desirable to have similar production temperatures for the extrudates for core-coat formulation pairs, as conjoint extrusion of the core and coat formulations through one co-extrusion die shall be feasible.

In this work, formulations with PEG 2,000 were processed at an optimal barrel temperature of 46 °C (Figure 38). Due to the melting temperatures of the pure components, the addition of PEG 1,500 resulted in a lower $T_{\text{barrelOptimal}}$, whereas the addition of POL caused a moderate increase in $T_{\text{barrelOptimal}}$ (Figure 38).

For co-ex dual, $T_{\text{barrelOptimal}}$ of F4, F5, and F7 (sustained release) were compared to those of F1 - F3 (immediate release) and for co-ex wax to those of F8 - F11 (wax mixtures). Formulation pair F2/F5 was assessed to be extrudable through one co-extrusion die as the optimal barrel temperature only differed by 3 °C. Core-coat formulation pair F5/F9 exhibited a difference of roughly 8 °C in $T_{\text{barrelOptimal}}$ (Figure 38). Still, this formulation pair was selected as formulation F9 represented the most suitable mechanical properties of all examined wax mixtures (F8 - F11, Figure 37 and Figure 38). A formulation optimisation of F9 was performed during co-extrusion experiments to reduce the difference in $T_{\text{barrelOptimal}}$ (F9b, Table 7).

3.2.3.2. Hot-Melt Co-Extrusion via Connected Twin-Screw Extruders

Considering the dissolution characteristics (section 3.2.2.4), the mechanical properties and the process temperature (both section 3.2.3.1), core-coat formulation pairs for co-extrusion were chosen (Table 7).

As a core material for both co-extrudates formulation F5 with 45 % CBZ showing sustained release characteristics was selected. The dual release co-extrudate - abbreviated as “co-ex dual” - has an immediate release coat (F2). The second - “co-ex wax” - was produced with a wax-coat (F9b) to restrict drug release to the cross-sections.

Table 7: Process parameters and resulting torque and pressure values of the co-extrusion batches

(co-)extrudate	formulation	feed rate [g/h]	screw speed [rpm]	temperature profile (from die to feeder) [°C]	torque [N*m]	pressure [bar]	
co-ex dual	coat (IR)	F2	400	40	45/42/42/42/45/55/55	11	70
	core (SR)	F5	200	10	45/43/43/43/45/55/50	11	50
co-ex wax	coat (wax)	F9b*	600	60	50/55/60/60/60/60/30	3	20
	core (SR)	F5	200	10	50/43/43/43/45/55/50	3	8

*F9b: 30 % PEG 2,000 (including 0.5 % colloidal silicium dioxide), 49 % white wax, and 21 % carnauba wax

Co-extrusion was performed by two 16 mm twin-screw extruders connected via a co-extrusion die (Figure 73, section 6.2.1.5). During the first experiments, there was an obstruction in the outer die tip. This blocking possibly occurred due to solid residuals of the (semi-)crystalline binder at the given process temperatures and a high drug-load. It was overcome by changing the inner die tip diameter from 3 to 2 mm, consequently increasing the space in the outer die. Thereby, the thickness of the coat layer was increased from 0.5 to 1 mm. Both co-extrudates were then produced with an inner die diameter of 2 mm and an outer die diameter of 4 mm.

Further optimisation was required during co-extrusion of the wax-coated formulation. Adding 30 % PEG 2,000 to the wax-coating (F9, Table 6) made a lowering of the die temperature possible. This way, the die temperature was more similar to the production temperature of the core (F5) allowing for the co-extrusion.

Adhesion between immiscible polymers was reported to be generally weak due to limited interdiffusion (Vynckier et al., 2014b). As the addition of PEG 2,000 caused an increase in hydrophilic properties of the wax-coating, an improvement of layer adhesion was assumed. Due to a poor powder flow of the wax-mixture (F9), 0.5 % colloidal silicium dioxide (F9b) was added to improve the feeding of the wax mixture into the barrel.

For the co-extrusion a low powder feed rate and a slow screw speed were utilised (Table 7) to achieve the possibility of scaling-up with the same loading in the barrel. During the process some pressure fluctuations were observed for the wax-coat. The slow screw speed of the core formulation (10 rpm) may have promoted a pulsatile material flow of the wax coat. This resulted in fluctuations in pressure and also affected the diameter of the core of co-ex wax. The co-extrusion of co-ex dual did not show any pulsatile material flow or pressure fluctuations, which may be due to the fact, that the excipients (PEGs) applied within the core and the coat formulation were more similar in viscosity.

Photographs of the resulting co-extrudates, optical microscopy images, and SEM micrographs are shown in Figure 39. For both co-extrudates straight rods with a smooth surface were generated and only rarely small surface defects were observed. Optical microscopy and SEM were performed to visualise and examine the cross-section of the co-extrudates and the interface between coat and core layer (section 6.2.3.4). Regarding the cross-section of the co-extrudates, the core layer may clearly be distinguished from the coat layer via SEM by its higher brightness (Figure 39). The interface between core and coat was smooth.

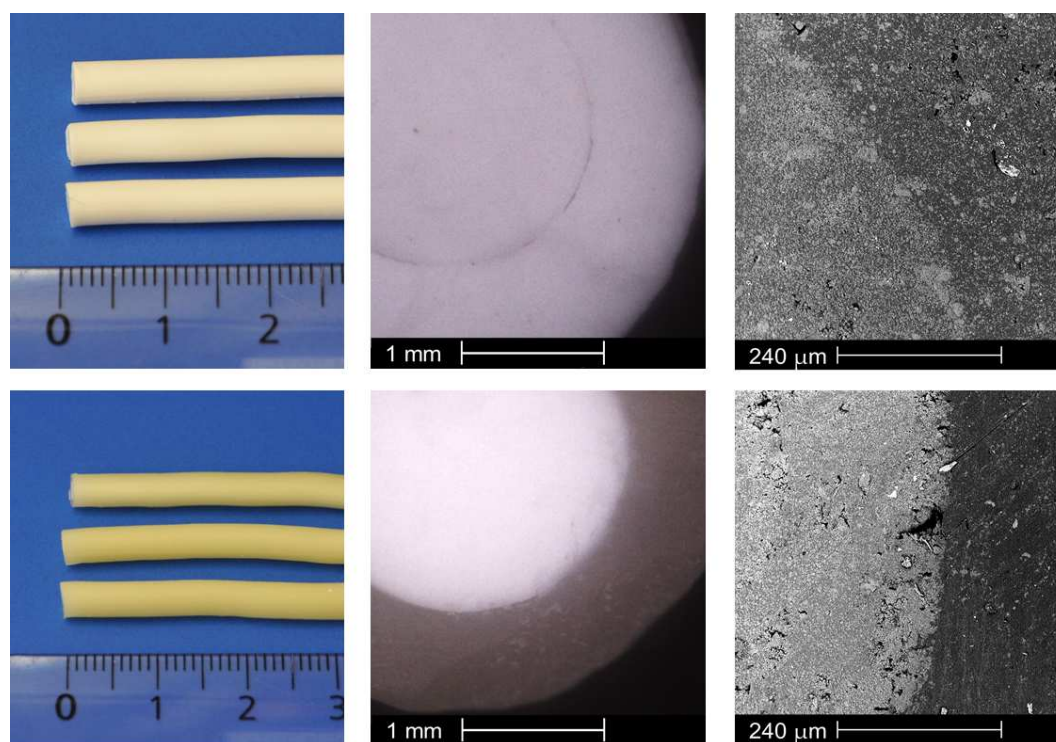


Figure 39: Dual drug release co-extrudates (first row) and wax-coated co-extrudates (second row); left: photograph (displayed scale in cm); middle: optical micrograph; right: SEM micrograph

Recently, the intersection between core and coat of co-extruded mini-matrices has been examined via micro-computer tomography (Vynckier et al., 2014c). The authors demonstrated that only 2.1 % of the total pore volume was located at the interface. This was postulated to be inherent in the co-extrusion die design and the specific formulation.

For the co-extrudates in this study, core and coat seem to be in close contact to each other in microscopic inspection (Figure 39). No air-entrapments or peeling of the coat-layer from the core were observed in any case.

A method to determine the adhesion of co-extrudate layers has been described in literature (Dierickx et al., 2012). The adhesion between core and coat was measured using a tensile tester. This method has been developed for formulations based on amorphous or partly amorphous polymers usually utilised for hot-melt extrusion. But this method did not reveal reproducible results for the presented co-extrudates made from comparatively

soft and waxy excipients. Therefore, in this study, layer adhesion was investigated further by testing the appropriateness of the formulations to be administered by the SDP (section 3.2.3.6).

As PEGs rapidly recrystallise at ambient conditions, the co-extrudates made from PEGs exclusively, showed no die swell as discussed above (diameter 4 mm). In contrast, a die swell was observed for the wax-coated co-extrudates (diameter 4.5 mm). This increase of the diameter of the co-extrudates was consistent with the results gained from the extrudates (section 3.2.3.1). An increase in thickness of about 50 % was described for lipid mono-, di-, and tri-layer extrudates as well (Oliveira et al., 2014). As discussed above, this die-swell may be explained by the elastic recovery of the wax-matrix. As the cross-section represents 9.4 mm² for the coat and 3.1 mm² for the core, a difference in the volume flow (g/h) by a factor of 3 was assumed to be appropriate. Nevertheless, within the co-extrusion process for co-ex dual a material flow of 400 and 200 g/h seemed to be more suitable, but finally resulted in a core diameter of approximately 2.5 mm and a coat layer thickness of approximately 0.75 mm.

3.2.3.3. Mechanical Properties

The mechanical properties of the co-extrudates were examined and compared to those of the extrudates (Figure 40).

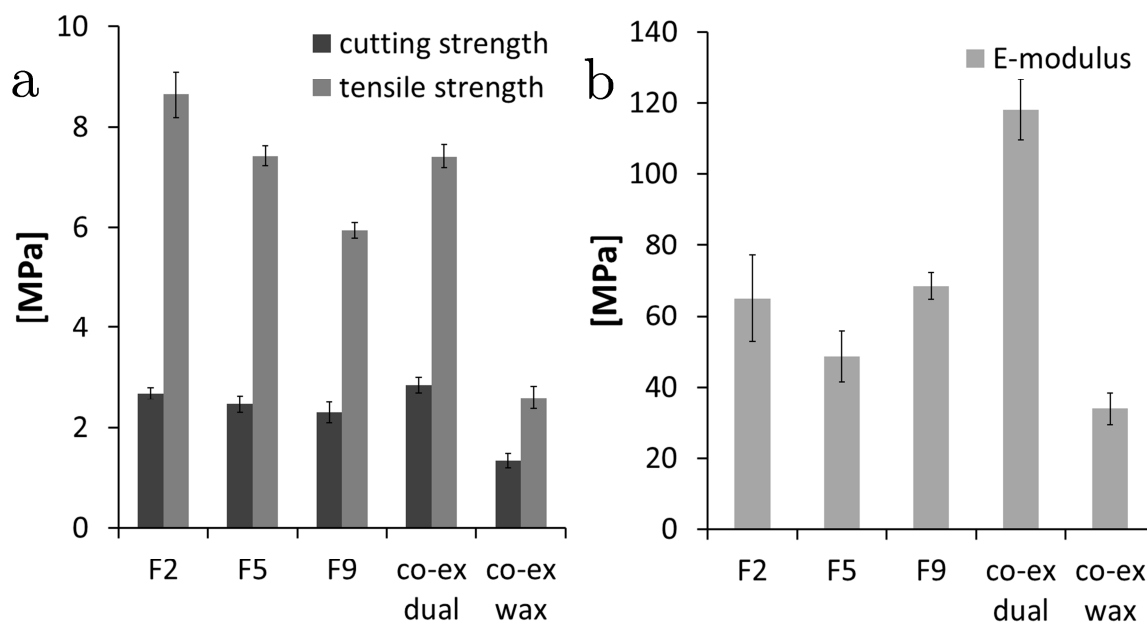


Figure 40: Cutting strength and tensile strength (a), and E-modulus of the co-extrudates in comparison to the extrudate formulations F2, F5, and F9; cutting strength determined by a Texture Analyser equipped with the cutting test set-up ($n = 10$, mean \pm SD), tensile strength and E-modulus determined by a three-point bending test ($n = 5$, mean \pm SD)

Using the Texture Analyser equipped with the cutting test set-up (section 6.2.3.1) cutting was feasible with a cutting strength of 2.9 ± 0.2 MPa for co-ex dual and 1.3 ± 0.1 MPa for co-ex wax. The tensile strength of the co-extrudates was determined as 7.4 ± 0.3 MPa for the dual drug release and 2.6 ± 0.2 MPa for the wax-coated formulation.

While co-ex dual showed values in the range of the two individual compositions which the co-extrudate consists of, cutting strength and the tensile strength of co-ex wax were considerably lower than the values of both F5 and F9. At the same time, 30 % PEG 2,000 was included in the wax-coating of the co-extrudate (F9b, Table 7). This may reduce the cutting strength and the tensile strength, as both were smaller for pure PEG 2,000 than for other PEG-formulations with CBZ (section 3.1.3.2).

The E-modulus constituted 118.1 ± 8.4 MPa for co-ex dual and was hence much higher than for formulations F2 and F5 (65.0 ± 12.2 MPa and 48.6 ± 7.1 MPa). For co-ex wax the E-modulus (33.9 ± 4.5 MPa) was found to be much lower than for F9 (68.5 ± 3.7 MPa, Figure 40).

3.2.3.4. Dissolution Studies

Dual Drug Release from Co-Extrudates

To investigate the liberation of the model drug, the co-extrudates were subject to dissolution testing (section 6.2.3.7).

The co-extruded dual drug release formulation contained 34.4 % CBZ in total and a biphasic drug release was obtained (Figure 41). As the coat formulation F2 contained 30 % CBZ (feed rate of 400 g/h) and the core formulation F5 45 % CBZ (feed rate of 200 g/h), approximately 57 % of the total CBZ dose was located in the immediate release coat and approximately 43 % was located in the sustained release core.

The fast releasing coat of the co-extrudate showed 85 % drug release within 30 to 45 min, meeting the USP requirements for immediate release formulations (USP 38 <1092>). The CBZ located within the core dissolved over several hours resulting in a sustained drug release.

Although only 71 % CBZ was released from the extrudate (F5) within 10 h, the CBZ release from co-ex dual was 95 % within 10 h (Figure 41). This may be due to the different dimensions of the sustained release layer, as the extrudate had a larger diameter (4 mm) than the core of the co-extrudate (2 mm). After erosion of the immediate release coat the core of co-ex dual had regarding to the CBZ content a larger surface than the extrudate (F5). This larger specific surface resulted in shorter diffusion ways and in a faster dissolution. These findings also explain, why the observed experimental dissolution of co-ex dual showed faster release characteristics for the second (sustained release) phase than the theoretical dissolution curve (Figure 41).

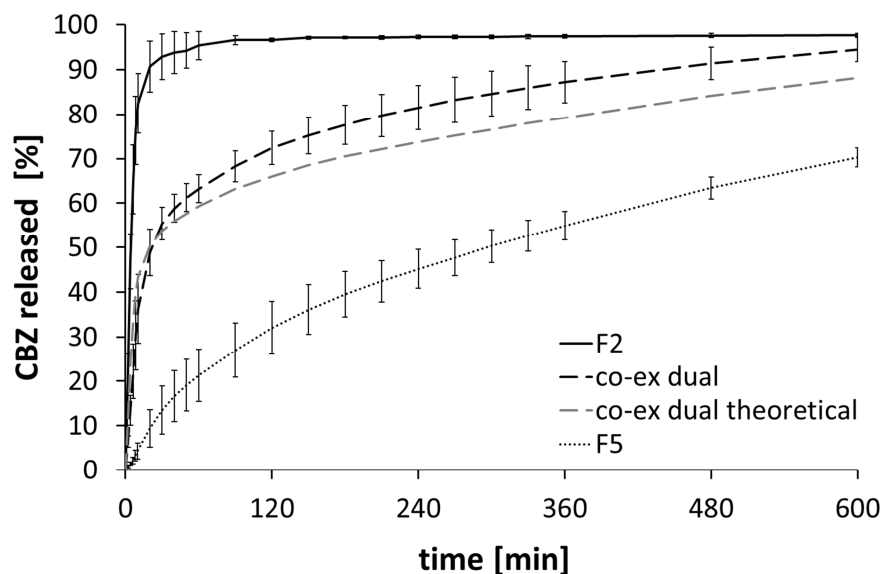


Figure 41: CBZ release of co-ex dual in comparison to the immediate release and sustained release extrudates (F2 and F5) and the theoretical CBZ dissolution of co-ex dual, all investigated extrudate pieces had the same geometry, 40 mg formulation per vessel corresponding to 12 - 18 mg CBZ; apparatus 1, 75 rpm in 900 mL of degassed, demineralised water at 37.0 ± 0.5 °C ($n = 6$; mean \pm CI; $\alpha = 0.05$)

Manufacturing of Wax-Coated Extrudates with a Larger Core-Diameter

Due to the design of the co-extrusion die and the selected formulations, only co-extrudates with an inner die diameter of 2 mm and an outer die diameter of 4 mm could be manufactured (section 3.2.3.2). To investigate, to which extent a larger diameter may change the dissolution rate, cut pieces of the sustained release extrudates (F5) were coated by immersion at 75 °C on a water bath as proposed by Reitz et al. (2008) and as described in section 6.2.1.6. The extrudate-pieces were immersed twice into a molten mixture with the same composition as used for co-ex wax (F9b, Table 7). Figure 42 illustrates the immersed formulation with a wax-coat thickness of 0.6 - 0.8 mm and a total diameter of 4.8 - 5.0 mm.

While being dipped into the hot wax-mixture the core was partially melting on the surface. The molten material of the core provided a close contact between core and coat. The interface was less smooth than after the co-extrusion process (Figure 39). In the cooled formulation some small air bubbles were visible in the outer part of the core, showing the migration of core material (Figure 42 c). Accordingly, the diameter of the core was reduced of approximately 0.2 mm.

During co-extrusion, hydrophilic PEG 2,000 was dispersed in the lipophilic carnauba- and bees wax due to the mixing by shear strain in the barrel. Therefore, the wax-coating of the co-ex wax formulation appeared homogeneous (Figure 39). As there was no mixing during the immersion process, the molten, low viscous PEG was only coarsely dispersed and PEG droplets could clearly be distinguished under SEM investigation by their higher brightness as compared to the wax, which showed lower brightness (Figure 42 c).

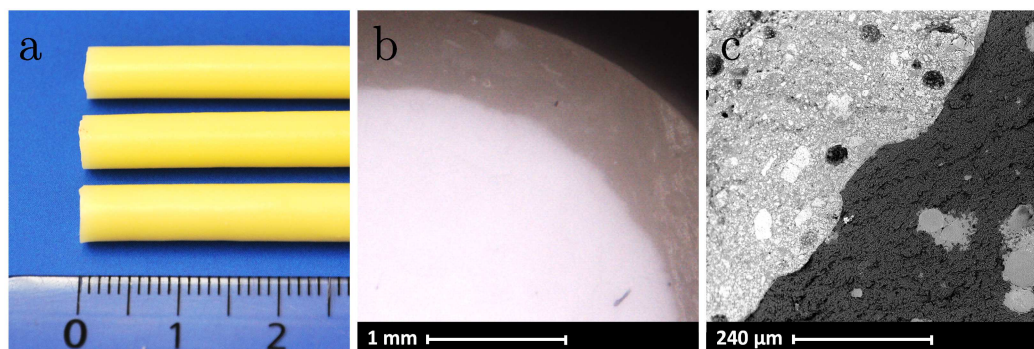


Figure 42: Wax-coated extrudate (F5, wax-coated by immersion into a molten wax-mixture); photograph, displayed scale in cm (a), optical microscopy image (b), and SEM micrograph (c)

The CBZ content within co-ex wax was 15.1 % in total (cores cross-section of $2 \times 3.1 \text{ mm}^2$) and the extrudate obtained by the immersion technique contained 28.5 % of CBZ (cores cross-section of $2 \times 13.9 \text{ mm}^2$). The manually wax-coated extrudates will be abbreviated as “ex wax” in the following paragraphs.

Sustained Drug Release from Wax-Coated Formulations

The extrudates with sustained release (F5), co-ex wax, and ex wax were investigated with regard to the CBZ release. A detailed examination of the release mechanisms was conducted (Table 8). Therefore different lengths of the extrudate pieces, meaning different masses of the formulations, were sliced manually with a surgery knife and submitted to dissolution testing (section 6.2.3.7). Due to the different drug-loadings in the formulations, different lengths were chosen for single, double, and triple doses (F5: 1, 2, and 3 mm; ex wax: 2, 4, and 6 mm; co-ex wax: 3, 6, and 9 mm).

While formulation F5 completely eroded during dissolution, the extrudate bodies of ex wax and co-ex wax still remained after 16 h of dissolution (Figure 43). Inside these wax cylinders approximately 50 % of the original volume of the CBZ formulation still remained.



Figure 43: Doses of the wax-coated extrudates by immersion (first row) and the wax-coated co-extrudates (second row) after dissolution of 16 h in 900 mL of degassed, demineralised water at $37.0 \pm 0.5 \text{ }^\circ\text{C}$, displayed scale in cm

Results of the dissolution testing are depicted in Figure 44 as absolute CBZ release (a), relative CBZ release (b), and CBZ release per surface area (c) over time.

Drug release from formulation F5 depended on the dose, whereas for co-ex wax and ex wax almost identical dissolution profiles independent of the investigated dose were observed (Figure 44 a). The higher core diameter of ex wax compared to co-ex wax led to a higher absolute drug dissolution rate. This means that by variation of the core-diameter tailored dissolution rates have been designed.

As may be seen from Figure 44 b, for all three formulations, higher masses resulted in lower dissolution rates. This may be explained by the different specific surfaces (see below) and was in line with results from other workgroups (Quintavalle et al., 2008; Quintavalle et al., 2007).

But the wax-coated formulations exhibited different dissolution profiles compared to the extrudates F5 due to the constant release-surfaces and thus the different release mechanisms: F5 released CBZ in all three dimensions over all surfaces, including the coat region. The extrudate surface was constantly decreasing during dissolution: This stands for an eroding mechanism, which may be represented by a cube root model. As can be seen in Table 8, the dissolution curves of F5 showed a good correlation with the cube root model (R^2 of 0.993, 0.972, and 0.957 for single, double, and triple dose). In literature a similar dosage form made from 40 % CBZ and 60 % PEG 4,000 was stated to correspond to a cube root release (Perissutti et al., 2002). Nevertheless, the square root model represented the CBZ release well, too - probably because different mechanisms emerged simultaneously within the process of dissolution.

In the case of the wax-coated (co-)extrudates dissolution of the coat region was completely inhibited by the wax coating, as the layer of coating neither was dissolved nor did the drug diffuse through the thick coating layer during dissolution. The coating allowed the model drug only to be liberated in one dimension via the cross-sections. Therefore, the magnitude of the surface for the wax-coated (co-)extrudates remained constant over several hours. After a burst at the beginning of the dissolution process, a constant mass of CBZ was released after 3 h (R^2 for zero order kinetics: 0.999, 0.996, and 0.992 for co-ex wax and 0.999, 0.999, and 1.000 for ex wax).

It may also be demonstrated by plotting the CBZ release per surface area over time that the wax-coating inhibited the dissolution from the coat region of co-ex wax and ex wax (Figure 44 c). After the burst at the beginning of the dissolution, the CBZ release resulted in linear release profiles with predominantly overlapping confidence intervals and with similar slopes (0.22 to 0.31 g/(m² * min)). These slopes were found in between the intrinsic dissolution rates of CBZ and CBZ DH (0.38 and 0.17 g/(m² * min), respectively), which were determined by Murphy et al. (2002).

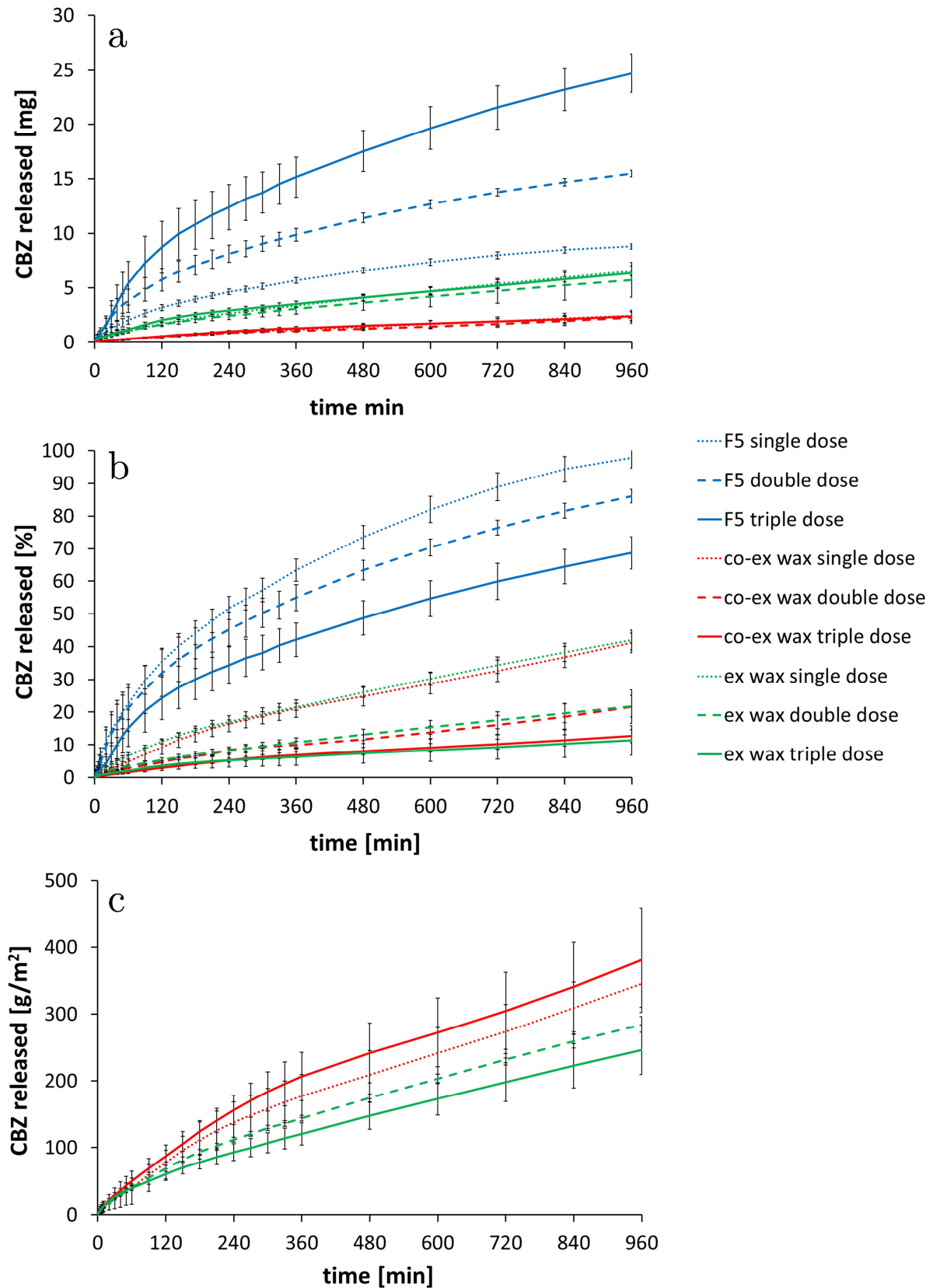


Figure 44: CBZ release of doses of different lengths of the formulations; absolute CBZ release (a), relative CBZ release (b), and absolute CBZ release per surface area (c); apparatus 1, 75 rpm in 900 mL of degassed, demineralised water at $37 \pm 0.5 \text{ }^\circ\text{C}$ ($n = 6$; mean \pm CI; $\alpha = 0.05$)

Table 8: Determination coefficients (R^2) of release mechanisms for the extrudate F5, co-ex wax, and ex wax depending on the extrudates length

extrudates length [mm]	F5			co-ex wax			ex wax		
	1	2	3	2	4	6	3	6	9
R^2 zero order (starting from 3 h)	-	-	-	0.999	0.996	0.992	0.999	0.999	1.000
R^2 square root	0.997	0.996	0.996	0.981	0.968	0.990	0.993	0.986	0.997
R^2 cube root	0.993	0.972	0.957	0.992	0.993	0.966	0.981	0.983	0.944
R^2 Korsmeyer-Peppas	0.994	0.973	0.982	0.998	0.998	0.998	0.998	0.999	0.995
n Korsmeyer-Peppas	0.690	0.810	0.777	0.746	0.745	0.744	0.708	0.643	0.578

Within the core of (co-)ex wax the included PEG 2,000 dissolves quickly, leaving the drug entrapped in the inherent wax-coat, which is to some extent visible in Figure 43. Therefore, a biphasic drug release profile was obtained (Cheng et al., 2010): The first part (up to approximately 180 min) was dominated by the drug release from the formulation through the pores formed by the dissolved PEG and the second - slower - part was based on the dissolution rate of CBZ DH.

The sustained release formulations of Wening et al. (2011) showed dissolution behaviour without a burst effect, but with a dose-dependency. The dose-dependency of the dissolution characteristics could be improved by the wax-coated (co-)extrudate formulations in this work. Still, the release rate of the wax-coated formulations (40 % CBZ in 16 h) was too low.

3.2.3.5. Solid State Properties

In order to confirm the results described above, the core of the wax-coated extrudate was investigated after dissolution by SEM (Figure 45) and XRPD (Figure 46). As a reference, CBZ DH was prepared from CBZ (section 6.2.1.1) and examined as well.

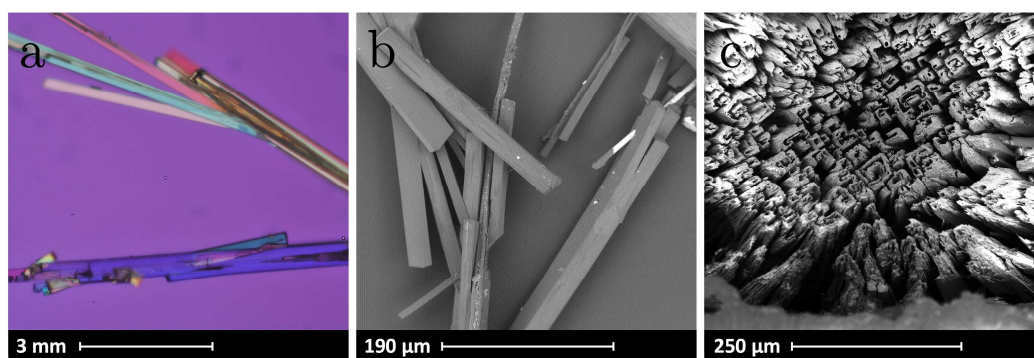


Figure 45: CBZ DH; optical microscopy image (a), SEM micrographs of the sole substance (b) and within the core of the wax-coated extrudate after dissolution for 16 h (c)

Figure 45 a and b present micrographs of CBZ DH crystals. Already in 1984 the growth of CBZ DH in aqueous condition was investigated via SEM (Laine et al., 1984): First, CBZ DH crystallises in whiskers that change to larger rigid crystals over time. These have the shape of platelets with a rectangular cross-section and a cavity inside. In Figure 45 a and b the needle shaped crystals of CBZ DH may be seen, whereas the wax-coated formulation comprised the more ridged crystals with distinct cavities (Figure 45 c).

Diffractograms of CBZ I, CBZ III, PEG 2,000, and CBZ DH as well as of the extrudates F2 and F5, co-extrudates co-ex dual, and the core of co-ex wax are depicted in Figure 46. CBZ DH showed characteristic reflections which were in agreement with literature data (Kobayashi et al., 2000; Tian et al., 2007) and may clearly be distinguished from CBZ I and CBZ III.

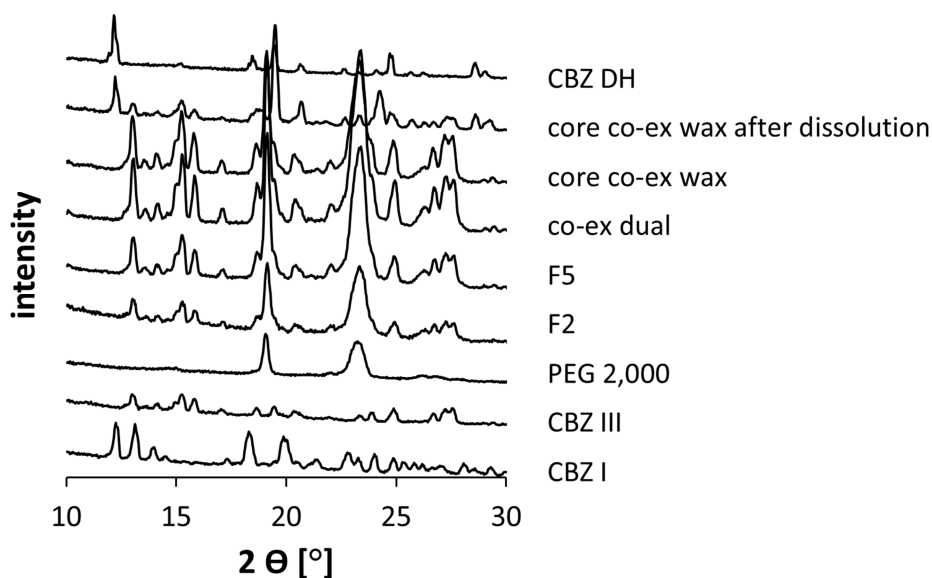


Figure 46: Diffractograms of pure substances (CBZ I, CBZ III, PEG 2,000, and CBZ DH), extrudates (F2 and F5), and co-extrudates (co-ex dual, core co-ex wax, and core co-ex wax after dissolution) depicted from 10 to 30° 2 Θ ; diffractograms of the excipients were normalised to the peak intensities within the formulations

As characteristic peaks of CBZ III, but not of CBZ I, may be found in all formulations after production, the diffractograms prove that only the required modification CBZ III was contained in F2, F5, and the co-extrudates. After dissolution, CBZ DH was detected within the core of co-ex wax as characteristic peaks of CBZ DH were identified at 12.2, 19.5, 20.7, 24.3, and 28.6° 2 Θ . Due to the reflections at 15.2 and 15.8° 2 Θ one may assume that CBZ III is still partly present, too.

3.2.3.6. Application of the Solid Dosage Pen

The co-extrudates exhibited mechanical properties allowing for practical handling and implementation of the SDP. Exemplarily, sections with lengths of 2, 4, and 6 mm (corresponding to 5, 10, and 15 DUs) were cut with the newly designed prototype of the device (section 3.2.2.5, Figure 33) to imitate the individual dosing. In no case coat and core were separated during the cutting process with the device. Thus, appropriate interfacial adhesion of the two layers and the suitability of the cutting blade and cutting mechanism of the SDP were proved.

The adhesion between core and coat was found to be mainly controlled by the extrusion temperature and the drug-loading (Dierickx et al., 2013). Adhesion forces increased with increasing drug-load (0, 30, and 50 % drug in crystalline form) due to a rougher surface of coat and core. The co-extrudates in this work contained CBZ with a relatively high loading (30 % and 45 %) and XRPD measurements revealed the presence of crystalline CBZ III within the co-extrudates (section 3.2.3.5, Figure 46). The crystallinity of CBZ III within the layers was supported by the determination of the CBZ III equilibrium solubility in PEG 2,000 (section 6.2.3.12), which was determined to be 8.1 ± 0.7 % (w/w) after 136 h. Moreover, within the extrusion process in all probability less drug will be solubilised than determined for the equilibrium solubility as the residence time of 3.5 to 4 min did not allow to reach the equilibrium solubility. Therefore, one can assume that more than 22 and 37 percentage points of CBZ will be in the crystalline state in modification III.

All in all, the layer adhesion was appropriate to the anticipated application, as the two layers adhered to one another when cut by the device. Even for the wax-coated co-extrudate, the adhesion forces between the rather hydrophilic core and hydrophobic coat could be sliced, which may be due to the inclusion of the hydrophilic PEG 2,000 into the wax-coat.

3.2.3.7. Uniformity of Dosage Units

Mass and content of doses with 5, 10, and 15 DUs were determined for co-ex wax and co-ex dual (sections 6.2.4.2 and 6.2.4.3) and are depicted in Table 9. Additionally, acceptance values (AV) were calculated with regard to Ph. Eur. 2.9.40 for co-ex dual (section 6.2.4.4, Table 9). As the determination of an AV needs a label claim, in this work AV were exemplarily calculated based on a label claim of 10, 20, and 30 mg CBZ.

The appropriateness of the SDP as a dosing device and the co-extrudates regarding their mechanical properties were demonstrated by small standard deviations (SDs) of the masses of cut slices for both co-extrudates (1.0 - 2.1 mg).

The content of co-ex dual was 97.9 to 102.8 % and showed SDs between 2.0 and 5.5 %, which represented a homogeneous distribution of CBZ in the formulations (Table 9). The SDs, decreasing with an increase in mass of the dose, were comparable to those of the extrudate formulations F2 and F5 (SD: 2.2 to 6.2 %, Table 4).

Table 9: Mass, content, and acceptance values based on label claims (AV, according to Ph. Eur. 2.9.40) for doses with 5, 10, and 15 DUs (corresponding to lengths of 2, 4, and 6 mm) of co-ex dual cut with the SDP (n = 10, mean \pm SD)

DUs	mass [mg]	content [%]	AV (label claim [mg])
5	29.4 \pm 1.6	99.6 \pm 5.5	15.1 (10)
10	61.1 \pm 1.6	97.9 \pm 2.7	10.5 (20)
15	88.7 \pm 1.5	102.8 \pm 2.0	10.4 (30)

In contrast, for co-ex wax the content varied: Exemplarily, for 10 DUs the content was analysed to be 86.6 \pm 13.3 % (n = 10) in one section of the co-extrudate and 114.6 \pm 12.3 % in another section. These deviations may be due to (A) a migration of the lipophilic CBZ molecule into the wax-coating, (B) the small CBZ dose in general, (C) incomplete mixing of the core material or (D) interfacial instabilities between the core and the coat-layer.

A. A migration of the CBZ molecule into the wax-coating was not likely for two reasons:

First, after extrusion, both core and coat recrystallised rapidly and the crystalline state of the drug was verified via XRPD measurements (Figure 46) and via distinction of the equilibrium solubility of CBZ in PEG as discussed above. In systems, in which all components are crystalline, diffusion coefficients are low.

Second, a partition coefficient of CBZ between the hydrophilic phase (PEGs) and the lipophilic phase (wax-mixture) was determined in the molten state of the excipients at 80 °C (section 6.2.3.12). Being stirred for 8 h, 89.5 % CBZ remained in the hydrophilic phase, which means in reverse that only 10.5 % CBZ had migrated into the lipophilic phase under these “accelerated” conditions. A reference without the molten wax-mixture constituted a CBZ content of 99.4 %.

B. The wax-coated co-extrudates had approximately only one third of the dose in comparison to the extrudate and co-ex dual and for small doses it is more challenging to achieve content uniformity.

C. Incomplete mixing of the core material was very unlikely, as the same bulk material was utilised as for the core of co-ex dual and for this co-extrudate no deviations occurred.

D. Interfacial instabilities - in terms of layer non-uniformity of the core - may be a result of pressure fluctuations (Vynckier et al., 2014b), which were observed during the process of this formulation. Other reasons mentioned for a layer non-uniformity are a mismatch of the melt temperature or a velocity mismatch (Vynckier et al., 2014b). Moreover, for double-layer drug delivery devices prepared by co-injection moulding the viscosity ratio between the core and coat layer played an important role in the formation of the interfacial shape, namely the coat thickness and layer uniformity (Vaz et al., 2003).

In this study, the barrel temperature of the coat (55 to 60 °C) and the core (43 to 55 °C) as well as the screw speed of the coat (60 rpm) and the core (10 pm) differed. The divergence of the barrel temperatures was the best compromise when choosing core and coat formulation pairs with the same mechanical properties for co-extrusion. But due to these differences, the wax-coated co-extrudates did not seem to provide appropriate content uniformity.

In contrast, for co-ex dual the uniformity of dosage units (Ph. Eur. 2.9.40) was found to be in accordance with the pharmacopoeial specifications for doses of 10 and 15 DUs and the determined AVs were comparable to those of the extrudates F2 and F5 (Table 4). The smallest investigated dose of co-ex dual (5 DU) resulted in an AV of 15.1 and therefore did not meet the requirements.

3.2.3.8. Stability Studies

To examine the mechanical properties over storing, stability testing was performed for co-ex dual and co-ex wax as described for the extrudates in section 3.2.2.7 (Table 10).

In line with the extrudates made from PEG exclusively, there was a tendency of F_{\max} to increase slightly during the six months of storage at 21.0 ± 0.2 °C and 45 % RH, but no significant effect was observed over the storing period. The tensile strength, however, showed a significant increase within the storing period. According to the results of the extrudates containing PEG 2,000, the E-modulus significantly increased for co-ex dual, whereas the increase for co-ex wax was not statistically significant. These findings are probably due to the recrystallisation of PEGs over the storing period leading to a more rigid behaviour. The recrystallisation of the wax-mixture was in contrast maybe already nearly completed before storing.

Table 10: Maximum cutting force (F_{\max} , $n = 10$), tensile strength, and E-modulus (both $n = 5$) after production and after six months of storage for the co-extrudates; mean \pm SD

formulation	after production			after 6 months of storage		
	F_{\max} [N]	tensile strength [MPa]	E-modulus [MPa]	F_{\max} [N]	tensile strength [MPa]	E-modulus [MPa]
co-ex dual	35.8 ± 2.0	7.4 ± 0.3	118.1 ± 8.4	39.4 ± 6.4	$9.9 \pm 0.4^*$	$170.0 \pm 7.0^*$
co-ex wax	26.4 ± 2.8	2.6 ± 0.2	33.9 ± 4.5	28.7 ± 2.3	$3.1 \pm 0.4^*$	45.3 ± 10.5

*significant difference of measured values after production and after six months of storage ($\alpha = 0.05$)

In the context of this investigation, the increase of tensile strength and E-modulus were acceptable, as the co-extrudates were still sliceable by the SDP. As discussed in detail in section 3.2.2.7, for an approved medicinal product, specifications for the mechanical properties would be needed and the mechanical properties would have to comply with the given specifications over the whole lifespan of the product.

To examine whether the dissolution behaviour varies over storage, dissolution testing was repeated for the co-extrudates and extrudate formulations F2, F3, F5, and F6 after storage (Figure 47).

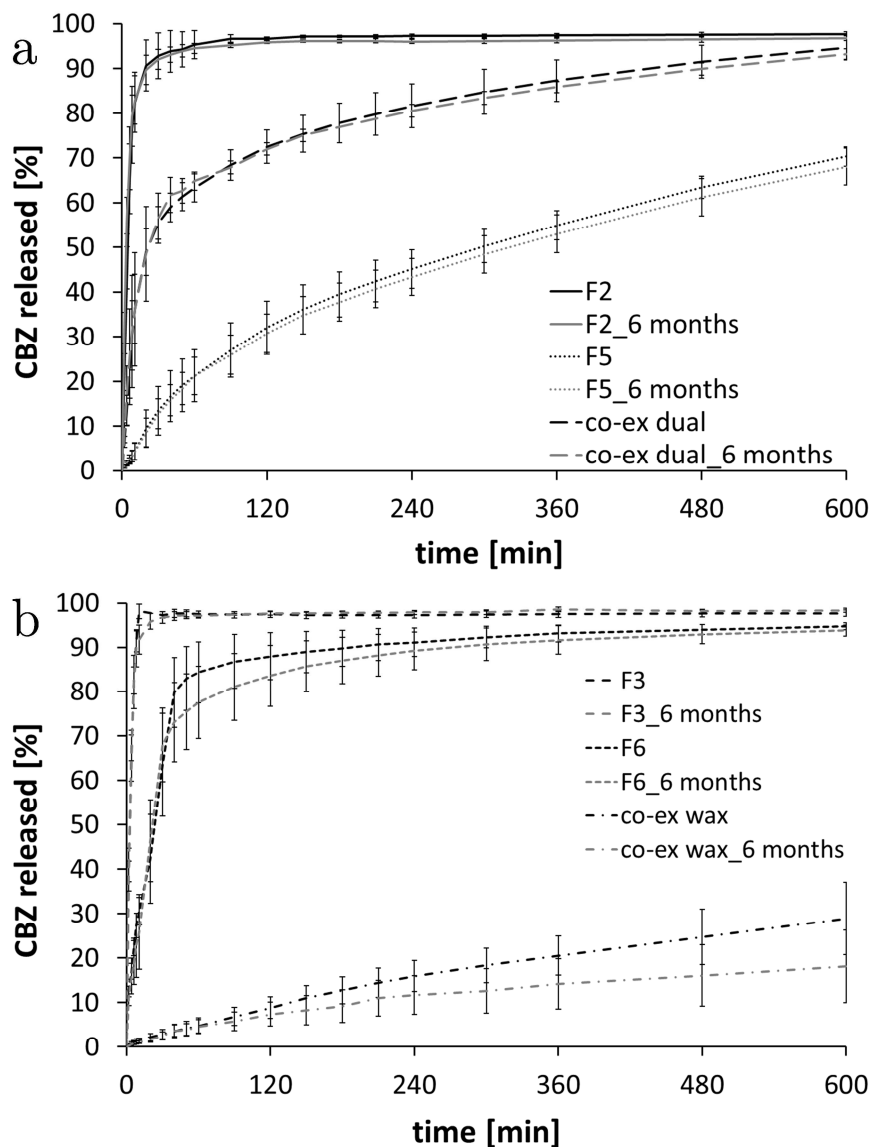


Figure 47: CBZ release of the extrudates and the co-extrudates after production (black lines) and after 6 months of storage at 21.0 ± 0.2 °C and 45 % RH (grey lines), formulation F2, F5, and co-ex dual (a), formulation F3, F6, and co-ex wax (b); apparatus 1, 75 rpm in 900 mL of degassed, demineralised water at 37.0 ± 0.5 °C ($n = 6$; mean \pm CI; $\alpha = 0.05$)

Figure 47 a reveals that for F2, F5, and co-ex dual no influence of storage on the CBZ release was observed after six months as the release profiles remained similar at the given storage conditions. As depicted in Figure 47 b, for F3, F6, and co-ex wax a tendency of decrease in dissolution rate was observed, but these results were not significant, as the confidence intervals of the respective profiles before and after storage overlapped ($\alpha = 0.05$). This tendency of decrease in dissolution rate was rated acceptable, as the samples were moreover openly stored.

In contrast, for an approved medicinal product specifications for the dissolution characteristics over storage would have to be defined and stability testing would be conducted in a primary package for the assessment of the lifespan. For this purpose, airtight sealed aluminium packages could serve as primary packaging, for instance. Open storage could be performed for determination of the in-use stability (e.g. several weeks).

3.2.4. Summary

Extrudates for the implementation of the SDP were developed, manufactured, and characterised on the basis of the experiences of the preliminary studies in the small-scale. Matching the dissolution behaviour, adjusting the mechanical properties, and approaching the process parameters of these extrudates represented a successful strategy for the selection of appropriate coat and core formulations for the co-extrudates.

The increase of the diameter of the prepared drug-loaded rods to 4 mm, and thus, their higher F_{\max} required a new design of the device. Due to their mechanical properties, all drug-loaded rods were sliceable by the newly designed device. For the extrudates, the exerted influence of their mechanical properties on cutting into tablet-like slices with the SDP was examined. The optical appearance of the sliced doses was improved by PEG 1,500 as added excipient and as no hard edges or splinters occurred, a safe swallowing was assumed which must later be investigated in clinical studies. The required cutting forces of extrudates were compared to literature data of the manual forces of different age groups, resulting in appropriateness even for the elderly and for school children, in patient-centred treatment, for instance. The evaluation of the mechanical properties showed that the tensile strength and the E-modulus were valuable indicators for the applicability of the SDP and thresholds for future formulation development were determined. Moreover, formulations which exhibited a cut were found to be more suitable for the utilisation of the SDP than those exhibiting a break. PEG 1,500 was demonstrated to be the more appropriate added excipient in comparison to POL, due to the better optical appearance and the smaller standard deviations in mass of the single doses sliced by the SDP. Due to a sufficient layer adhesion of core and coat and adequate mechanical properties even the co-extrudates were suitable for the application of the SDP.

By the utilisation of different excipients and drug-loadings tailored dissolution kinetics were achieved with immediate-, dual-, and sustained release characteristics. Dose dependent dissolution behaviour of sustained release formulations was minimised by applying a wax-coat. Extrudates exhibiting sustained release characteristics showed cube root kinetics, whereas wax-coated formulations followed a zero order release mechanism. The dissolution profiles of the extrudates and co-extrudates did not alter after a storing period of six months at ambient temperature and 45 % RH.

Solid state analysis revealed the presence of crystalline CBZ in the required modification III within the crystalline carrier in all formulations.

Differences of the process parameters between the core- and the coat-layer resulted in unsatisfying content uniformities for co-ex wax. In contrast, the pharmacopoeial requirements for content uniformity were met by extrudates containing PEG 1,500 as well as by the dual drug release co-extrudates.

3.3. Micropellet-Loaded Rods

3.3.1. Introduction and Objectives

The SDP has been introduced for individual dosing of monolithic, tablet-like drug carriers sliced from a drug-loaded rod. However, so far, the drug release from these sliced drug carriers depended on the dose, geometry, and size of the cut slices (Wening, 2011).

The objective of this part of the thesis was to overcome this drawback by the development of formulations including multiparticulates that provide dissolution profiles which are independent of the number and masses of cut slices and of the over-all dose. This way, the advantages of multiparticulate and monolithic dosage forms may be combined.

Therefore, sustained release micropellets (spherical particles with a size $< 500 \mu\text{m}$) were incorporated into a matrix via ram-extrusion by a HPCR. During the development of those micropellet-loaded rods (MPLRs), some challenges had to be faced and examined: On the one hand, the coating of the pellets may be subject to undesirable interactions with the matrix. On the other hand, the coating may be damaged mechanically during ram-extrusion. Both effects would lead to a change of the release properties of the micropellets incorporated within the matrix.

In addition, this chapter will focus on the mechanical properties of the MPLRs, their individual dosing by the SDP, and storage stability of the system.

In this section, CBZ was utilised as model drug, too. This attempt only represents a general proof of concept: the drug-loading of the MPLRs was limited due to the drug content of the micropellets and the restricted fraction of pellets that may be incorporated into the matrix. Hence, the therapeutic dose of CBZ (Kearns et al., 2003) will hardly be reached. Nevertheless, for highly potent drugs, like carvedilol, hydrochlorothiazide, or dexamethasone, for example, this concept would establish new perspectives. Furthermore, the limited drug-loading may considerably be improved by the utilisation of extrusion-spheronisation for the micropellet-manufacturing or the continuous MicroPx[®] fluid bed technology introduced by Glatt GmbH (Binzen, Germany) to produce highly drug-loaded micropellets providing a drug-load of up to 95 % (Pöllinger, 2013).

3.3.2. Feasibility Study

In this work, the choice of the matrix material had to be taken in the light of minimising the solubility of the coating material in the matrix, but also to allow for the dosing of the produced rods via cutting them into tablet-like slices. The mechanical properties of rods containing PEG 2,000 with an addition of PEG 1,500 permitted application via the SDP in the best way (section 3.2.2). As the utilised PEGs moreover showed low melting temperatures (section 3.2.2.1, Table 3), a matrix composition of 70 % PEG 2,000 and 30 % PEG 1,500 was utilised for the MPLRs. The compatibility of the matrix- and the coating materials will be investigated further in section 3.3.4.5. Furthermore, the residence

time of the matrix material and the coated micropellets within the barrel will have to be optimised to decrease the contact time at elevated temperatures (Miller et al., 2007).

In a first step, the process parameters for the manufacturing of MPLRs by the HPCR were investigated to examine whether the processing of layered pellets via ram-extrusion at high pressures is feasible in general. Thus, coated pellets with a diameter below 710 μm were utilised for incorporation into ram-extrudates and an experimental design (DoE) was performed. A 2^3 full factorial design with the extrusion temperature (43 and 45 $^{\circ}\text{C}$), the equilibration time (10 and 20 min), and the piston velocity (100 and 300 mm/min) as factors (and factor levels) was conducted (section 6.2.2).

The limits for the extrusion temperature (T_{extr}) and the equilibration time (t_{equil}) were known from the production of the small-scale ram-extrudates (sections 3.1.3.1 and 3.2.2.1). For the ram-extrusion of glycerides, extrusion rates from 20 to 500 mm/min have already been evaluated by other workgroups (Oliveira et al., 2013; Pinto and Silverio, 2001). When ram-velocities of 20 to 320 mm/min were applied an extrusion pressure of 3 to 15 MPa occurred for extrudates manufactured by Perissutti et al. (2002), who found a significant increase in the extrusion pressure by increased ram-velocities.

Table 11 presents the experiments conducted within the DoE. The occurring pressure within the barrel, F_{max} , tensile strength, and E-modulus of the produced MPLRs were examined as yield variables.

Table 11: Factors, factor levels, and yield variables of the DoE

Experiment name	Run order	T_{extr} [$^{\circ}\text{C}$]	t_{equil} [min]	v_{piston} [mm/min]	Pressure [MPa]*	F_{max} [N]	Tensile strength [MPa]	E-modulus [MPa]
N1	1	43	10	100	4.1	25.6 ± 4.2	6.2 ± 0.4	257.8 ± 15.5
N2	11	45	10	100	1.8	28.0 ± 3.1	6.3 ± 0.4	255.3 ± 5.9
N3	9	43	20	100	3.4	29.6 ± 5.6	6.5 ± 0.4	267.2 ± 6.9
N4	8	45	20	100	1.4	29.2 ± 3.4	6.3 ± 0.2	263.1 ± 7.2
N5	3	43	10	300	5.8	31.0 ± 3.8	7.1 ± 0.5	260.3 ± 10.8
N6	10	45	10	300	2.5	30.3 ± 2.3	6.4 ± 0.3	255.3 ± 10.5
N7	6	43	20	300	4.9	31.2 ± 3.1	7.1 ± 0.1	238.4 ± 15.8
N8	2	45	20	300	2.2	30.6 ± 1.9	6.3 ± 0.2	244.0 ± 13.8
N9	5	44	15	200	2.9	24.8 ± 4.5	6.3 ± 0.2	257.0 ± 11.3
N10	4	44	15	200	3.5	28.3 ± 3.3	6.4 ± 0.2	245.6 ± 9.0
N11	7	44	15	200	3.1	28.3 ± 4.1	6.3 ± 0.3	251.5 ± 10.2

* The pressure was calculated as mean of values recorded for the steady state in extrusion (between the 5th and 10th second).

Pressure values ranged from 1.4 MPa for the factor-level combination N4 (45 °C, 20 min, 100 mm/min) to 5.8 MPa for the factor-level combination N5 (43 °C, 10 min, 300 mm/min).

For the yield variables F_{\max} , tensile strength, and E-modulus no significant effects were observed regarding T_{extr} , t_{equil} , and v_{piston} within the experimental space. Thus, for pressure values between 1.4 and 5.8 MPa the process was demonstrated to result in extrudates with similar mechanical properties.

But the three factors T_{extr} , t_{equil} , and v_{piston} affected the pressure and thus a linear regression model for this yield variable was built. The summary plot depicted in Figure 48 illustrates the satisfying fit of the built model: The coefficient of determination ($R^2\text{Adj}$), which describes the quality of the model, was 0.945 and the coefficient of prediction (Q^2), which characterises the prediction quality of the model, was 0.888. The model validity (lack of fit), which explains the systematic proportion of the error, which is not explicable by the model or random scattering, was 0.811 and the reproducibility, which provides information about errors that occur at the repetition of experiments, was 0.957.

Figure 49 presents the coefficients plot for the three examined factors. As expected an increase in extrusion temperature or equilibration time led to lower pressure values in the barrel. For example, elevating the temperature by 1 °C resulted in a decrease of pressure of 1.3 MPa. This may be explained by a softening and a decrease in viscosity of the material depending on temperature and time. The impact of the equilibration time on the related factor space was less important than the barrel temperature itself. Thus, one may assume that the plasticisation of the material was already almost complete at the lowest level of 10 min equilibration time.

Although the investigated temperature range was narrow (43 - 45 °C), the extrusion temperature showed the highest effect due to the (semi-)crystalline structure of the excipients and the proximity to their melting temperature (49.2 °C for PEG 1,500 and 54.0 °C for PEG 2,000; determined by DSC measurements).

An increase in the piston velocity resulted in an increase in pressure due to higher shear forces in the die region. This effect was smaller than the effect of the temperature even though the studied range was quite large (100 to 300 mm/min). Interactions between the factors were not significant.

A contour plot of the examined factors T_{extr} (x-axis), v_{piston} (y-axis), and t_{equil} on the yield variable pressure is presented in Figure 50. As the equilibration time had a minor impact on the pressure occurring in the barrel within the investigated range, the three contour plots for the different t_{equil} were similar. For the production of the MPLRs a barrel temperature of 45 °C, an equilibration time of 10 min, and a piston velocity of 200 mm/min were selected with the aim of a low pressure and a short contact time in the barrel (Miller et al., 2007). Besides, the surface of the rods had a better appearance at higher piston velocities in the analysed range. This adjustment resulted in the feasibility study in occurring pressures of 2 to 2.5 MPa (Figure 50, turquoise region).

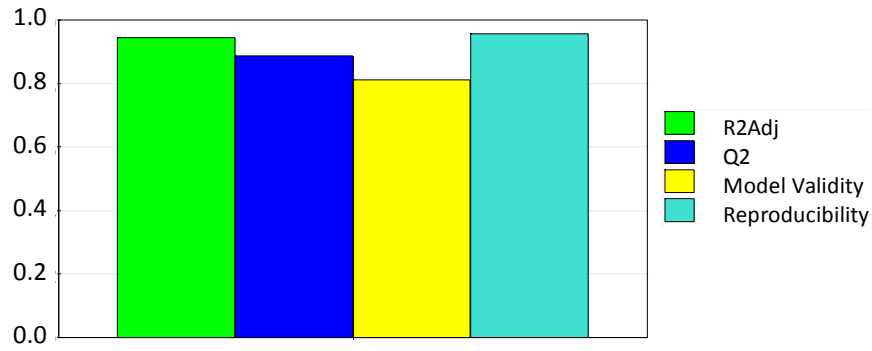


Figure 48: Summary plot for the optimised linear regression model for the yield variable pressure; $n = 11$, $DF = 7$

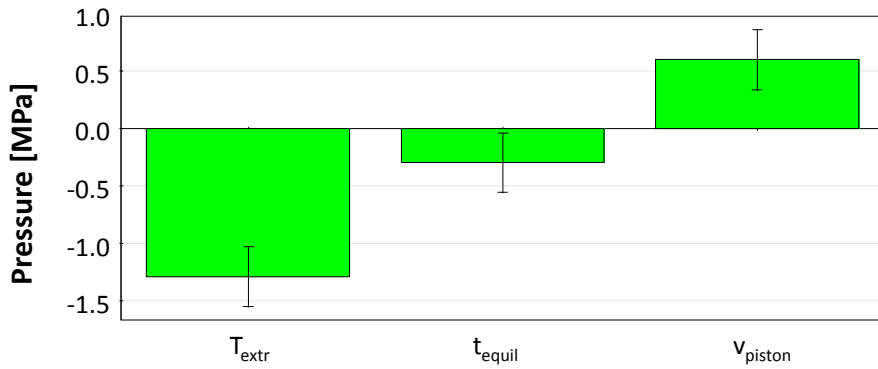


Figure 49: Coefficients plot (coefficient \pm CI); scaled and centred coefficients for the yield variable pressure depending on the examined factors extrusion temperature (T_{extr}), equilibration time (t_{equil}), and piston velocity (v_{piston}); $n = 11$, $DF = 7$, coefficient of variation = 0.309, $\alpha = 0.05$

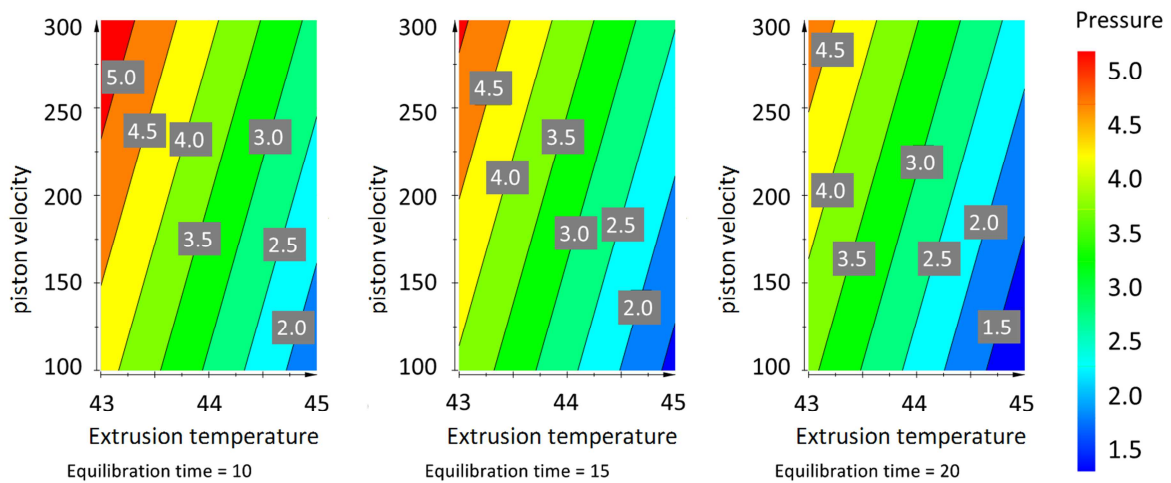


Figure 50: Contour plot for the yield variable pressure on the examined factors extrusion temperature, piston velocity, and equilibration time

3.3.3. CBZ Layering on Micropellets

3.3.3.1. Layering Process

In the first step, the aim was to layer CBZ on starter cores to obtain CBZ micropellets. Starter cores made from sugar provoked a crack formation of a film coating during dissolution, as the sugar built up a hydrostatic pressure and attracted water into the core (Cuppok et al., 2011). This phenomenon resulted in a high dissolution rate due to drug release through water filled cracks. In contrast, drug dissolution from coated microcrystalline cellulose (MCC) spheres was found to be mainly based on drug diffusion through the intact film coating, yielding a constant and slower drug release (Cuppok et al., 2011). As this is the aim of this work as well and MCC-Pellets are moreover known to show narrow particle size distribution and high mechanical resistance (Schilling and McGinity, 2010), which makes them suitable for further processing via ram-extrusion, Cellets® 200 and 350 were chosen as starter cores.

In preliminary studies, hypromellose (HPMC) with a viscosity of 3 and 6 mPa*s has been utilised as binder for the CBZ-layering. To examine the efficacy of the drug layering, the CBZ recovery was calculated by division of the measured by the calculated CBZ content. This recovery of CBZ on preliminary batches was found to be 38.1 to 57.1 % for the lower viscous HPMC grade and was not markedly increased for the higher viscous HPMC grade for the examined layering parameters (57.3 %). The low recovery of the drug may be due to a low pigment binding capacity of HPMC. Figure 51 presents SEM micrographs of the starter cores (Figure 51 a and b) and pellets layered with CBZ and HPMC (Figure 51 c and d). A visible peeling of the layer may refer to the insufficient drug binding capacity of the polymeric binder (Figure 51 c).

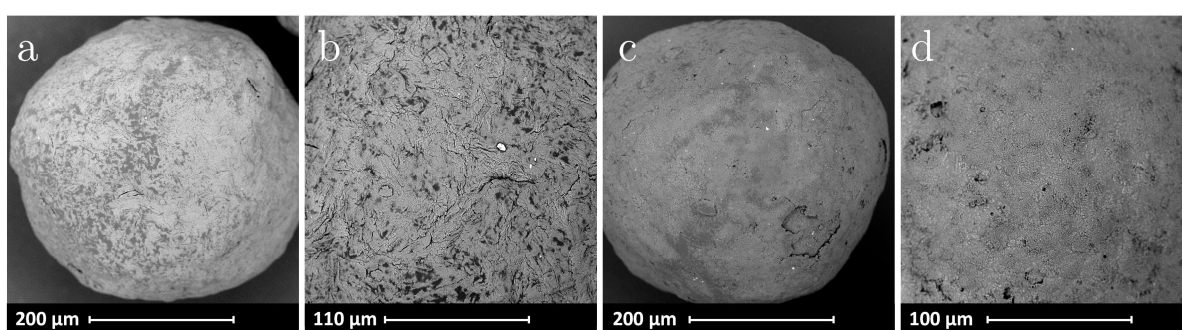


Figure 51: SEM micrographs of the surface of Cellets® 350 (a, b) and the CBZ layered pellets from the preliminary studies with a 3 mPa*s grade of HPMC (c) and a 6 mPa*s grade of HPMC (d)

In contrast to the observed unsatisfactory pigment tolerance of HPMC, PVA-PEG has already shown a high pigment binding capacity and flexibility of the pigment-containing films (Bühler, 2007; Kolter, 2004). Moreover, the polymer has been proved to be a suitable binder for suspension layering processes with a solid content up to 45 % even for coarse

drug particles (Suhrenbrock et al., 2011). Thus, PVA-PEG was utilised as binder in further experiments (batches A to E, Table 12).

For the batches A, B, and D Cellets® 350 and for the batches C and E Cellets® 200 were utilised as starter cores. 200 g of starter cores were layered in a fluidised bed coater (Mycrolab, Hüttlin, Germany) with PVA-PEG as binder and a solid content of the layering dispersion of 20 % (section 6.2.1.7). The composition of the layering suspension, the process parameters, and the resulting CBZ content of the layered micropellets are presented in Table 12.

Table 12: Layering suspension, process parameters, and CBZ content of the CBZ-layering with PVA-PEG, batches A - E ; solid content of 20 %, spray pressure of 0.8 bar, all batches were cured for 30 min at 43 °C

batch	A	B	C	D	E
layering suspension					
binder level [%]*	20	20	20	25	25
CBZ proportion [%]	16	16	16	15	15
layering parameters					
inlet air temperature [°C]	53 - 55	58 - 61	60 - 64	53 - 55	54 - 56
spray rate [g/min]	2.8	4.4	4.4	4.2	4.2
product temperature [°C]	34 - 35	32 - 34	31 - 32	31 - 33	31 - 32
microclimate [bar]	0.5	0.5	0.5	0.2	0.15
CBZ content					
calculated CBZ content [%]	13.3	13.3	13.3	12.5	12.5
measured CBZ content [%] (n ≥ 2, mean)	9.1	9.6	11.2	11.0	10.8
CBZ recovery [%]	68.4	72.2	84.2	87.8	86.2

*binder level: percentage of the binder-mass to the sum of binder- and drug-mass (section 6.2.1.7)

In order to minimise the mass to be administered to the patient, the drug-loading of the formulation should be maximised. Starting from batch A with a recovery of 68.4 %, parameters were therefore varied in order to increase the recovery of the drug (Suhrenbrock, 2011). Hence, the product temperature was decreased from 34 - 35 °C (batch A) to 31 - 34 °C (batches B - E). At the same time the spray rate was increased from 2.8 g/min (batch A) to 4.2 - 4.4 g/min (batches B - E). Moreover, for batches D and E, the pressure of the microclimate was decreased to optimise the air void around the spray nozzle. Additionally, the binder level was increased from 20 % (batches A - C) up to 25 % (batches D and E). The optimised process conditions resulted in an increased CBZ recovery of 87.8 and 86.2 % for batches D and E.

The lowest recovery in the work of Suhrenbrock et al. (2011) was 93.7 %. In consideration of the small-scale (200 g pellets per batch), the small starter cores as well as the utilisation of a different drug in this study, the CBZ recovery of 72.7 - 87.8 % for batches B to E was judged as a satisfying result.

The pellet fraction below 500 μm for batches A, B, and D and below 400 μm for batches C and E were selected for further analysis and for the sustained release coating of the pellets (section 3.3.4).

3.3.3.2. Particle Size Measurements and Surface Properties

The starter core size and the size of the layered pellets were analysed by dynamic image analysis (DIA) employing a double camera system (section 6.2.3.5). The pellet sizes were analysed as $x_{C_{\min}}$ -values, representing the smallest of all possible maximum cords for the particle projection. Results are presented as x_{50} -values and inter-quartile spans (IQS) in Table 13.

The starter cores had an x_{50} -value of $384.0 \pm 0.6 \mu\text{m}$ (Cellets[®] 350) and $279.7 \pm 0.2 \mu\text{m}$ (Cellets[®] 200) and - as anticipated - a narrow particle size distribution. In general, pellets with larger x_{50} -values (Cellets[®] 350, batches A, B, and D) showed smaller IQSs (28.8 ± 0.3 to $31.4 \pm 0.3 \mu\text{m}$) and pellets with smaller x_{50} -values (Cellets[®] 200, batches C and E) exhibited larger IQSs (57.1 ± 0.7 to $58.0 \pm 0.8 \mu\text{m}$). However, the IQSs of the CBZ micropellets (batches A - E) stayed in the same range as the corresponding starter cores, indicating a homogeneous layering of the pellets.

Table 13: Particle size (x_{50}) and inter-quartile span (IQS) of the starter cores (Cellets[®] 200 and 350) and the CBZ-layered pellets (batches A - E) in μm , $n = 3$, mean \pm SD

	Cellets [®] 200	Cellets [®] 350	batch A	batch B	batch C	batch D	batch E
x_{50}	279.7 ± 0.2	384.0 ± 0.6	408.3 ± 0.4	409.2 ± 0.4	293.1 ± 0.9	419.4 ± 0.3	303.8 ± 1.4
IQS	57.1 ± 0.9	28.8 ± 0.3	30.4 ± 0.3	29.1 ± 0.2	57.1 ± 0.7	31.4 ± 0.3	58.0 ± 0.8

The size of the pellets was crucial to monitor: They should be extruded through a die with a diameter of 4 mm. As general rule of bulk mechanics, the diameter of a funnel (or die) should be at least 5 to 6 times the particle diameter in order to avoid bridging. Furthermore, it may be expected that smaller pellets are advantageous for the generation of a homogeneous distribution of the drug in the rods and therefore in the sliced single doses as well.

Figure 52 illustrates SEM micrographs of the CBZ micropellets from batch B (Figure 52 a and b) and E (Figure 52 c and d) in overview and in detail. While the surface of HPMC-layered micropellets in the preliminary studies was smooth (Figure 51 c and d), the surface structure of the PVA-PEG-layered pellets was rough and porous (Figure 52). This is in accordance with Suhrenbrock et al. (2011), who have already observed a roughness of

this layering, which emerged due to a steric arrangement of needle shaped drug particles. Even an increase in binder level from 20 % (batches A - C) to 25 % (batches D and E) did not change the morphology of the surface.

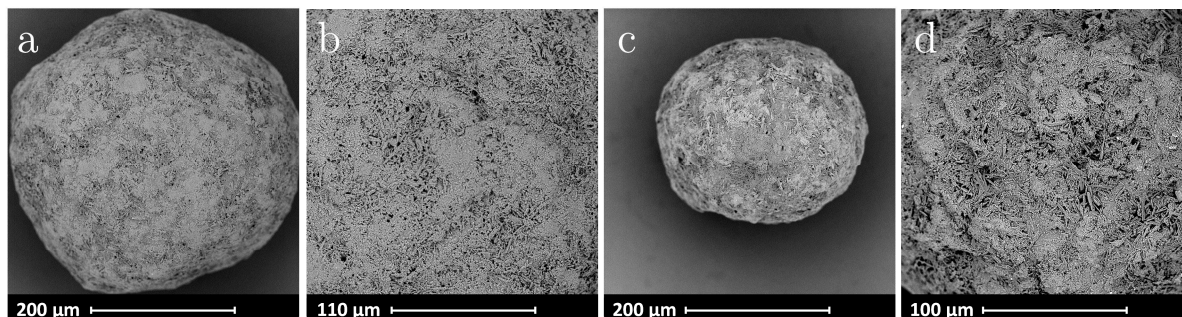


Figure 52: SEM micrographs of the CBZ-layered pellets, exemplarily batch B (a - b) and batch E (c - d); overview (a, c) and detail of the surface (b, d)

Despite the uneven surface morphology, CBZ micropellets with a uniform drug layer and a content of approximately 10 % were manufactured with PVA-PEG as binder (Table 12).

3.3.3.3. Dissolution Studies

Dissolution testing of the layered pellets was performed with a paddle apparatus at 75 rpm in 900 mL of degassed, demineralised water ($n \geq 3$) under sink conditions (section 6.2.3.7). Dissolution profiles of batches A - E are depicted in Figure 53.

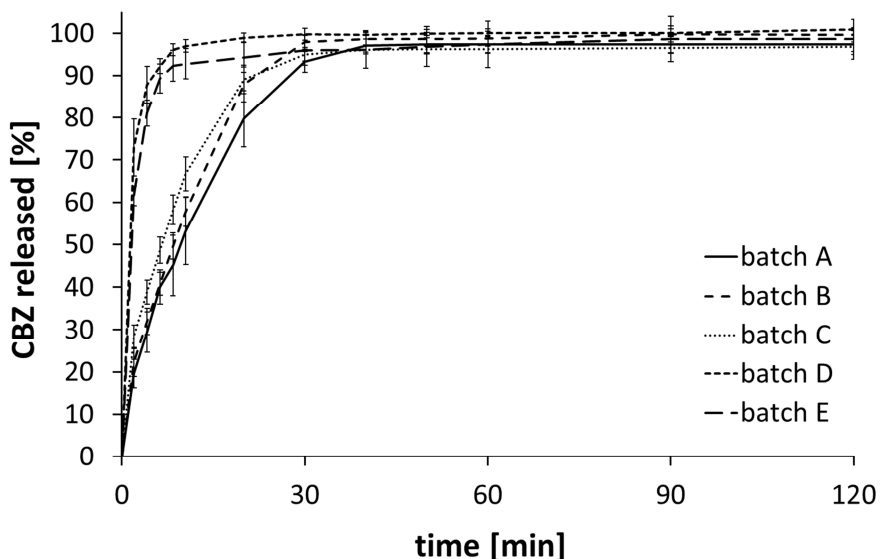


Figure 53: CBZ release of the CBZ micropellets (batches A - E); apparatus 2, 75 rpm in 900 mL of degassed, demineralised water at 37.0 ± 0.5 °C ($n \geq 3$; mean \pm SD)

All CBZ micropellets showed immediate release properties, as the binder PVA-PEG dissolved rapidly in water and liberated the drug immediately (Figure 53). The CBZ release from batches D and E was slightly faster than from batches A, B, and C. This may be due to the higher binder level (25 % for batches D and E), as the utilised binder was a well soluble polymer that did not lead to swelling but may have enhanced the wettability of the poorly soluble drug.

Nevertheless, all batches were utilised for the sustained release coating experiments presented in the next section (section 3.3.4) as the drug release was 96.3 - 99.9 % after 45 min for all formulations.

3.3.4. Sustained Release Coating of CBZ Micropellets

3.3.4.1. Coating Process

In a second step, the CBZ micropellets (section 3.3.3) were coated with a sustained release polymer film to obtain sustained release properties (section 6.2.1.8). Table 14 summarises the six batches of sustained release coated micropellets, the corresponding coating suspensions, the process parameters, and the resulting CBZ contents.

One coating suspension included a mixture of Eudragit® RS and Eudragit® RL in the ratio of 9:1 (batch 1). The other coating suspensions contained PVAc (batches 2 and 3) and PVAc/PVA-PEG (batch 4 in a ratio of 9:1; batches 5 and 6 in a ratio of 8:2). Batches 2 and 3 were both coated with PVAc as polymer, but differed in the applied percentage of coating suspension: The calculated weight gains were 22 % and 14 % according to a desired coating film thickness of 15 and 10 μm . As described in section 6.2.1.8 different excipients were utilised as anti-tacking agents and plasticisers.

The CBZ micropellets were coated in a fluidised bed coater in a batch size of 70 - 150 g. For batches 1 - 5 CBZ micropellets based on Cellets® 350 were utilised and batch 6 contained CBZ micropellets based on Cellets® 200. The process parameters, such as inlet air temperature, volumetric flow, spray rate or microclimate were varied to optimise the coating process.

For batch 2 some agglomerates were observed ($\geq 600 \mu\text{m}$), which affected the specific surface during coating and led to a decrease in the total yield, which was defined as mass of product per mass of material input. As over-wetting was suspected to be the reason for this effect, for batches 3 to 6 the spray rate was decreased and the volumetric flow was slightly increased in order to prevent agglomeration (Table 14).

The pellets were dried for 12 h and fractions below 500 μm for batches 1 to 5 and below 400 μm for batch 6 were selected for further analysis and the MPLR manufacturing (section 3.3.5).

The CBZ content of the sustained release coated pellets was analysed to be between 8.0 and 9.7 %, depending on the starting material.

Table 14: Starting material, coating suspension, process parameters, and CBZ content of the sustained release coated micropellets, batches 1 - 6, with a solid content of 20.0 % for batch 1, 17.1 % for batches 2 - 5, and 20.8 % for batch 6, spray pressure of 0.8 bar

batch	1	2	3	4	5	6
starting material (Table 12)	A	B	D	A/B	D	E
coating suspension						
polymer(s)	Eudragit® RS/RL (9:1)	PVAc	PVAc	PVAc/ PVA-PEG (9:1)	PVAc/ PVA-PEG (8:2)	PVAc/ PVA-PEG (8:2)
process parameters						
temperature [°C]	40 - 42	45 - 47	45 - 46	43 - 47	41 - 45	39 - 42
volumetric flow [m ³ /h]	15	18 - 20	20	20 - 23	20 - 23	20 - 25
spray rate [g/min]	2.3	2.4	1.1	1.1	0.9	0.8
product temperature [°C]	28 - 31	36 - 37	36 - 37	36 - 38	35 - 37	35 - 37
microclimate [bar]	0.5	0.3	0.3	0.4	0.4	0.3
after treatment	curing for 150 min at 40 °C		cool-down within the coater (32°C)			
content						
measured CBZ content [%] (n ≥ 2, mean)	8.5	7.8	9.7	8.0	9.6	9.4

3.3.4.2. Particle Size Measurements and Film Properties

The size of the sustained release pellets was investigated via DIA (dynamic image analysis, section 6.2.3.5) and the coating film thickness was calculated by subtracting the x_{50} -value of the CBZ micropellets from the one of the sustained release micropellets and dividing the result by two (Table 15).

Regarding the x_{50} -values, the particle size of the sustained release coated pellets was found to be between 426.3 ± 0.4 and 448.4 ± 0.6 μm for the larger CBZ micropellets (batches 1 - 5) and 312.6 ± 0.3 μm for the smaller CBZ micropellets (batch 6). The sustained release pellets showed a favourably narrow particle size distribution (IQS of 31.7 ± 0.1 to 40.0 ± 0.7 μm for batches 1 - 5 and 55.3 ± 0.6 μm for batch 6).

Table 15: Particle size (x_{50}), inter-quartile span (IQS), and calculated film thickness [μm] of the sustained release coated micropellets, batches 1 - 6, for particle size and IQS: $n = 3$, mean \pm SD

batch	1	2	3	4	5	6
x_{50}	426.3 ± 0.4	448.4 ± 0.6	428.9 ± 0.0	432.7 ± 0.4	434.5 ± 0.4	312.6 ± 0.3
IQS	35.3 ± 0.4	40.0 ± 0.7	31.7 ± 0.1	31.8 ± 0.1	36.1 ± 0.5	55.3 ± 0.6
film thickness [μm]*	9	20	5	12	8	4

*calculated by dividing the mean difference of x_{50} of the CBZ micropellets and the sustained release coated micropellets by two

The calculated weight gain for the coating process [%] was computed on the desired coating film thickness [μm]. For all batches the coating film thickness was anticipated to be above 10 μm to obtain a homogeneous film coating thickness. Due to aggregation tendencies during the coating for batches 3, 5, and 6 the coating was stopped before the calculated mass of coating-suspension had been applied onto the pellets. Therefore, the coating was thinner than intended (5, 8, and 4 μm).

SEM micrographs were recorded to visualise and examine the film properties via the surface morphology (Figure 54) and the cross-cut images (Figure 55) of the coated pellets. All sustained release coatings covered the rough surface of the CBZ micropellets with a smooth surface and for batches 1 to 5 hardly any fissures or holes were observed in spite of the low film thicknesses. For batches including talc as anti-tacking agent (batches 1 and 6) the insoluble particles may clearly be seen on the surface of the coated micropellets.

For batch 6, containing CBZ micropellets with the lower x_{50} -values, the pellet surface contained some defects and uneven structures, which possibly resulted from the pellets sticking to one another during the coating process. These defects and uneven structures in the coating may lead to a faster drug release or even uncontrolled liberation of CBZ from the pellets. To investigate this hypothesis further, dissolution testing was performed as described in the next section (section 3.3.4.3).

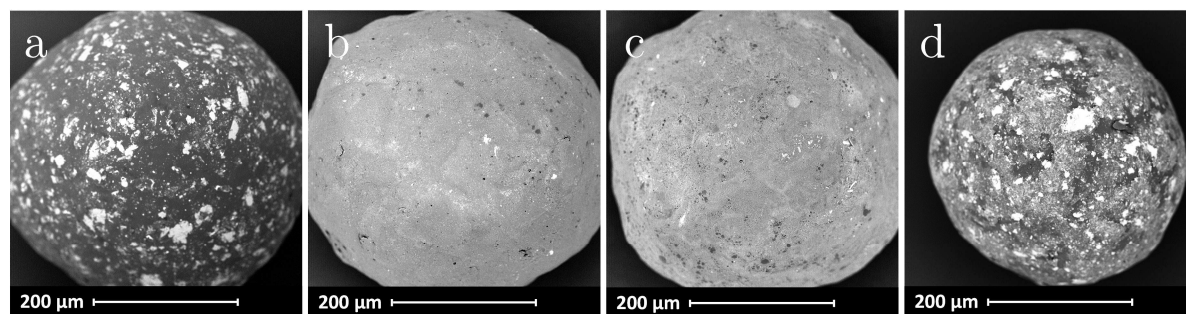


Figure 54: SEM micrographs of the surface of the sustained release pellets, exemplary depicted for batches 1, 2, 4, and 6 (a - d)

The cross-sections of the cut micropellets are presented in Figure 55. In all SEM micrographs the starter cores may clearly be distinguished from the film layers. Regarding the micrographs, one may assume that both the CBZ layering and the sustained release coating were homogeneously distributed and the film had a dense structure and a good integrity.

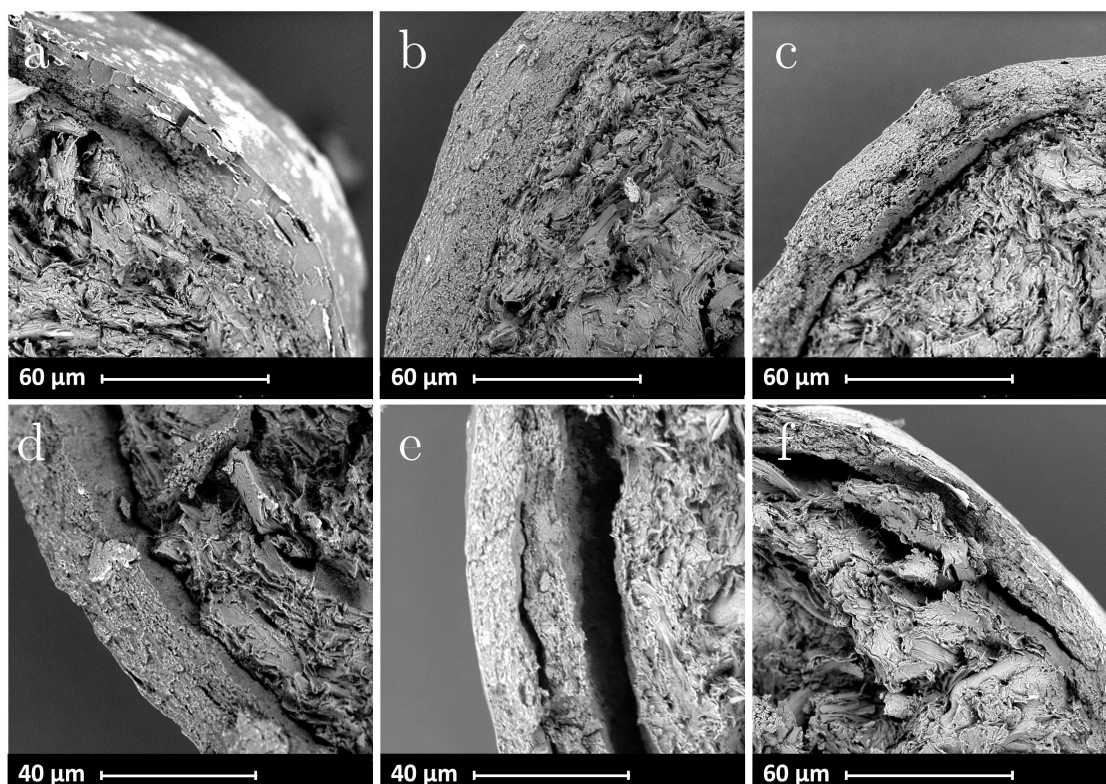


Figure 55: SEM micrographs of the cross-cut of the sustained release pellets, batches 1 - 6 (a - f)

The calculated and the observed thicknesses of the sustained release coating film were similar (Table 15, Figure 55). For instance, the film thickness of batch 3 (Figure 55 c) was thinner than the one of batch 2 (Figure 55 b), which was in line with the calculated values.

3.3.4.3. Dissolution Studies

The sustained release coated pellets were subject to dissolution testing (section 6.2.3.7). The resulting drug release profiles are presented in Figure 56.

While batches 1 to 3 showed constant drug release over time, batches 4 to 6 exhibited dissolution profiles with decreasing slope due to the different composition of the sustained release film coatings.

Batches 1 to 3 were composed from a Eudragit®-blend or PVAc. Interestingly, the dissolution profiles of batches 2 and 3, both containing PVAc seemed to be similar, although the film thickness varied between 5 and 20 μm . Therefore, one can assume that the film thickness was not discriminative for dissolution rate.

Ho et al. (2009) found that a difference in film thickness of 36 μm did not determine drug release. In their study, drug release was not predominately governed by drug diffusion through the polymeric film (PVAc/PVA-PEG-blend), but probably limited by the low drug solubility of theophylline. In contrast, for a hydrophilic drug the release was dependent on the film thickness as presumably not the solubility, but the diffusion rate through the coating limited the drug release (Haaser et al., 2013).

For batches 1, 2, and 3, the CBZ release was constant over time (R^2 for zero order kinetics: 0.990, 0.990, and 0.986) and 50 % of the drug was released after 570, 960, and 860 min. As these dissolution properties were rated as low and the film thickness did not have a major impact on the dissolution rate, PVA-PEG as a more hydrophilic polymer was added to the coating (batches 4 to 6, Table 14).

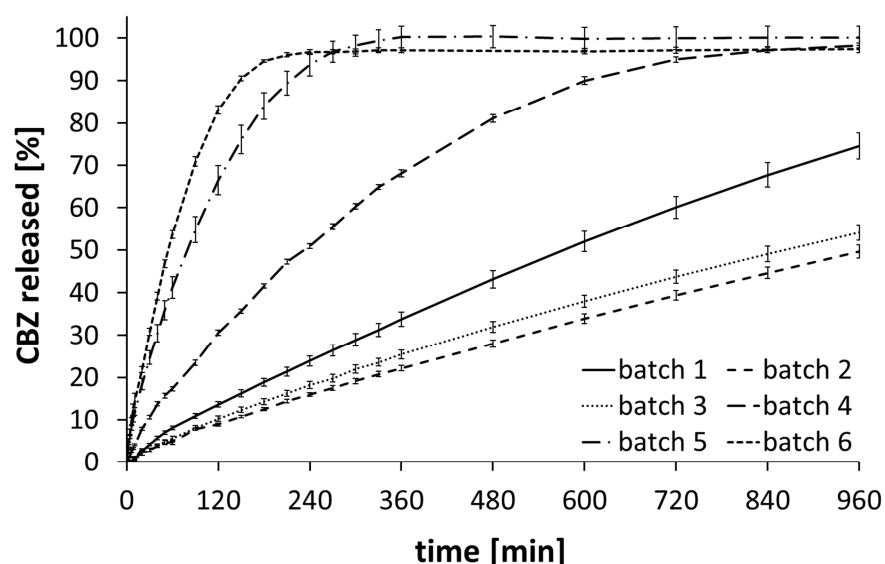


Figure 56: CBZ release of the sustained release micropellets (batches 1 - 6); apparatus 2, 75 rpm in 900 mL of degassed, demineralised water at 37.0 ± 0.5 °C ($n \geq 3$; mean \pm SD)

PVA-PEG acted as pore-forming agent enhancing the dissolution, but also altered the shape of the dissolution profiles, which were no longer following zero order kinetics.

For batches 4, 5, and 6, 50 % CBZ was released after 47, 78, and 232 min. The drug release from batch 4 was slower than from batch 5 due to the higher film-thickness (12 μm vs. 8 μm) and the lower proportion of PVA-PEG (10 % vs. 20 %). For batches 5 and 6 dissolution characteristics were similar to each other, when compared to batches 1 to 4. For batch 6 a controlled sustained release was achieved in spite of the rough and apparently inhomogeneous structure of the coating film (Figure 54). Drug release was complete after 360 and 240 min (101.6 ± 0.7 and 96.8 ± 0.6 %) for batches 5 and 6, which was assessed as suitable for a sustained release formulation. Batches 5 and 6 only varied in the size of the CBZ micropellets and the film thickness, and the drug release from the smaller and more thinly coated pellets from batch 6 was a little faster than from batch 5.

The SEM micrographs in Figure 57 illustrate the different morphologies of the sustained release coated pellets after 16 h of dissolution. Batch 2 is exemplarily shown for the pellets coated without a pore-forming agent (Figure 57 a - c) and batch 4 is presented as an example of a coating containing PVA-PEG as pore former (Figure 57 d - f).

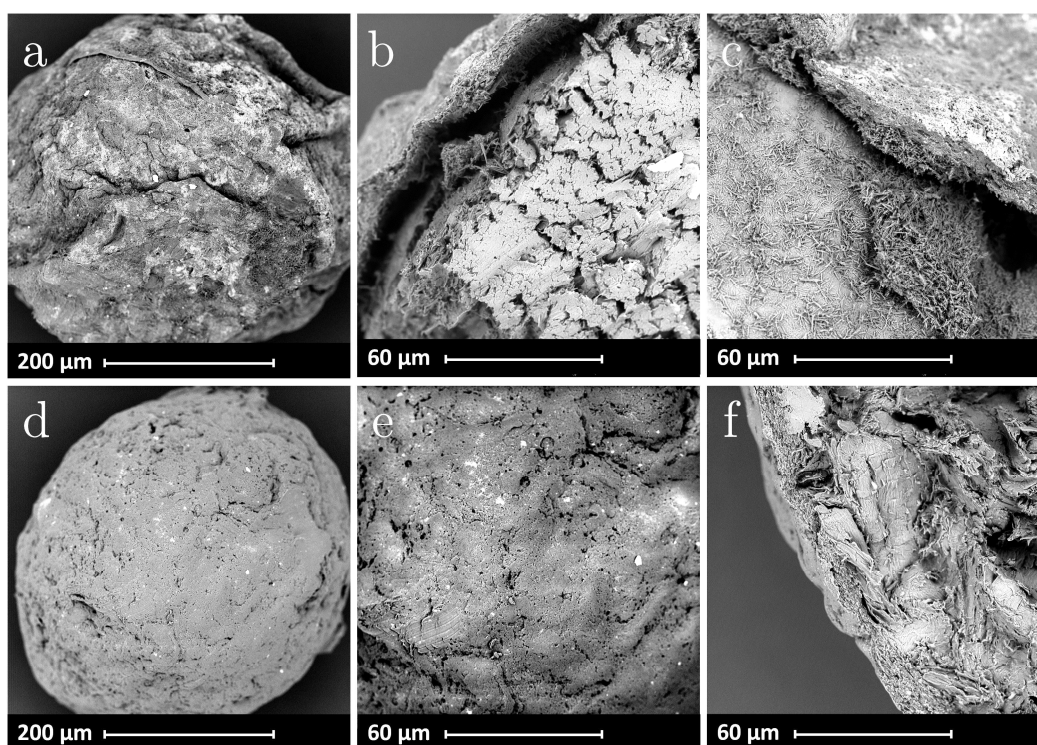


Figure 57: SEM micrographs of the sustained release coated micropellets, batch 2 (a - c) and batch 4 (d - f), of the surface (a, d, and e) and the cross-cut (b, c, and f) after 16 h of dissolution in 900 mL of degassed, demineralised water at 37.0 ± 0.5 °C

After dissolution, the PVAc-coated micropellets showed an irregular, wavy, but still intact surface (Figure 57 a). During dissolution, the sustained release coating swells and at the same time water is taken up into the emerging cavity between the core and the sustained

release coating, where CBZ transforms rapidly into CBZ DH (Kobayashi et al., 2000) and both CBZ and CBZ DH partly dissolve. Thus, a saturated CBZ-solution with CBZ DH crystals was generated inside the pellet. Therefore, the CBZ release rate was time-independent for batches 1 to 3 as long as a saturated drug solution was existent between the core of the insoluble pellet and the polymer coating (Ho et al., 2009). Moreover, this observed dissolution mechanism of the drug possibly explains why the film thickness had no major impact for the examined batches 2 and 3 (20 and 5 μm) in this study. The release rate depended on the solubility of the drug and therefore it was supposed that for drugs showing higher solubility higher release rates would be obtained. As only 50 % of the drug was liberated after 16 h, CBZ DH crystals were still visible between core and coating-layer in the micrographs (Figure 57 b and c).

XRPD measurements revealed that the pellets contained CBZ III before dissolution and CBZ DH afterwards (Figure 58), which corroborates the statements above.

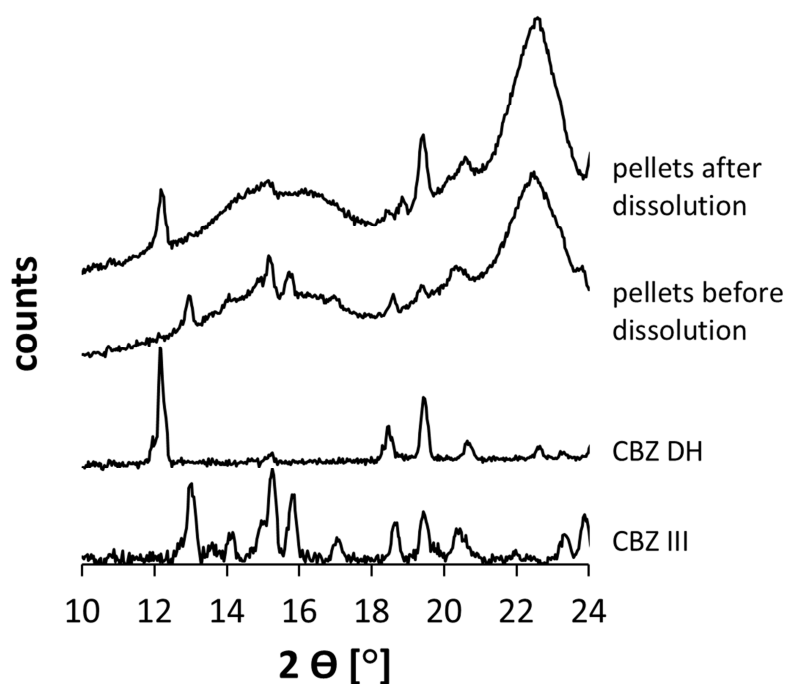


Figure 58: Diffractograms of CBZ III and CBZ DH, the pellets of batch 2 before and after dissolution; depicted from 10 to 24° 2θ ; measured values of the polyimide films were subtracted from the sample values

The micrographs of batch 4 differed: The surface of the sustained release coated pellets was rather smooth and pores were observed (Figure 57 e). The drug dissolution process from similarly coated pellets was subdivided into three parts: (1) A fast water influx through the polymeric membrane, (2) dissolution of the water-soluble polymers (creating the pores in the membrane) and (3) solubilisation of the drug (Ensslin et al., 2008; Ho et al., 2009; Strübing et al., 2008). The fast uptake of water and the dissolution of PVA-PEG after several minutes did not result in a fast, but slow drug release (Ensslin et

al., 2008). After 16 h of dissolution no CBZ DH crystals were visible as the drug had already been released completely (Figure 56 and Figure 57).

As batch 3 did not differ from batch 2 with regard to drug dissolution, it was not included for further examination.

3.3.4.4. Pressure Compatibility

A mechanical rupture of the sustained release coating within the extrusion-process would result in accelerated and uncontrolled dissolution properties. Thus, the sustained release coated pellets need to be robust against a certain pressure emerging in the barrel and the die of the HPCR during ram-extrusion of MPLRs, even if this pressure works in a diametric way. For the tableting of multiparticulates it has already been shown that similar drug release profiles from pellets coated with PVAc or PVAc/PVA-PEG were obtained before and after compression for pressures of 102 and 106 MPa due to the high flexibility of the polymer films (Ensslin et al., 2009; Sawicki and Lunio, 2005).

To evaluate whether the pellets may be processed via ram-extrusion their tensile strength was determined and compared to the pressure occurring during ram-extrusion in the HPCR. For the feasibility study the occurring pressures ranged from 1.8 - 5.8 MPa (section 3.3.2).

The tensile strength of the starter cores and the sustained release micropellets was investigated via a Texture Analyser (section 6.2.3.3) and calculated from the first maximal force for a particle deformation of 50 % and the diameter of each pellet ($n = 30$) according to literature (Kleinebudde et al., 1999; Shipway and Hutchings, 1993). A testing velocity of 0.04 mm/s was utilised (Schilling and McGinity, 2010), as in preliminary studies this testing velocity gave similar values as gained by a testing velocity of 0.1 mm/s (Krueger et al., 2013; Thommes and Kleinebudde, 2006), but lower standard deviations were obtained.

Figure 59 presents the tensile strength of the sustained release pellets and the starter cores. The tensile strength of the micropellets in this work ranged from 12.6 ± 2.7 to 18.4 ± 2.9 MPa. For uncoated MCC microspheres (300 - 500 μm) a tensile strength of approximately 34 MPa was determined by Schilling and McGinity (2010), whereas for coated MCC spheres approximately 24 MPa were measured. The absolute values may only be compared with caution, as they were calculated by a different equation (Hiramatsu-Oka equation).

Schilling and McGinity (2010) proposed that the mechanical properties were mainly due to the high strength of the MCC-starter cores and that the increase in particle diameter by the coating would lead to smaller calculated values of the tensile strength. In this work, the effect of the coating on the tensile strength was ambiguous and likely to depend on the coating polymer and film coating thickness (Aulton et al., 1994).

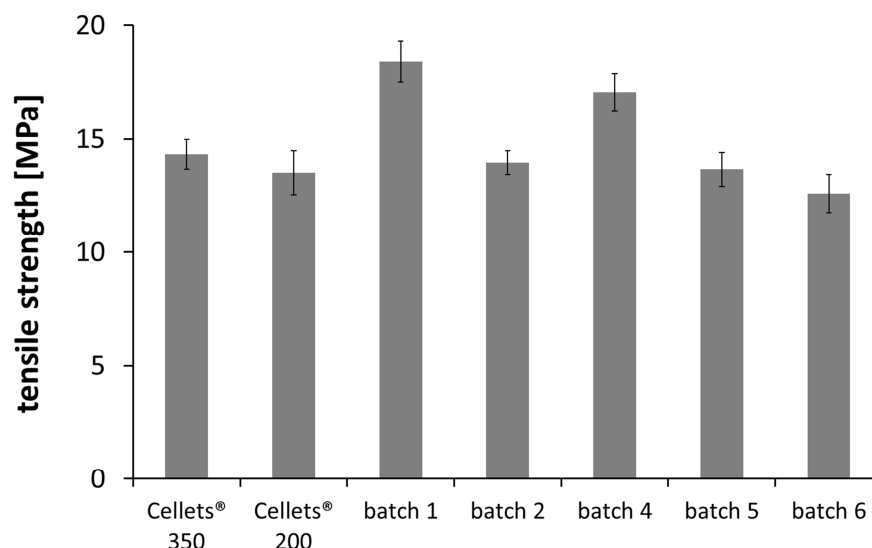


Figure 59: Tensile strength of the starter cores (Cellets® 350 and 200) and the sustained release coated CBZ micropellets (batches 1, 2, and 4 - 6), determined by the Texture Analyser ($n = 30$, mean \pm SD)

The same authors found that a film which had similar tensile properties to the uncoated spheres resulted in the most suitable film coating for compaction of spheres into tablets (Aulton et al., 1994).

To conclude, the tensile strengths of the sustained release CBZ micropellets were similar to the ones from the uncoated Cellets® and, moreover, far above the pressure occurring during the ram-extrusion of the MPLRs in the feasibility study (≤ 5.8 MPa, section 3.3.2).

3.3.4.5. Matrix Compatibility

Besides the pressure resistance of the coated pellets, the compatibility of the polymer coating with the matrix was crucial to investigate.

For instance, Schilling and McGinity (2010) found an increase of the drug dissolution rate after the extrusion of coated pellets in a matrix to be more likely a result of the partial solubilisation of the film in the matrix, than a result of the mechanical rupture of the film due to shear forces or elevated pressure during extrusion.

These findings were in line with earlier studies by Schmidt and Bodmeier (2001): Developing a multiparticulate drug delivery system based on pellets which were embedded into a tablet-shaped PEG matrix, they found the suitability of a PEG-matrix to be dependent on the molecular weight of PEG.

To evaluate undesirable interactions between the sustained release polymers and the matrix during ram-extrusion, DSC measurements were conducted (section 6.2.3.10) based on a method by Schilling and McGinity (2010): The matrix material of the MPLRs (PEG-mixture) was either heated in pure form or mixed with an equal quantity of the film building polymer. The DSC-samples were heated to 20 °C above the extrusion temperature ($T_{\text{extr}} = 45$ °C) with a heating rate of 10 °C/min. This temperature was then hold for 10 min simulating filling of the barrel, appropriate equilibration time in the

barrel, and subsequent ram-extrusion. After cooling rapidly to 20 °C, a second heating run was performed. According to the aforementioned authors a reduction in the melting enthalpy of the matrix from the first to the second heating cycle can be interpreted as partial polymer solubility. The relative crystallinity of the matrix after processing was calculated by dividing the melting enthalpies of the second run by the melting enthalpies of the first run. Results are depicted in Figure 60.

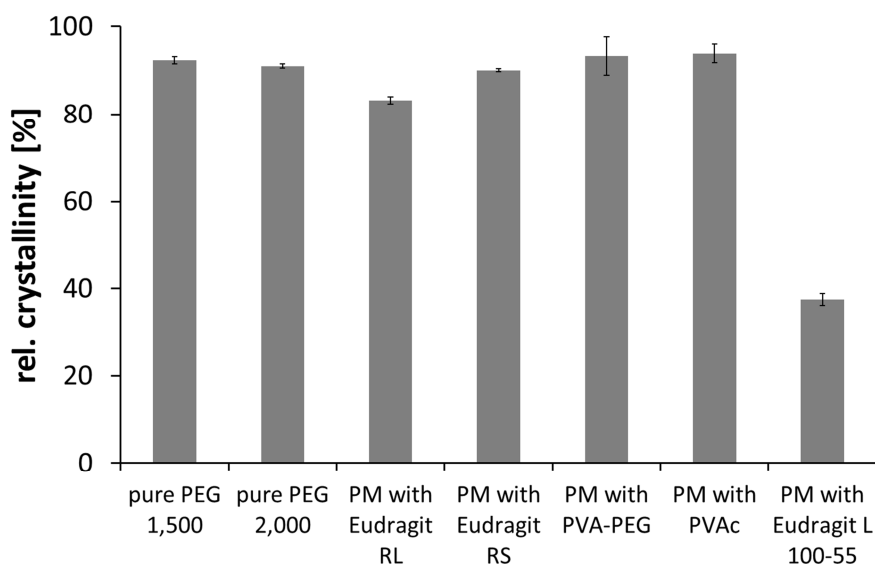


Figure 60: Relative crystallinity [%] of the matrix materials (PEG 1,500 and 2,000) and the physical mixtures (PM) of the PEG-mixture utilised for the MPLRs with different polymers (Eudragit® RL, Eudragit® RS, PVA-PEG, PVAc, and Eudragit® L 100-55), PM in the ratio of 1:1; n = 2, mean ± SD

For the pure matrix components PEG 1,500 and PEG 2,000 a relative crystallinity of 92.3 % and 91.0 % was estimated (Figure 60). These findings were in agreement with results from Schilling and McGinity (2010), who recorded only a slight decrease in crystallinity of PEGs 4,000 and 8,000 when heated alone (92 and 96 %).

The physical mixtures with coating polymers Eudragit® RL and Eudragit® RS resulted in slightly smaller values of the relative crystallinity: While Eudragit® RS (type B Ph. Eur.) induced a reduction of relative crystallinity to 90.1 ± 0.4 %, Eudragit® RL (type A Ph. Eur.) decreased the relative crystallinity to a higher extent (83.2 ± 0.8 %). This may be explained by the ratio of quaternary ammonium groups in the two polymers: Eudragit® RL (high permeability) includes twice as many ammonium groups as Eudragit® RS (low permeability). Thus, the more hydrophilic Eudragit® RL showed a higher solubility in PEGs.

The relative crystallinity of the matrix with PVA-PEG and PVAc was higher (93.3 ± 4.3 % and 93.9 ± 2.1 %) and therefore in the same range as values of the pure matrix substances.

In order to verify the method and to compare the results to those of Schilling and McGinity (2010), a physical mixture with Eudragit® L 100-55 was analysed as well, although this polymer was not utilised in this study. The relative crystallinity of the PM of the PEG-mixture with Eudragit® L 100-55 resulted in 37.5 ± 1.4 %, showing a harsh decrease compared to the other coating polymers. Measurements of the mentioned workgroup demonstrated as well that Eudragit® L 100-55 reduced the relative crystallinity of PEG 4,000 and 8,000 as matrix materials (9 and 24 %). In conclusion, the PEG matrix seemed to be suitable for the polymers Eudragit® RL/RS, PVA-PEG, and PVAc as their relative crystallinity was only slightly decreased by the thermal treatment cycle during the DSC measurements.

Nevertheless, regarding the matrix compatibility some limitations of these DSC measurements have to be faced: First, plasticisers and surface active substances included in the coating suspension may change the solubility of the film coating in the matrix. These effects were not analysed in this work, as only the pure coating polymers were subject to investigation. Second, and more importantly, the DSC measurements only modelled the production process of the ram-extrusion, but the effects in the dosage form that may appear in the long run were not modelled. Interactions like partial dissolution of the polymer within the matrix or the migration of plasticisers may not only appear in the course of the production process of the MPLRs, but also over storing time (Schilling and McGinity, 2010; Schmidt and Bodmeier, 2001). The storage stability of the MPLRs was therefore investigated further and will be discussed in section 3.3.5.5.

3.3.5. Embedding of Micropellets into Rods

3.3.5.1. Ram-Extrusion via a HPCR

Based on the feasibility study (section 3.3.2) MPLRs containing 30 % (w/w) coated micropellets (batches 1, 2, and 4 to 6) and PEG(-mixtures) as matrix were manufactured by ram-extrusion via a HPCR (section 6.2.1.9).

Table 16 shows the MPLR formulations together with the production parameters and the mean pressure observed during ram-extrusion. Additionally, pressure profiles recorded during the production of the MPLRs are presented in Figure 61.

For MPLRs containing PEG 2,000 and PEG 1,500 in the ratio of 7:3 (MPLR batches 1, 2, and 4 to 6) an extrusion temperature of 45 °C, an equilibration time of 10 min, and an extrusion rate of 200 mm/min were utilised. These values were selected to minimise the time of interactions between the coating of the pellets and the matrix and to minimise the pressure during ram-extrusion according to the results of the feasibility study. Furthermore, PEG 20,000 was exemplarily utilised as matrix material for batch 1 with different production parameters (Table 16).

Table 16: MPLR formulations, extrusion temperature (T_{extr}), equilibration time (t_{equil}), and pressure* observed during ram-extrusion (mean \pm SD), $v_{\text{piston}} = 200$ mm/min

formulation	T_{extr} [°C]	t_{equil} [min]	pressure [MPa]*
MPLR batch 1	45	10	3.2 ± 0.1
MPLR batch 1_PEG 20,000_1	63	5	5.9 ± 0.1
MPLR batch 1_PEG 20,000_2	63	10	3.4 ± 0.1
MPLR batch 1_PEG 20,000_3	62	10	6.8 ± 0.1
MPLR batch 2	45	10	2.9 ± 0.1
MPLR batch 4	45	10	2.6 ± 0.1
MPLR batch 5	45	10	2.0 ± 0.1
MPLR batch 6	45	10	1.4 ± 0.0

*Pressure was calculated as mean of values recorded for the steady state in extrusion (between the 5th and 10th second and the 10th and 15th second for MPLR batches with PEG 2,000 and PEG 20,000, respectively)

For the ram-extrusion of MPLR batches 1, 2, and 4 to 6 the occurring pressures did not exceed 3.2 ± 0.1 MPa. For the extrusion of MPLRs containing the higher molecular weight PEG (MPLR batches 1_PEG 20,000_1 - 3) pressures up to 6.8 ± 0.1 MPa resulted from the chosen process parameters.

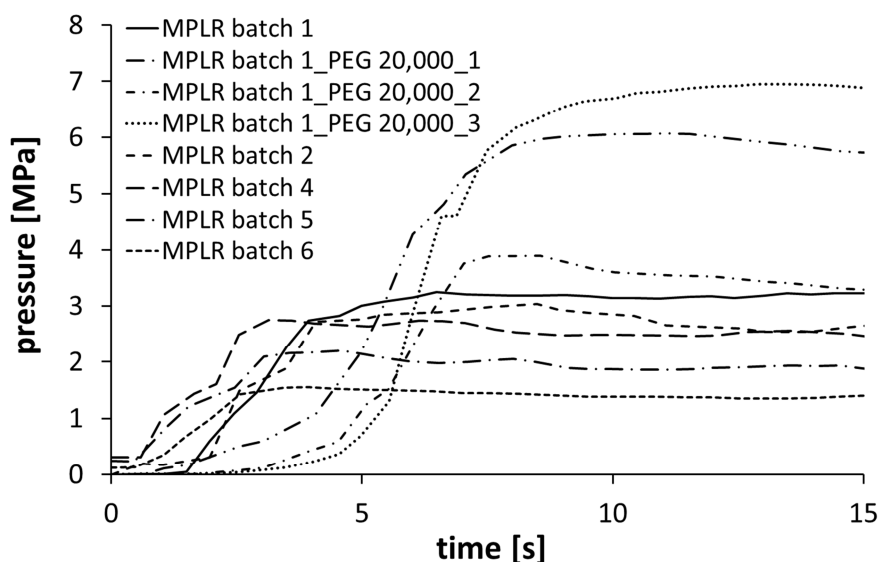


Figure 61: Extrusion profiles recorded during the production of the MPLRs via ram-extrusion, MPLR batches 1, 2, and 4 - 6 and MPLR batches 1_PEG 20,000_1 - 3

Regarding the extrusion temperature the process was not very robust, as the (semi-)crystalline excipients were processed near their melting temperature (T_m PEG 20,000: 64 °C). The process parameters of MPLR batch 1_PEG 20,000_2 and MPLR batch 1_PEG 20,000_3, for instance, differed only slightly in the extrusion

temperature. Still, decreasing the temperature of 1 °C strongly affected the viscosity of the formulation and finally resulted in doubling of the pressure value (Table 16).

Figure 61 presents the pressure profiles recorded during the production of the MPLRs by ram-extrusion. Three different stages occurred within the ram-extrusion process: (1) a compression stage, in which the material was compressible by low forces, (2) an increase in pressure, before the material was forced through the die, and (3) a steady state stage reflecting continuous extrusion. A long and uniform steady state stage - as observed for both matrices - is indicative for a material with good extrusion properties leading to a satisfying quality of extrudates (Podczeck et al., 2008).

The sustained release coated micropellets of batch 2 and the corresponding MPLRs are exemplarily illustrated in Figure 62.

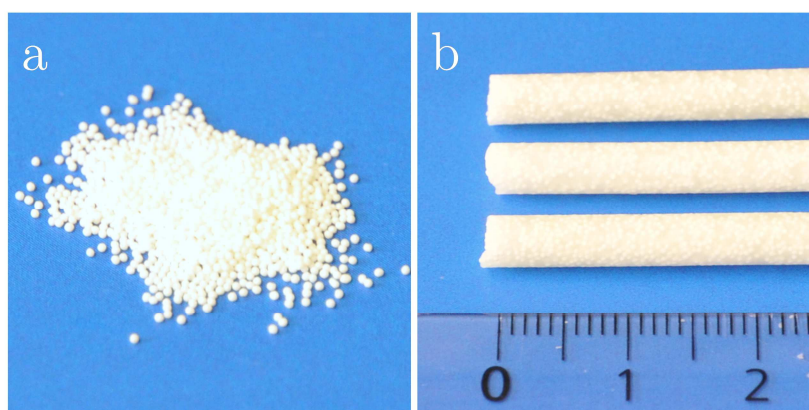


Figure 62: Sustained release coated micropellets and MPLRs (both batch 2), displayed scale in cm

In line with the interpretation of the extrusion profiles, the ram-extrudates showed a dense structure and a smooth extrudate surface. The micropellets were clearly visible inside the rods near the surface and did not seem to be damaged mechanically.

3.3.5.2. Mechanical Properties

As described for the small-scale ram-extrudates and the drug-loaded rods, the mechanical properties of the MPLRs based on PEG 2,000 and PEG 1,500 were determined by a Texture Analyser (sections 6.2.3.1 and 6.2.3.2). Table 17 presents F_{\max} , tensile strength, and E-modulus of MPLR batches 1, 2, and 4 - 6.

F_{\max} and the tensile strength of the MPLRs were smaller compared to the extrudates which had the same diameter and contained PEGs 2,000 and 1,500 as well (35.8 ± 2.4 to 37.2 ± 1.6 N and 7.4 ± 0.2 to 8.6 ± 0.5 MPa). Besides, the tensile strength of the MPLRs was smaller than the one of the small-scale ram-extrudates containing PEG 2,000 and 30 % CBZ (8.2 ± 1.7 MPa).

Table 17: F_{\max} ($n = 10$), tensile strength, and E-modulus (both $n = 5$) for MPLR batches 1, 2, 4 - 6, determined by a Texture Analyser equipped with a cutting test set-up or with a three-point bending rig; mean \pm SD

formulation	F_{\max} [N]	tensile strength [MPa]	E-modulus [MPa]
MPLR batch 1	27.7 ± 2.1	6.4 ± 0.2	202.4 ± 4.0
MPLR batch 2	25.1 ± 3.3	7.0 ± 0.3	257.3 ± 6.6
MPLR batch 4	25.4 ± 2.3	5.9 ± 0.5	241.6 ± 6.7
MPLR batch 5	26.3 ± 1.9	6.3 ± 0.5	243.5 ± 23.1
MPLR batch 6	26.5 ± 2.9	6.7 ± 0.3	220.7 ± 11.2

These observed differences may have occurred because of the larger fraction of the added excipient PEG 1,500 in the MPLRs (21 % in the MPLRs versus 0 to 15 % in the other extrudates). A higher fraction of PEG 1,500 may have decreased F_{\max} , as the cuttability was majorly influenced by the binder (section 3.1.3.2).

In contrast, the E-modulus resulted in markedly higher values of the MPLRs (202.4 ± 4.0 to 257.3 ± 6.6 MPa) than of the extrudates (48.6 ± 7.1 to 65.0 ± 12.2 MPa). In fact, the E-moduli of the MPLRs were more comparable to those of the small-scale ram-extrudates made from PEG 2,000 and containing 30 % CBZ (579 ± 82 MPa). Thus, the different manufacturing technique and the incorporation of different particle sizes ($\leq 500 \mu\text{m}$ for the coated pellets versus $132.6 \mu\text{m}$ as x_{50} -value for the CBZ particles) may have resulted in a less flexible behaviour expressed in an increase of the E-modulus of the MPLRs.

Figure 63 exemplarily illustrates the cross-sections of sliced MPLRs. Cutting the rods with a razor blade resulted in non-deformed and smooth cross-sections (Figure 63 a) with properly sliced coated micropellets, which remained tightly embedded within the matrix material (Figure 63 b - d).

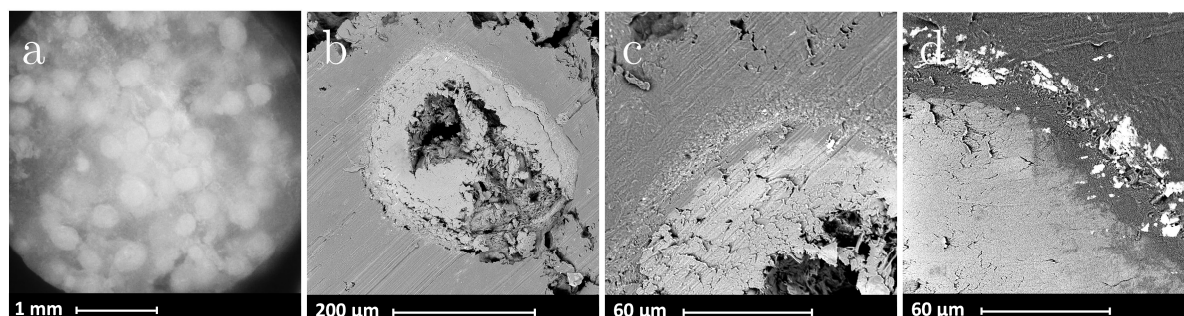


Figure 63: Cross-sections of the sliced MPLRs, optical microscopy image (a) and SEM micrographs (b - d) exemplary of batch 4 (a - c) and batch 1 (d) in overview (b) and detail (c - d)

These sliced pellets at the cross-section may result in an instantaneous drug release during dissolution, but regarding the ratio of cut pellets at the cross-section to intact pellets inside the matrix, this effect was assumed to be small. Still, the dependency of the dissolution behaviour of the MPLRs on the number of pieces and thus on the number of cross-sections will be investigated further in the next section.

3.3.5.3. Disintegration Time and Dissolution Studies

The aim of the development of the MPLRs predominantly was, to produce a drug release which is independent of the dose, geometry, and size of the cut slices. Therefore, the disintegration of the MPLRs is important, as the release characteristics may be altered by the matrix until the disintegration of the dosage form is completed. Hence, a fast disintegration is desirable.

Disintegration testing was performed according to Ph. Eur. 2.9.1 (section 6.2.3.6): MPLR pieces (10 mm in length) were placed into the tubes of the basket-rack assembly and discs were added to avoid previously detected floating tendencies of the MPLR pieces. The disintegration was observed within the immersion fluid during the movement of the basket-rack assembly.

In Figure 64 the disintegration time of the MPLR batches containing lower and higher molecular weight PEGs are presented. MPLR batch 4 adhered to the discs and the walls of the basket-rack assembly for unknown reasons. Thus, the disintegration times of this batch could not be precisely determined.

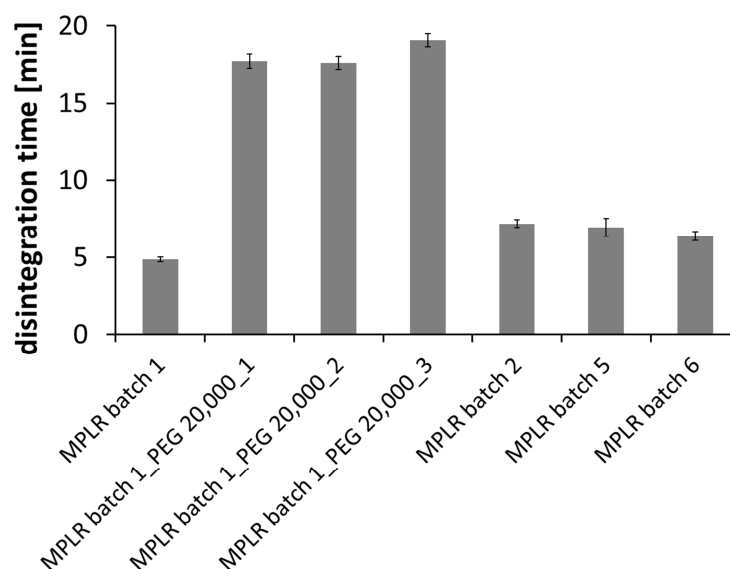


Figure 64: Disintegration of MPLRs (batches 1, 2, 5, and 6, and batches including PEG 20,000); disintegration tester Ph. Eur. (DT2 Sotax), in degassed, demineralised water at 37 ± 2 °C, with discs (n = 6; mean \pm SD)

For the MPLRs, in addition to the disintegration properties the dissolution characteristics were investigated in a paddle apparatus according to Ph. Eur. 2.9.3 (section 6.2.3.7). Figure 65 illustrates the dissolution profiles of the sustained release coated pellets from batch 1 in comparison to the corresponding MPLRs made from the lower and the higher molecular weight PEGs and including 30 % (w/w) pellets.

MPLRs made from PEG 2,000 and 1,500 disintegrated within 5 to 7 min, which was assessed as a suitable disintegration time, as a disintegration time below 15 min would fulfil the pharmacopoeial requirements for an immediate release dosage form. When PEG 20,000 was utilised as matrix material, the disintegration time increased to 18 to 19 min bearing the risk of influencing the CBZ liberation from the matrix within this time span.

The differences in disintegration time of matrices made from PEG with different M_w may also be an explanation for the observed variances in dissolution rate for the small-scale extrudates (section 3.1.3.3).

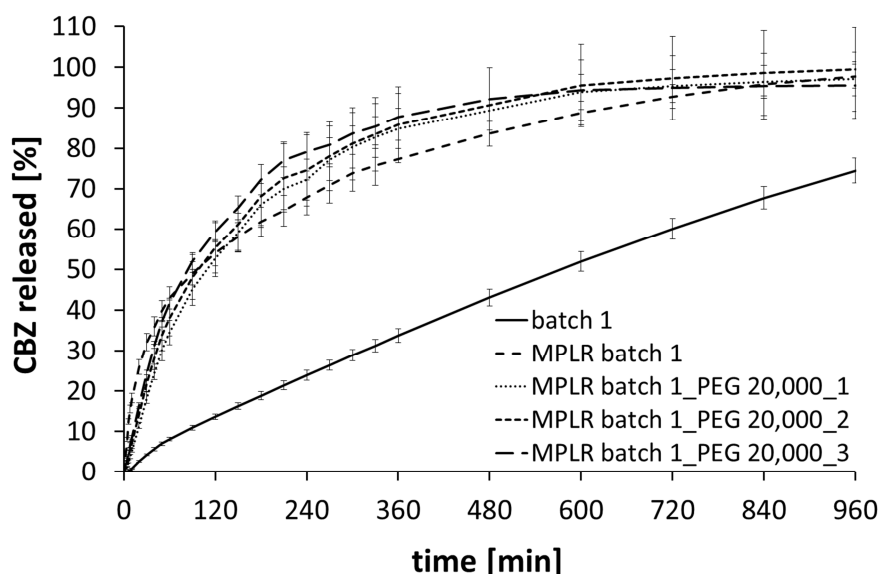


Figure 65: CBZ release of sustained release pellets from batch 1 and the corresponding MPLRs with PEG 2,000 (MPLR batch 1) and MPLRs with PEG 20,000 as matrix, manufactured with different production parameters (MPLR batches 1_PEG 20,000_1 - 3); apparatus 2, 75 rpm in 900 mL of degassed, demineralised water at 37.0 ± 0.5 °C ($n \geq 3$; mean \pm SD)

Independently of the selected matrix and the investigated process parameters, the MPLRs showed a faster CBZ release and the shape of the release curves was altered compared to the pellets before embedding. This effect may be due to an undesirable interaction of the Eudragit® RS/RL polymer with the matrix, but also of the used plasticiser (2.4 % triethyl citrate, TEC) with the matrix. Lower molecular weight PEGs (PEG 600 and 1,000) were found to be non-suitable carrier materials for Eudragit® RS/TEC-coated pellets, as they dissolved the coatings and led to a significantly higher permeability (Schmidt and Bodmeier, 2001). In contrast, storage stability was confirmed by the same workgroup over

a six months period for Eudragit® RS/TEC-coated pellets incorporated in PEGs 4,000 and 10,000 as matrices, if stored at 4 °C. In the present work, TEC as hydrophilic plasticiser may have leached in the PEG matrix independently from the utilised M_w of PEG, resulting in an enhanced drug release due to an increase in water permeability of the coating (Schultz et al., 1997).

Figure 66 depicts the results of the dissolution testing of batch 2 containing PVAc and batches 4 - 6 containing PVAc/PVA-PEG as polymers and the corresponding MPLR batches. For these batches the MPLRs exhibited similar dissolution characteristics as the non-embedded pellets. Only MPLR batch 4 showed a small burst effect which was not noticed for the pellets of batch 4. The dissolution rates of MPLR batches 5 and 6 were a little lower than those of the non-embedded pellets.

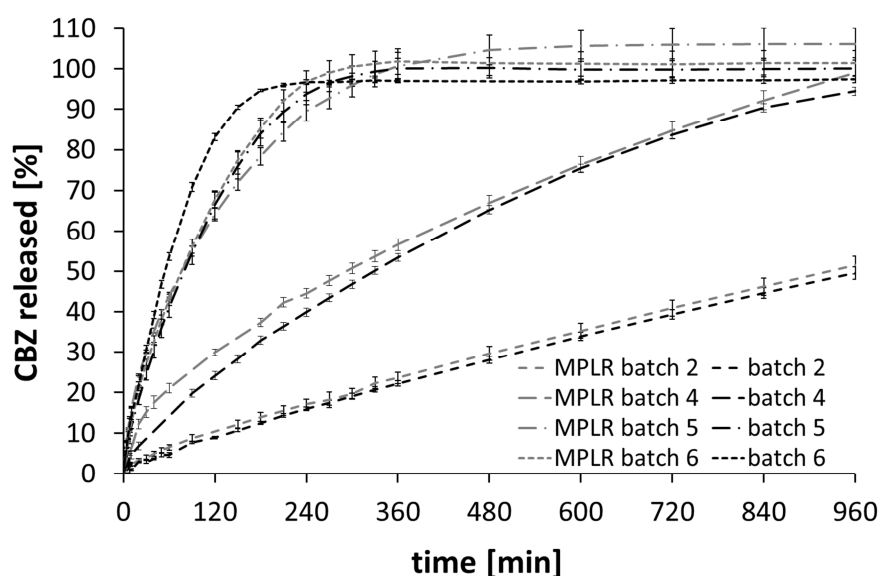


Figure 66: CBZ release of the sustained release micropellets (batches 2 and 4 - 6) and the corresponding MPLRs (MPLR batches 2, and 4 - 6); apparatus 2, 75 rpm in 900 mL of degassed, demineralised water at 37.0 ± 0.5 °C ($n \geq 3$; mean \pm SD)

One major idea behind the development of the MPLRs was the achievement of dissolution profiles, which were independent of the number and masses of administered pieces and of the over-all dose.

Figure 67 a exemplarily shows the CBZ release of pellets from batch 2 and the corresponding MPLRs. The MPLRs had a total mass of 300 mg, cut into one, two, or four pieces of 300, 150, or 75 mg each. The examination of different numbers and masses of MPLR pieces also involves the number of cross-sections, which varied from 2 to 8. The dissolution profiles demonstrate the independence of the dissolution characteristics of the number and masses of the pieces. Thus, the quantity of cut micropellets at the cross-sections of the MPLRs may be neglected compared to the total number of pellets (section 3.3.5.2).

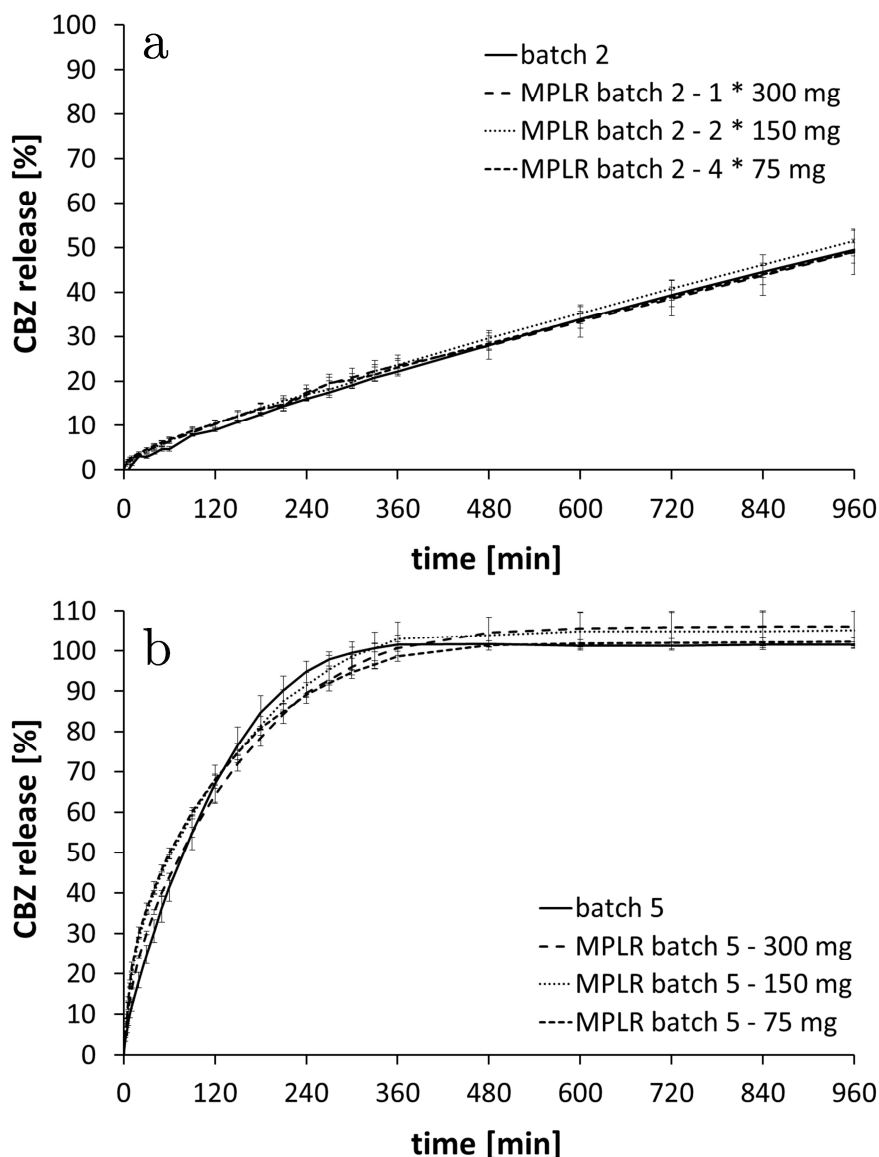


Figure 67: CBZ release of the sustained release micropellets (batch 2 (a) and batch 5 (b)) and different numbers and masses of pieces of MPLR batch 2 (a) and different doses of MPLR batch 5 (b); apparatus 2, 75 rpm in 900 mL of degassed, demineralised water at 37.0 ± 0.5 °C ($n \geq 3$; mean \pm SD)

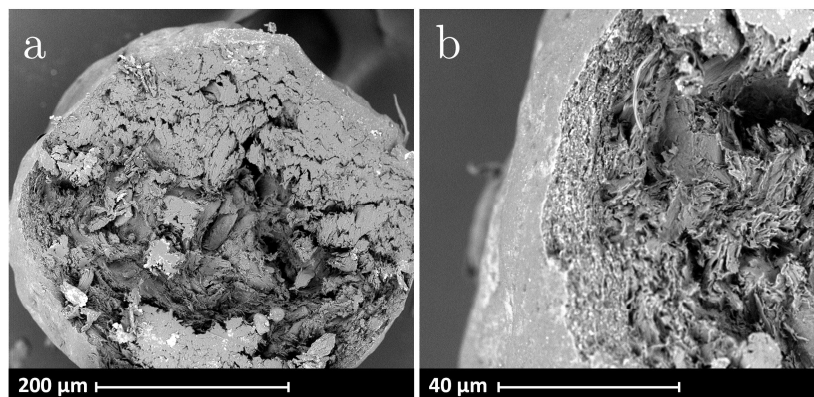


Figure 68: SEM micrographs of the cross-cut of a pellet which was embedded in MPLR batch 4 after 16 h of dissolution in 900 mL of degassed, demineralised water at 37.0 ± 0.5 °C; in overview (a) and detail (b)

The dissolution profiles of different doses of the MPLRs are exemplarily shown for batch 5 in Figure 67 b. The liberation of the drug was found to be independent of the investigated dose as dissolution profiles of doses of 75, 150, and 300 mg formulation proved to be similar.

The pellets of the MPLRs after dissolution were investigated via SEM and were still found intact, comparable to the non-embedded pellets after dissolution (Figure 57). Figure 68 exemplarily depicts the cross-cut of a pellet which had been embedded into a rod (MPLR batch 4) after 16 h of dissolution.

3.3.5.4. Application of the Solid Dosage Pen

The MPLRs containing a pellet-loading of 30 % (w/w) were investigated with regard to the application via the SDP: Exemplarily, ten doses with 10 DUs (corresponding to 4 mm length) were sliced from the MPLRs with the SDP (section 6.2.4.1). Mass and content of the doses were determined and are presented in Table 18.

Table 18: Mass and content of doses with 10 DUs (corresponding to 4 mm length), cut from the MPLRs with the SDP, $n = 10$, mean \pm SD; and the x_{50} -values of the corresponding micropellets, $n = 3$, mean \pm SD

MPLR batch	1	2	4	5	6
mass [mg]	62.4 \pm 0.9	61.2 \pm 1.1	62.2 \pm 1.0	60.6 \pm 0.7	60.9 \pm 0.8
content [%]	91.1 \pm 4.2	108.0 \pm 7.8	124.4 \pm 7.6	109.6 \pm 5.4	100.5 \pm 3.6
batch	1	2	4	5	6
x_{50} -value	426.3 \pm 0.4	448.4 \pm 0.6	432.7 \pm 0.4	434.5 \pm 0.4	312.6 \pm 0.3

The standard deviation of the mass of the sliced doses was not larger than 1.1 mg for all batches and hence comparable to those observed for the extrudates and the co-extrudates (sections 3.2.2.6 and 3.2.3.7).

As one major disadvantage, the content of the single doses sliced from the MPLRs varied from 91.1 \pm 4.2 to 124.4 \pm 7.6 %. This unsatisfying result may be explained by the process of ram-extrusion in which hardly any distributive mixing is performed. Moreover, a tendency of separation of the pellets and the milled PEG particles during the filling of the HPCR barrel has been observed. This separation was probably due to the different particle sizes (x_{50} -value of the milled PEG: 343 \pm 13 μ m vs. x_{50} -values of the pellets: 426 \pm 0.4 - 448.4 \pm 0.6 for batches 1 to 5) and different bulk densities of the milled PEG (0.60 g/mL) and of the sustained release micropellets (0.82 g/mL). A difference in density was not observed among the different sustained release micropellet batches. A further separation may also happen during ram-extrusion, as the softened PEGs probably behave differently under compression than the non-softened pellets. The problem of

inhomogeneity may be improved or even overcome by the utilisation of a single screw extruder as conducted by Schilling and McGinity (2010).

MPLRs batch 6 including smaller micropellets (x_{50} -value of $312.6 \pm 0.3 \mu\text{m}$) demonstrated a content of 100.5 % with a standard deviation $\leq 4 \%$ (Table 18). The mixture showed less pronounced separation when filled into the barrel, due to a smaller particle size difference ($30 \mu\text{m}$) compared to particle size differences of 84 to $106 \mu\text{m}$ for batches 1 to 5.

3.3.5.5. Stability Studies

To examine if the dissolution behaviour changed after storage, stability testing was performed over a period of 10 weeks ($21.0 \pm 0.2 \text{ }^\circ\text{C}$; 45 % RH) and the dissolution testing was repeated for the sustained release micropellets and the MPLRs.

Figure 69 a exemplarily depicts the dissolution profiles of batch 2 and the corresponding MPLRs after production and after storage. For batch 2, the drug dissolution rate of the pellets slightly decreased after 10 weeks, whereas the MPLRs exhibited a slightly faster CBZ release after storage. For batch 1 similar effects were observed (data not shown). On the one hand these findings may be explained by the curing of the polymer coating of the sustained release pellets leading to a slight decrease in dissolution rate (Ensslin et al., 2009) and on the other hand solubilisation tendencies of the film coating in the PEG-matrix of the MPLRs led to a slight increase in dissolution rate.

For batches 5 and 6 the dissolution characteristics neither changed for the pellets nor for the MPLRs after storage (Figure 69 b and c). The corresponding pellets contained a blend of PVAc/PVA-PEG and the addition of PVA-PEG to a PVAc film has already demonstrated a positive effect on the storage stability (Ensslin et al., 2009). A plasticising effect of PVA-PEG on PVAc films and a reduction in glass transition temperature (T_g) after the addition of PVA-PEG to PVAc casted films have previously been reported (Müller et al., 2008) and might be the reason for the improved storage stability.

Moreover, a lower spray rate was utilised in the coating process for batches 4, 5, and 6. For these batches a proceeding coalescence of the film forming particles may have led to a denser and thus more robust film (Ensslin et al., 2009).

In line with these explanations, batch 4, containing only 10 % PVA-PEG, exhibited a small decrease in dissolution rate after storage for the pellets, but not for the MPLRs (data not shown).

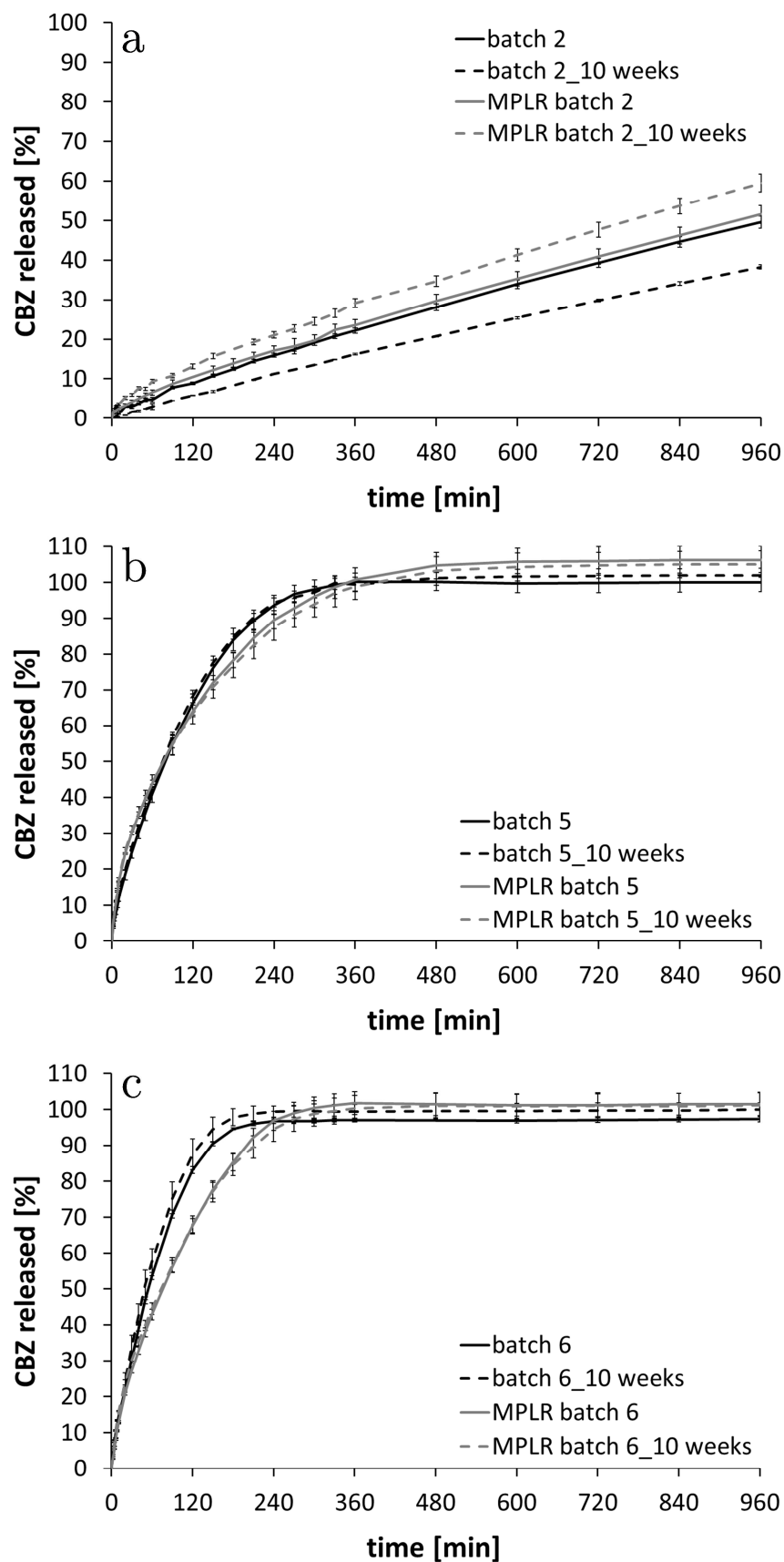


Figure 69: CBZ release of the sustained release micropellets and the MPLRs after production and after 10 weeks of storage; batch 2 (a), batch 5 (b), and batch 6 (c); apparatus 2, 75 rpm in 900 mL of degassed, demineralised water at 37.0 ± 0.5 °C ($n \geq 3$; mean \pm SD)

3.3.6. Summary

CBZ micropellets were successfully manufactured by layering CBZ on MCC microspheres with PVA-PEG as binder with high binding capacity for solids. Coating of the CBZ micropellets with Eudragit® RS/RL and PVAc resulted in sustained release profiles showing constant drug release over time, but low dissolution rates. The addition of PVA-PEG as a pore-forming agent within the PVAc film increased the drug dissolution rate of the sustained release micropellets. The different mechanisms of drug liberation depended on the applied coating polymers and were amongst others explained by examination of the pellet surface morphology and cross-cuts via SEM before and after dissolution.

The tensile strength of the sustained release pellets, which had a size of approximately 300 to 450 µm depending on the utilised starter cores, was more than two times higher than pressures occurring during ram-extrusion. Due to relative crystallinities above 93 % for PVAc and PVA-PEG a low solubility of the coating films within the PEG matrix was assumed. Thus, with PVAc and PVAc/PVA-PEG the sustained release pellets were successfully incorporated into MPLRs by ram-extrusion and drug release properties of the pellets were remained after they had been embedded into the matrix. However, differences in size and density of the pellets and the particles of the matrix-material resulted in separation of the mixture for pellets above 400 µm during the filling of the barrel prior to ram-extrusion.

The mechanical properties of the MPLRs permitted the application of the SDP and for embedded particles with a size below 350 µm a precise drug delivery of single doses was feasible. Moreover, the MPLRs provided drug liberation, which was independent of the number and masses of pieces and of the over-all dose. Storage stability was proven for MPLRs containing PVAc/PVA-PEG coated pellets.

4. Summary

This work focuses on the development, the manufacturing, and the characterisation of melt-extruded rods for the application by the Solid Dosage Pen (SDP) - a device which permits individual dosing by cutting slices of pre-defined heights from these rods. The field of application of the SDP was broadened to drugs with higher doses, like the chosen model drug carbamazepine (CBZ), by the production of rods with a larger diameter (4 mm) and the new design of the existing prototype of the SDP.

First, small-scale production techniques were elaborated to conduct an excipient screening for the formulation development. A high pressure capillary rheometer allowed for the manufacturing of ram-extrudates with only 10 g material input. This way, the exploration of mechanical properties, dissolution behaviour, and solid state characteristics was feasible at small-scale. Second, and based on the experiences in the small-scale, extrudates containing polyethylene glycols (PEGs) and poloxamers as excipients were produced by twin-screw melt-extrusion. Furthermore, co-extrusion as a new and more sophisticated technique was successfully applied. By the adjustment of the dissolution behaviour, the mechanical properties, and the process parameters of the extrudates appropriate coat and core formulations were chosen. Third, for the embedding of multiparticulates into a matrix, CBZ micropellets were manufactured and coated with Eudragit® RS/RL, PVAc and PVAc/PVA-PEG. These micropellets, sized 300 to 450 µm, were then successfully incorporated into rods via ram-extrusion due to their adequate tensile strength and due to a low solubility of the film coating within the matrix.

By the utilisation of different matrices, added excipients, pore-forming agents, drug-loadings and applied production techniques tailored dissolution kinetics were achieved with immediate, biphasic, and sustained release characteristics. For hydrophilic matrices like PEGs with different molecular weights, a higher CBZ-loading resulted in lower drug dissolution rates. For lipophilic matrices like stearic acid or poly(ϵ -caprolactone) the dissolution rates were low and pore-forming agents only marginally impinged on the CBZ release. Nevertheless, for drugs with a higher solubility, matrix formulations based on lipophilic matrices could be valuable. Extrudates exhibiting sustained release characteristics showed cube root kinetics, whereas wax-coated (co-)extrudates followed a zero order release mechanism after 3 h. Dissolution profiles with constant CBZ release over time and without a burst effect were made accessible by the micropellet-loaded rods (MPLRs) containing Eudragit® RS/RL and PVAc coated CBZ micropellets. The addition of PVA-PEG as a pore-forming agent within the PVAc film increased the drug dissolution rate of the sustained release micropellets but also changed the dissolution mechanism. The different mechanisms of drug liberation depended on the applied coating polymers and were explained amongst others by the investigation of the pellets' surface morphology and cross-cuts via SEM before and after dissolution. Finally, dose-dependent dissolution behaviour of sustained release formulations was minimised by

applying a wax-coating via co-extrusion and even completely overcome by the embedding of micropellets into rods. The dissolution profiles of the extrudates and co-extrudates as well as the micropellet-loaded rods containing PVAc/PVA-PEG coated pellets did not alter after storage at ambient temperature and 45 % RH. As an outlook, the approach of the MPLR opens up new possibilities like enteric-coated dosage forms for the SDP.

For the first time, the mechanical properties of rods intended for the application by the SDP were systematically investigated by the evaluation of the maximum cutting force, the tensile strength and the E-modulus. While cuttability was mainly influenced by the utilised binder, both tensile strength and E-modulus were affected by the CBZ-loading. Moreover, the mechanical properties were purposefully modulated by suitable excipients and the optical appearance of the sliced doses was improved by PEG 1,500. The formulations in conjunction with the device were shown to be generally suitable for patient-centred treatment: The required cutting forces for the drug-loaded rods (below 41.9 ± 1.7 N) were in the range of the manual forces of different age groups, resulting in appropriateness even for the elderly and for school children.

Due to their adequate mechanical properties and - in the case of the co-extrudates - due to a suitable layer adhesion of core and coat, all drug- and micropellet-loaded rods were sliceable by the newly designed SDP. As no hard edges or splinters occurred, a safe swallowing can be assumed. The mass uniformity of sliced doses was influenced by the mechanical properties of the rods: Firstly, formulations which exhibited a cut were more suitable for the utilisation of the SDP than those exhibiting a break. Secondly, tensile strength and E-modulus were shown to be valuable indicators for the applicability of the SDP. A tensile strength below 9.1 ± 0.3 MPa and an E-modulus below 135.9 ± 7.2 MPa were determined as thresholds for future formulation development. Regarding the uniformity of dosage units the pharmacopoeial requirements were met for extrudates containing PEG 1,500 and also for the dual drug release co-extrudates. Contrarily, for the wax-coated co-extrudate differences of the process parameters between the core- and the coat-layer resulted in unsatisfying content uniformities. For MPLRs including particles sized below 350 μ m a precise drug delivery of single doses was reached.

A thorough understanding of the solid state properties of CBZ within the formulations was built up within this work. Solid state analysis via XRPD, SEM or Raman-spectroscopy, for example, revealed that the utilised manufacturing techniques did not change the modification of the drug and all formulations enclosed the required modification of CBZ III.

To conclude, innovative production processes, new analytic methods and novel formulations were established for peroral solid dosage forms for the SDP. The melt-extruded formulations allowed for individual dosing by the SDP and could therefore provide a new platform in personalised medicine as well as in paediatrics and geriatrics.

5. Zusammenfassung

Im Rahmen dieser Arbeit wurden Schmelzextrudate für die perorale Applikation durch ein neuartiges Dosiersystem, den Solid Dosage Pen (SDP), entwickelt, hergestellt und charakterisiert. Der SDP ermöglicht die individuelle Dosierung fester zylindrischer Arzneiträger durch das Abteilen tablettenartiger Scheiben. Die Anwendbarkeit dieses Dosiersystems wurde für höher dosierte Arzneistoffe wie den Modellarzneistoff Carbamazepin (CBZ) ausgeweitet, indem Schmelzextrudate mit größerem Durchmesser (4 mm) produziert wurden und der Prototyp des SDP angepasst wurde.

Für die Formulierungsentwicklung wurden zunächst Produktionsmethoden im Kleinstmaßstab ausgearbeitet, um die mechanischen Eigenschaften, das Freisetzungverhalten und die Festphaseneigenschaften zu untersuchen. Ein Hochdruck-Kapillarrheometer wurde hierfür als Kolbenextruder mit nur 10 g Materialeinsatz verwendet. Basierend auf den gewonnenen Kenntnissen aus dem Kleinstmaßstab wurden Extrudate aus Polyethylenglykolen (PEG) und Poloxamer mit Hilfe der Doppelschnecken-Schmelzextrusion produziert. Des Weiteren wurde die Co-Extrusion als neue und anspruchsvolle Technik erfolgreich angewendet, wobei für die Auswahl geeigneter Kern- und Mantelformulierungen der konzentrischen Co-Extrudate das Freisetzungverhalten, die mechanischen Eigenschaften und die Prozessparameter der Einzel-Extrudate aneinander angepasst wurden. Darüber hinaus wurden 300 bis 450 µm kleine, mit Eudragit® RS/RL, PVAc oder PVAc/PVA-PEG befilmte, CBZ-Mikropellets hergestellt. Mittels Kolbenextrusion gelang eine erfolgreiche Einbettung dieser Pellets in eine Extrudat-Matrix auf Grund einer ausreichenden Bruchfestigkeit der Pellets und geringer Löslichkeit des Polymerfilms in der Matrix.

Durch die Verwendung unterschiedlicher Matrices, Hilfsstoffe, Porenbildner, Arzneistoffbeladungen und Produktionsmethoden ist es in dieser Arbeit gelungen, Freisetzungskinetiken mit unveränderter Freisetzung, biphasischem Freisetzungverlauf und verlängerter Freisetzung zu erzielen. Für hydrophile Matrices wie PEG führte eine höhere CBZ-Beladung zu geringeren Freisetzungsraten, wohingegen diese für lipophile Matrices wie Stearinsäure oder Poly(ϵ -caprolacton) insgesamt gering waren und die Freisetzung auch durch die Verwendung von Porenbildnern nur geringfügig beschleunigt werden konnte. Diese lipophilen Matrixformulierungen könnten für Arzneistoffe mit einer höheren Löslichkeit dennoch wertvoll sein. Extrudate, die eine verlängerte Freisetzung zeigten, folgten einer Kubikwurzel-Kinetik, wohingegen die Co-Extrudate mit Wachsmantel nach einer vermehrten Freisetzung des Arzneistoffs zu Beginn der Freisetzung im späteren Verlauf einer Kinetik nullter Ordnung folgten. Profile mit einer konstanten Freisetzung von CBZ ohne stärkere Freisetzung zu Beginn wurden durch die in Extrudate eingebetteten, mit Eudragit® RS/RL oder PVAc befilmten Mikropellets ermöglicht. Der Zusatz von PVA-PEG als Porenbildner in den PVAc-Polymerfilm steigerte die Freisetzung unter Änderung des Mechanismus. Die unterschiedlichen

Freisetzung-mechanismen konnten unter anderem durch die Untersuchung der Morphologie der Pelletoberfläche und der Querschnitte der Pellets, die vor und nach der Freisetzung erfolgte, erklärt werden. Die Abhängigkeit des Freisetzungsverhaltens von der Extrudatlänge und der Dosis konnte durch die Co-Extrudate mit Wachsmantel verringert und schließlich durch die Einbettung von Mikropellets in Extrudate völlig überwunden werden. Die Freisetzungsprofile der Einzel- und Co-Extrudate sowie der Extrudate mit PVAc/PVA-PEG befilmten Mikropellets waren nach einer Lagerzeit bei Raumtemperatur und 45 % relativer Feuchte unverändert. Als Ausblick in die Zukunft könnten auch magensaftresistente Arzneiformen für den Gebrauch des SDP durch die in Extrudate eingebettete, befilmte Mikropellets ermöglicht werden.

Im Rahmen dieser Arbeit wurden zum ersten Mal die mechanischen Eigenschaften der Arzneiträger für die Anwendung des SDP durch die Bestimmung und Bewertung der maximalen Schneidkraft, der Biegefestigkeit und des E-Moduls systematisch untersucht. Während die maximale Schneidkraft am stärksten durch die verwendete Matrix bestimmt wurde, zeigten die Biegefestigkeit und der E-Modul auch eine Abhängigkeit von der Arzneistoffbeladung. Darüber hinaus wurden die mechanischen Eigenschaften zielgerichtet durch geeignete pharmazeutische Hilfsstoffe moduliert. Die optische Erscheinung der abgeteilten Arzneiträger wurde durch PEG 1500 verbessert. In der Literatur beschriebene maximale manuelle Kräfte verschiedener Altersgruppen überstiegen die benötigten maximalen Schneidkräfte der hergestellten Arzneiträger, weswegen diese zusammen mit dem Dosiersystem als geeignet für patientengerechte Behandlung bewertet wurden. Auf Grund ihrer adäquaten mechanischen Eigenschaften und - im Falle der Co-Extrudate - auf Grund der geeigneten Adhäsion ihrer Schichten waren alle hergestellten Extrudate mit dem angepassten SDP schneidbar. Da keine harten Kanten oder Splitter bei der Dosierung auftraten, wurde von einer sicheren Verabreichung der abgeteilten Arzneiträger ausgegangen. Deren Einheitlichkeit der Masse wurde wiederum von den mechanischen Eigenschaften beeinflusst: Formulierungen, die einen Schnitt bei der Dosierung zeigten, waren besser geeignet, als solche die brachen. Außerdem wurde gezeigt, dass die Biegefestigkeit (unter $9,1 \pm 0,3$ MPa) und der E-Modul (unter $135,9 \pm 7,2$ MPa) wertvolle Indikatoren für die Anwendbarkeit des Dosiersystems waren. Aus den Untersuchungen konnten somit Schwellenwerte für die Formulierungsentwicklung abgeleitet werden.

Die Anforderungen des Europäischen Arzneibuches bezüglich der Gleichförmigkeit einzeldosierter Arzneiformen wurden für Extrudate mit PEG 1500 sowie für die Co-Extrudate mit biphasischem Freisetzungsprofil erfüllt, jedoch für Co-Extrudate mit Wachsmantel auf Grund unterschiedlicher Prozessparameter der Kern- und Mantelformulierung nicht. Für die in Extrudate eingebetteten Mikropellets mit einer Größe unter $350 \mu\text{m}$ konnte für die abgeteilten Arzneiträger ein gleichförmiger Arzneistoffgehalt erzielt werden.

In dieser Arbeit wurde ein fundiertes Verständnis der Festphaseneigenschaften des CBZ in den Arzneiträgern erarbeitet. Mittels Untersuchungsmethoden wie Röntgen-diffraktometrie, Rasterelektronen-Mikroskopie oder Raman-Spektroskopie wurde gezeigt, dass es durch die verwendeten Herstellungsmethoden nicht zur Umwandlung der Kristallstruktur kam, weshalb alle Arzneiträger die erforderliche Modifikation CBZ III enthielten.

Zusammenfassend lässt sich sagen, dass durch innovative Herstellungsverfahren neue Arzneiformen für den SDP etabliert wurden und diese durch geeignete analytische Methoden auf ihre Eigenschaften und Eignung untersucht wurden. Die durch Schmelzextrusion hergestellten Arzneiträger ermöglichen eine individuelle Dosierung mit Hilfe des SDP und könnten daher eine neue Technologie-Plattform für die personalisierte Medizin sowie für die Pädiatrie und Geriatrie darstellen.

6. Experimental Part

6.1. Materials

Table 19: The model drug carbamazepine (CBZ); particle size ($n = 3$, mean \pm SD) determined by dynamic image analysis (section 6.2.3.5)

substance	batch no	source of supply	particle size [μm]*		
			X ₂₅	X ₅₀	X ₇₅
carbamazepine F	0005927194	BASF Pharma, Switzerland	63 \pm 3	133 \pm 6	277 \pm 12

Table 20: Substances utilised as excipients for the extrusion

substance	name/grade	source of supply
amino-polymethylmethacrylat (aPMMA)	Eudragit® E PO	Evonik, Darmstadt, Germany
carnauba wax	Ph. Eur. 6.0	Caesar & Loretz, Hilden, Germany
colloidal silicium dioxide	Aerosil® 200	Evonik, Hanau, Germany
poly(ϵ -caprolactone)	Capromer® PD1-20	BASF Corporation, New York, USA
hydroxypropyl cellulose (HPC)	Klucel™	Ashland, Wilmington, USA
hydroxypropyl methylcellulose, hypromellose (HPMC)	Pharmacoat® 606	Shin-Etsu, Tokyo, Japan
hydroxypropyl methylcellulose acetate succinate (HPMC AS)	Aqoat® AS-MF	Shin-Etsu, Tokyo, Japan
isomalt	Galen IQ® 720	Beneo-Palatinit, Mannheim, Germany
mannitol	Pearlitol® C 160	Roquette, Lestrem, France
poloxamer 188	Kolliphor® P 188 micro	BASF, Ludwigshafen, Germany
polyethylene glycol (PEG)		Clariant, Frankfurt am Main, Germany
$M_w = 1,500$ g/mol	Polyglycol 1500 S	
$M_w = 2,000$ g/mol	Polyglycol 2000 S	
$M_w = 4,000$ g/mol	Polyglycol 4000 P	
$M_w = 10,000$ g/mol	Polyglycol 10000 P	
$M_w = 20,000$ g/mol	Polyglycol 20000 P	
polyethylene oxide (PEO)		Colorcon, Dartford, United Kingdom
$M_w = 100,000$ g/mol	Polyox™WSR N-10	
$M_w = 200,000$ g/mol	Polyox™WSR N-80	
$M_w = 1,000,000$ g/mol	Polyox™WSR N-12K	

polyvinyl pyrrolidone/polyvinyl acetate copolymer (PVP-PVA copolymer)	Kollidon® VA 64	BASF, Ludwigshafen, Germany
polyvinyl alcohol-polyethylene glycol graft polymer (PVA-PEG)	Kollicoat® IR	BASF, Ludwigshafen, Germany
povidone, polyvinyl pyrrolidone, (PVP)	Kollidon® 12 PF Kollidon® 17	BASF, Ludwigshafen, Germany
stearic acid	Baerocid® SMS-1A	Baerlocher, Lingen, Germany
stearoyl macrogol-32 glycerides	Gelucire® 50/13	Gattefossé, Saint-Priest, France
sucrose palmitate	Surfhope® D-1616	Mitsubishi-Kagaku, Tokyo, Japan
white bees wax (<i>cera alba</i>)	Ph. Eur. 7.0	Caesar & Loretz, Hilden, Germany
xylytol	Xylisorb® 300	Roquette, Lestrem, France

Table 21: Substances utilised for the layered micropellets

substance	name/grade	source of supply
ammonio methacrylate copolymer dispersion, type A - NF	Eudragit® RL 30 D	Evonik, Darmstadt, Germany
ammonio methacrylate copolymer dispersion, type B - NF	Eudragit® RS 30 D	Evonik, Darmstadt, Germany
glycerol monostearate 60	DAC 2010	Caesar & Loretz, Hilden, Germany
hypromellose (HPMC)	Pharmacoat® 603 Pharmacoat® 606	Harke, Mülheim an der Ruhr, Germany
micropellets (microcrystalline cellulose)	Cellets® 200 Cellets® 350	Harke, Mülheim an der Ruhr, Germany
polysorbate 80	Ph. Eur. 7.0	Caesar & Loretz, Hilden, Germany
polyvinyl alcohol-polyethylene glycol graft polymer (PVA-PEG)	Kollicoat® IR	BASF, Ludwigshafen, Germany
polyvinyl acetate (PVAc) dispersion stabilised with PVP and sodium lauryl sulphate	Kollicoat® SR 30 D	BASF, Ludwigshafen, Germany
propylene glycol	Ph. Eur. 7.0	Caesar & Loretz, Hilden, Germany
talc	Talcum Pharma G	C. H. Erbslöh, Krefeld, Germany
titanium dioxide	Aeroxide® P25	Evonik Industries, Essen, Germany
triethyl citrate	Citrofol® A1	Jungbunzlauer, Ladenburg, Germany

6.2. Methods

6.2.1. Manufacturing Methods

6.2.1.1. Production of CBZ Modification I and CBZ Dihydrate

CBZ modification I (CBZ I) was prepared by heating 3 g CBZ III powder (carbamazepine F, BASF Pharma, Switzerland) at 170 °C in an oven (kelvitron[®] t, Heraeus Instruments, Germany) for 2 h (Lefebvre et al., 1986). To produce CBZ dihydrate (CBZ DH), 1 g CBZ III was suspended in 1 L of distilled water and stirred for 1 h. Then, the insoluble part was separated via a polypropylene filter (0.45 µm) and the solution was transferred into crystallising dishes for the evaporation of the water.

CBZ III, CBZ I and CBZ DH were characterised via XRPD in transmission mode (section 6.2.3.8) and DSC (section 6.2.3.10) to confirm the modification by comparison to literature (Grzesiak et al., 2003; McMahon et al., 1996).

6.2.1.2. Melting and Moulding

The excipients were completely molten on a water bath (W 200, Memmert, Germany) at approximately 10 °C over their melting temperature. 10 - 30 % CBZ (w/w) was dispersed in the melt utilising a pestle and the suspension was then grouted into the casting moulds (Figure 70) and cooled to room temperature. The mini-moulds have a diameter of 4 mm and the longitudinal moulds measure 4 x 50 mm.

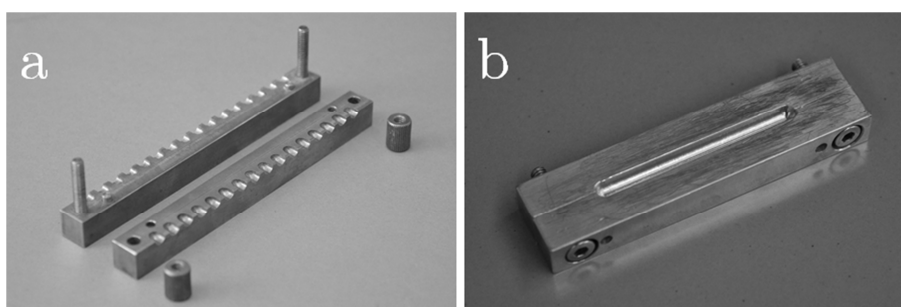


Figure 70: Casting moulds for mini-moulds (Haupt et al., 2013) (a) and longitudinal moulds (b)

6.2.1.3. Small-Scale Ram-Extrusion

The manufacturing of the small-scale ram-extrudates is presented in a scheme below (Figure 71).

40 g of sole excipient or 10 g of CBZ-loaded formulation were prepared by mixing with mortar and pestle. Each powder was then filled into the pre-heated barrel of the high pressure capillary rheometer (HPCR, Rosand[®] RH2000, Malvern, United Kingdom). The HPCR barrel has an inner diameter of 15 mm and a length of 250 mm, resulting in a maximum capacity of 40 mL. It is thermo-stated with an electrically heated jacket with an accuracy of ± 0.7 °C. The temperature of the three heating zones was set collectively.

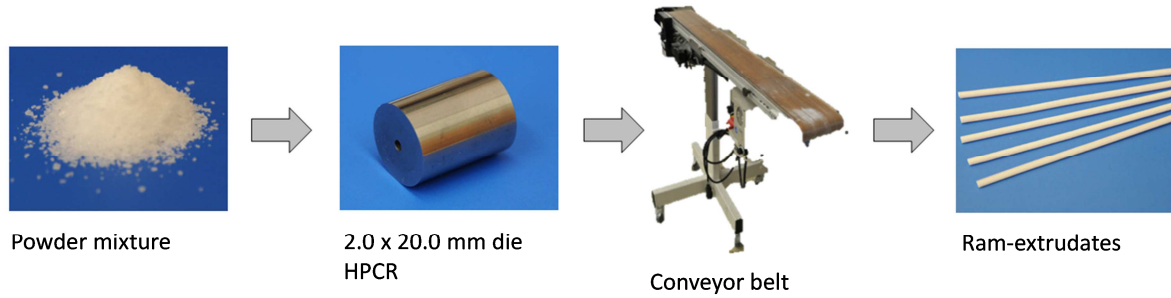


Figure 71: Manufacturing of small-scale ram-extrudates

After manual pre-compression of the material and an equilibration time the ram-extrudates were shaped through a 2.0 x 20.0 mm die (feeding angle of 180°) with a defined piston velocity (v_{piston}). For pressure measurements during extrusion a 10.5 MPa transducer incorporated in the wall of the barrel above the die region was utilised. The pressure transducer mastered a measurement rate of 20 Hz.

A conveyor belt with a length of 1.30 m, adjustable for height and conveying speed (model 846102.001, Brabender, Germany) was used to convey and cool the ram-extrudates down to room temperature.

6.2.1.4. Hot-Melt Extrusion of Extrudates

PEG flakes and the previously prepared wax mixtures were ground in an ultra centrifugal mill (ZM 200, Retsch, Germany) at 6,000 rpm with sieve no. 1.5. PEGs, POL and CBZ were mixed with a batch size of 300 g in a tumbling mixer (Turbula[®] T2A, W.A. Bachofen, Switzerland) at 50 rpm for 30 min.

The extrudates were produced employing a Pharma 16 HME twin-screw extruder (Thermo Fisher Scientific, Germany). The barrel length was 25 D (400 mm) and the die had a diameter of 4.0 mm and a length of 2.5 mm. The temperature of the six heating zones was set collectively and dependent on the formulation (Table 3). A screw speed of 60 rpm and a feeding rate of 600 g/h (KT 20, K-Tron Soder, Switzerland) were utilised. The screw configuration contained four conveying- (4½, 3, 3½, 7 L/D from die to feeder) and three mixing-zones (3, 1, 3 L/D) as depicted in Figure 72.

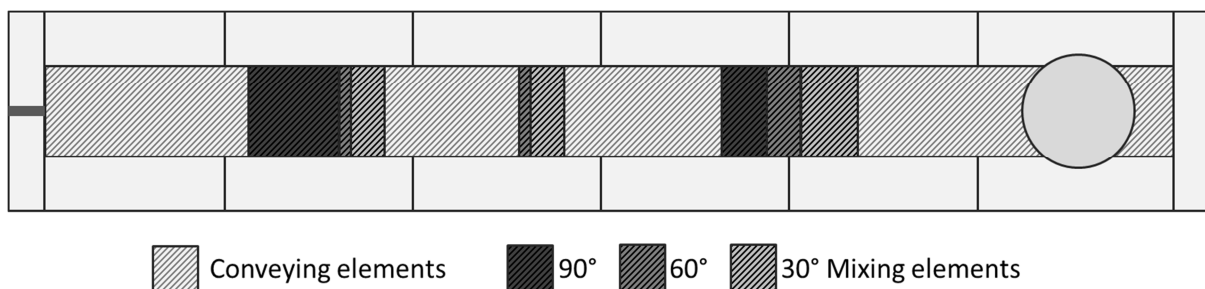


Figure 72: Screw configuration for the hot-melt extrusion, from die (left) to feeder (right)

All conveying elements helices had a pitch of 1 L/D. The angle of the mixing elements varied from 30° over 60° to 90°. A conveyor belt (model 846102.001, Brabender, Germany) was used to transport and cool the extrudates to room temperature. To collect extrudates, which were produced within steady state of the extrusion process, samples (approximately 100 g) were only taken after 10 min.

6.2.1.5. Hot-Melt Co-Extrusion

PEG flakes and the previously prepared wax mixtures were ground in an ultra centrifugal mill (ZM 200, Retsch, Germany) at 6,000 rpm with sieve no. 1.5. PEGs, POL and CBZ were mixed with a batch size of 300 g in a Turbula[®] mixer (T2A, W.A. Bachofen, Switzerland) at 50 rpm for 30 min.

Co-extrusion was performed using two Prism Eurolab 16 twin-screw extruders (Thermo Fisher Scientific, Germany) connected by a co-extrusion die (Figure 73). The co-extrusion die was specially designed and produced by Guill (USA) and was equipped with an outer die tip (diameter of 4 mm) and an inner die tip (diameter of 2 mm).

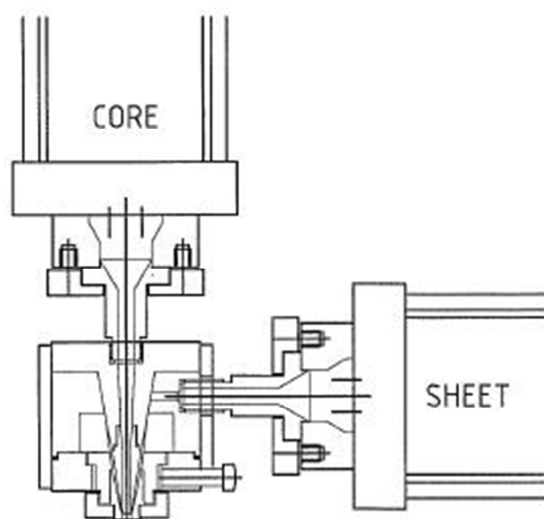


Figure 73: Co-extrusion die set-up (Vynckier et al., 2014b) with cylindrical core and annular coat (sheet)

Feed rate (Flexwall powder feeders, Brabender, Germany), screw speed, and temperature of the equipment were adapted to each formulation during co-extrusion (Table 7). The screw configuration was the same as described in section 6.2.1.4 (Figure 72).

6.2.1.6. Immersion of Extrudates

One extrudate formulation (F5: 45 % CBZ, 40 % PEG 2,000, 15 % PEG 1,500; section 6.2.1.4) was cut into extrudate pieces with 50 mm in length by a surgery knife. Subsequently, they were coated by immersion (Reitz et al., 2008) into a molten mixture two times at 75 °C on a water bath (W 200, Memmert, Germany). Consistent to the wax-coat of the co-extrudates (formulation 9b in Table 7) the molten mixture contained 49 %

bees wax, 30 % PEG 2,000, and 21 % carnauba wax and was manually dispersed prior to immersion.

6.2.1.7. CBZ Layering on Micropellets

The polymeric binder (HPMC or PVA-PEG) was dissolved for 24 h in water with moderate stirring by a magnetic stirrer. Then, the slightly soluble drug was added in small portions and finally dispersed with an Ultra Turrax® (IKA-T18 digital, IKA, Germany) equipped with a dispersing element (S 18 N 19 G) at 25,000 rpm for 10 min. During the layering process in the fluidised bed coater Mycrolab (Hüttlin, Germany) the suspension, which had a total mass of 500 g, was stirred continuously.

The solid content of the layering-suspension was kept constant at 20 %, whereas the CBZ content, the binder, and thus the binder level were varied (Table 12). The binder level is defined in Equation 1.

$$\text{binder level [\%]} = \frac{\text{mass binder}}{\text{mass binder} + \text{mass CBZ}} * 100$$

Equation 1: Binder level

200 g of starter cores were fluidised with a constant air flow rate of 8 m³/h for pre-heating and 15 - 18 m³/h for the spraying process. The spray pressure (0.8 bar) and the nozzle diameter (0.8 mm) were kept constant for all experiments. Further process parameters like the inlet air temperature and the spray rate are depicted in Table 12. A suspension-mass of 200 g was applied within 45 to 70 min depending on the spray rate (Table 12).

After the layering, the CBZ micropellets were cured in an oven (kelvitron® t, Heraeus Instruments, Germany) for 30 min at 43 °C to ensure coalescence of the polymer particles to a film.

In order to obtain defined particle size fractions for further processing, the layered pellets were sieved in a sieve tower on a shaker (AS 200 Control, Retsch, Germany) with 1.5 mm amplitude for two min. The fractions below 500 µm for batches A, B, and D and below 400 µm for batches C and E were selected for further analysis and for the sustained release coating of the pellets (section 6.2.1.8).

6.2.1.8. Sustained Release Coating of CBZ Micropellets

To obtain the excipient suspension for batch 1, talc (5.9 %) and triethyl citrate (TEC, 2.4 %) were homogenised in water utilising an Ultra Turrax® homogeniser (IKA-T18 digital, IKA, Germany) equipped with a dispersing element (S 18 N 19 G) at 25,000 rpm for 10 min. Eudragit® RS D 30 (35.3 %) and Eudragit® RL D 30 (3.9 %) were mixed in a proportion of 9 to 1 (w/w) by gently stirring with a magnetic stirrer. The excipient suspension was then poured slowly into the Eudragit®-dispersion.

For the excipient suspension of batches 2 and 3, glycerol monostearate 60 (0.7 %), polysorbate 80 (0.3 %), propylene glycol (0.7 %), and 100 mL of demineralised water were

heated up to 80 °C under stirring with a magnetic stirrer. Titanium dioxide (0.4 %) was added in small portions during emulsification with the Ultra Turrax® as described in section 6.2.1.7. The excipient suspension was cooled to approximately 25 °C and then Kollicoat® SR 30 D (49.9 %) was added under magnetic stirring.

The suspensions for batches 4 - 6 were obtained by dissolving PVA-PEG (1.5 % or 3.0 %) for 24 h in demineralised water with moderate stirring by a magnetic stirrer. Then, the coating suspension was prepared as described for batches 2 and 3 (with 44.9 % or 39.9 % Kollicoat® SR 30 D). Thus, a proportion of PVAc to PVA-PEG (w/w) of 9:1 (batch 4) and 8:2 (batches 5 and 6) was obtained. For batch 6, talc instead of glycerol monostearate was utilised as anti-tacking substance (5.9 %).

All suspensions had a total batch size of 500 g and were continuously stirred during the coating process to prevent sedimentation and agglomeration of insoluble components. CBZ micropellets were coated (Mycrolab, Hüttlin, Germany) at a spray pressure of 0.8 bar and with a nozzle diameter of 0.8 mm. Further process parameters were adapted for each batch and are presented in Table 14. A suspension-mass of 80 - 130 g was applied within 50 - 90 min depending on the batch size (70 - 150 g) and the spray rate (Table 14).

The film-coated pellets were dried for 12 h and sieved in a sieve tower on a shaker (AS 200 Control, Retsch, Germany) with 1.5 mm amplitude for 2 min to obtain defined particle size fractions. The fractions below 500 µm for batches 1 - 5 and below 400 µm for batch 6 were selected for further analysis and manufacturing of the micropellet-loaded rods (MPLRs). The yield of the sieved fractions varied between 25 and 80 %.

6.2.1.9. Ram-Extrusion of Micropellet-Loaded Rods

Polyethylene glycols (PEG 1,500, PEG 2,000, and PEG 20,000) were used as hydrophilic matrix for the MPLRs. Flaked qualities were ground in an ultra centrifugal mill (ZM 200, Retsch, Germany) at 6,000 rpm with sieve no. 1.5. Subsequently, milled PEGs and the pellets were premixed in a ratio of 7:3 (w/w) by a Turbula® mixer (T2A, W.A. Bachofen, Switzerland) for 15 min at 50 rpm. Then, the MPLRs were manufactured via ram-extrusion with a high pressure capillary rheometer (HPCR, Rosand® RH2000, Malvern, United Kingdom). The set-up of the HPCR is described in more detail in section 6.2.1.3. The three heating zones of the barrel were pre-heated collectively for one hour. For the feasibility study the corresponding temperature was 43 - 45 °C and for the MPLR batches the barrel was heated up to 45 °C.

Next, 20 g of the mixture (15 g for the feasibility study) were filled into the barrel and automatically pre-compressed at a piston velocity of 100 mm/min up to a maximal pressure of 2 MPa. The MPLRs for the feasibility study (section 6.2.2) were extruded after an equilibration time of 10 - 20 min through a die (4 x 20 mm, feeding angle 180 °). The piston velocity as pre-defined extrusion rate was varied from 100 - 300 mm/min. For the MPLR batches an equilibration time of 10 min and an extrusion rate of 200 mm/min were utilised. Finally, a conveyor belt (model 846102.001, Brabender, Germany) was used to transport and cool the MPLRs to room temperature.

6.2.2. Feasibility Study

A design of experiments (DoE) was performed to analyse the impact of the process parameters (factors) on the yield variables. The four yield variables were the pressure during ram-extrusion as well as the maximum cutting force, the tensile strength, and the E-modulus of the produced MPLRs. The MPLRs contained 30 % (w/w) coated pellets ($\leq 710 \mu\text{m}$), and 70 % of a mixture of PEG 1,500 and PEG 2,000 in a ratio of 3:7. They were manufactured as described in section 6.2.1.9.

The DoE observed three factors (extrusion temperature, equilibration time, and piston velocity) on two factor levels, a lower and an upper level (-1; +1). The extrusion temperature was varied from 43 - 45 °C, the equilibration time from 10 - 20 min, and the piston velocity from 100 - 300 mm/min.

A 2^3 full factorial design with three replications of a centre point with a medium setting (level 0: 44 °C, 15 min, and 200 mm/min) was carried out. The experiment run order was fully randomised. The statistical analysis was based on a linear regression model and calculated with MODDE 9.0 (Umetrics, Sweden). To enhance the model a backward regression was conducted by deleting non-significant effects.

6.2.3. Analytical Methods

6.2.3.1. Maximum Cutting Force of the Extrudates

For the small-scale ram-extrudates and the extrudates the maximum cutting force F_{max} was determined at room temperature by Test Apparatus H10KM (Hess, Germany) equipped with a 1,000 N load cell and applying a cutting speed of 1.67 mm/s.

For the extrudates, the co-extrudates and the MPLRs F_{max} was examined using a Texture Analyser (TA.XTplus, Stable Micro Systems, United Kingdom) with a pre-testing and testing-velocity of 1.67 mm/s at room temperature. The cutting strength [MPa] was applied, when normalisation of F_{max} with regard to the extrudate cross-sectional area [mm^2] was necessary.

Both instruments were equipped with specifically developed cutting test set-ups (Figure 74) to measure F_{max} ($n = 10$). Figure 74 a illustrates the cutting test set-up for the Texture Analyser and Figure 74 b presents the newly developed cutting test set-up for the Test Apparatus with a more rigid and changeable cutting knife based on the guillotine-like mechanism described in literature (Wening and Breitzkreutz, 2010; Wening et al., 2012). The Texture Analyser allowed for the recording of force-displacement curves with a measurement-rate of one data point per μm .

For the extrudates and the co-extrudates the assessment of F_{max} was repeated after 6 months of storage at $21.0 \pm 0.2 \text{ }^\circ\text{C}$ at a relative humidity of 45 % in a climate chamber.

6.2.3.2. Tensile Strength and E-modulus of the Extrudates

The tensile strength and the E-modulus of the extrudates were examined using a Texture Analyser (TA.XTplus, Stable Micro Systems, United Kingdom) with a pre-testing velocity of 1 mm/s, a testing velocity of 0.1 mm/s, and a trigger force of 0.049 N.

The Texture Analyser was equipped with a three-point bending rig (Figure 74 c). The three-point bending test was performed five times for each sample (25 mm length) and force-displacement curves were recorded with one data point per μm .

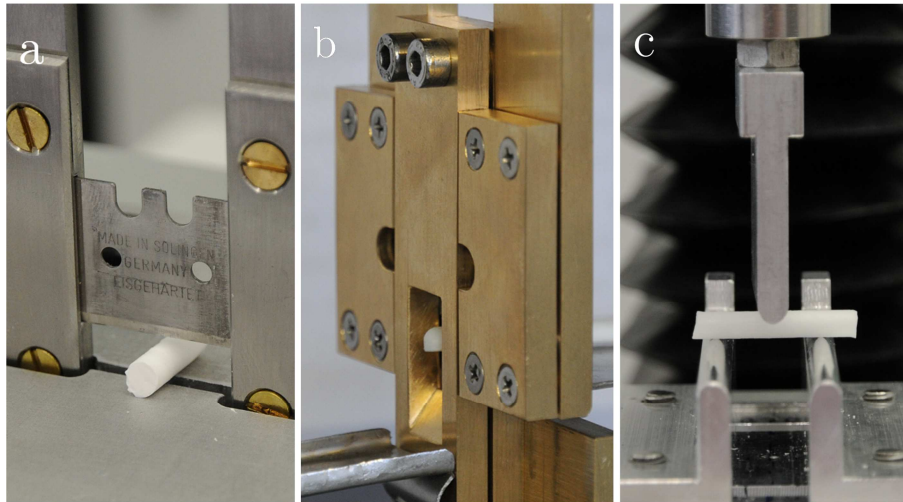


Figure 74: Cutting test set-ups for the assessment of F_{max} for implementation with the Texture Analyser (a) and with the Test Apparatus H10KM (b); three-point bending rig for the three-point bending test with the Texture Analyser for the assessment of the tensile strength and the E-modulus (c)

The tensile strength σ and the E-modulus E (Young's modulus) were calculated following Equation 2 and Equation 3 (Perissutti et al., 2002) with F_{max} as maximum force at break [N], l as the support span of the rig ($l = 17$ mm, according to Roberts and Rowe (1996)), r as radius of the sample [mm], d as the diameter of the sample, and ξ as the vertical displacement of the sample midpoint [mm].

$$\sigma = \frac{F_{\text{max}} * l}{\pi * r^3}$$

Equation 2: Tensile strength σ

$$E = \frac{4 * l^3 * F_{\text{max}}}{3 * \pi * d^4 * \xi}$$

Equation 3: E-modulus E

For the investigation of the temperature-dependency of the tensile strength and the E-modulus the small-scale ram extrudates were stored at different temperatures (17 °C, 20 °C, and 35 °C) until the examination (n = 10).

For the extrudates and the co-extrudates the assessment of the tensile strength and the E-modulus were repeated after 6 months of storage at 21.0 ± 0.2 °C at a relative humidity of 45 % in a climate chamber.

6.2.3.3. Tensile Strength of the Micropellets

To investigate the tensile strength of the starter cores and the sustained release micropellets, the first maximal force for a particle deformation of 50 % was determined by a Texture Analyser (TA.XTplus, Stable Micro Systems, United Kingdom) according to a method by Kleinebudde et al. (1999). The measurement was conducted with a 5 mm punch, a pre-testing velocity of 0.5 mm/s, a triggering force of 0.01 N, and a testing velocity of 0.04 mm/s (Schilling and McGinity, 2010). The diameter of each pellet (n = 30) was recorded by the distance of contact. The tensile strength σ was calculated with the first maximal force F and the diameter d of the pellet according to Equation 4 (Shipway and Hutchings, 1993). All tests were conducted at constant temperature of 21.0 ± 0.2 °C and at a relative humidity of 45 % RH in a climate room.

$$\sigma = \frac{1.6 * F}{\pi * d^2}$$

Equation 4: Tensile strength σ according to Shipway and Hutchings, 1993

6.2.3.4. Microscopy

Optical microscopy and scanning electron microscopy (SEM)

Optical microscopy and scanning electron microscopy (SEM) were performed utilising a Phenom G2 pro (PhenomWorld, The Netherlands) to visualise and examine the surface morphology of the formulations, the interface between core and coat layer in the co-extrudates, the film integrity of coated pellets, and the cross-section of the cut coated pellets. The microscope was utilised with a working voltage of 5 to 10 kV. The samples were attached to aluminium stubs with the help of double-sided carbon tape. Sputter-coating prior to SEM was not required as no charging of the samples under SEM occurred.

Polarised Light Microscopy and Hot Stage Microscopy (HSM)

Polarised light microscopy was utilised for the examination of the morphology of the CBZ crystals and physical changes in combination with excipients upon heating (Leica Microsystems, Germany). For hot stage microscopy (HSM) samples were prepared on a temperature controlled microscopy stage (THMS 600). A little quantity of each sample was placed on a glass slide and was heated at a heating rate of 10 °C/min with the

temperature control system TMS 94 (both Linkam Scientific Instruments, United Kingdom).

6.2.3.5. Dynamic Image Analysis

The pellet size was analysed by dynamic image analysis (Camsizer[®] XT, Retsch, Germany) employing a double camera system. The device was equipped with the X-Fall unit for size determination of the pellets; and with the X-Jet unit for CBZ and PEG. The speed of the conveying trough was adapted to each pellet sample and the dispersion pressure was set to 30 kPa to detect every particle separately without destroying it. The particle sizes were analysed as $x_{c_{min}}$ -values, representing the smallest of all possible maximum cords for the particle projection. Three measurements were conducted with 1 g of sample each. The quantiles x_{25} , x_{50} , and x_{75} , and the inter-quartile span (IQS) were evaluated for the size of CBZ, PEG, the starter cores, the CBZ microparticles, and the sustained release micropellets.

6.2.3.6. Disintegration Time

Disintegration testing was performed according to Ph. Eur. 2.9.1 with a disintegration apparatus A (DT2, Sotax, Switzerland). Six samples of the MPLRs (150 mg each) were given into the tubes of the basket-rack assembly and discs were added. Degassed, demineralised water served as immersion fluid, which was filled into a 1 L, low-form beaker and subsequently tempered to 37 ± 2 °C. The disintegration was observed within the immersion fluid during movement of the basket-rack assembly and the disintegration time [min] was stopped separately for each sample ($n = 6$, mean \pm SD).

6.2.3.7. Dissolution Testing

Apparatus 1 (Basket)

Dissolution testing for the small-scale ram-extrudates, the extrudates and co-extrudates was performed with apparatus 1 (DT 700, Erweka, Germany) at 75 rpm in 900 mL of degassed, demineralised water ($n = 6$) according to Ph. Eur. 2.9.3. The bath temperature was kept constant at 37.0 ± 0.5 °C and sink conditions were maintained during the experiments. Samples were withdrawn automatically (PVP 80, Erweka, Germany) each 2 min (0 - 10 min), then each 10 min (10 - 60 min) and each 30 min (60 - 360 min) and finally each 2 h (6 - 24 h where applicable) for the determination of CBZ. The CBZ concentration was analysed spectrophotometrically at a wavelength of 285 nm (Lambda 2, Perkin-Elmer, USA). In preliminary studies it has been shown, that the excipients did not have a notable impact on the UV-spectra at the corresponding wavelength. The CBZ concentration was calculated following a calibration function (Figure 75).

Dissolution studies were repeated for the extrudates and the co-extrudates after 6 months of storage at 21.0 ± 0.2 °C and at a relative humidity of 45 % in a climate chamber.

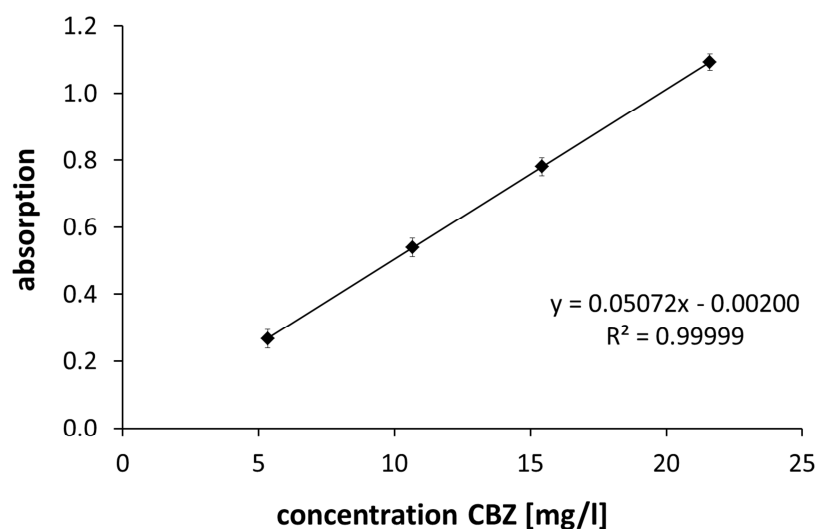


Figure 75: UV-absorption of CBZ in degassed, demineralised water at 37.0 ± 0.5 °C, Lambda 2, Perkin-Elmer, USA; wavelength of 285 nm; cuvette 1 cm; $n = 6$, mean \pm SD

Apparatus 2 (Paddle)

Dissolution studies of the (coated) micropellets and the MPLRs were performed with apparatus 2 (DT 700, Erweka, Germany) at 75 rpm in 900 mL of degassed, demineralised water ($n \geq 3$) according to Ph. Eur. 2.9.3. The bath temperature was set to 37.0 ± 0.5 °C and sink conditions were maintained. To prevent floating of the pellets, they were inserted into the filled vessel by an air stream through a tube. Samples were withdrawn automatically and the CBZ concentration was analysed spectrophotometrically as described above.

Dissolution studies were repeated after 10 weeks of storage at 21.0 ± 0.2 °C at a relative humidity of 45 % in a climate chamber.

6.2.3.8. X-Ray Powder Diffraction (XRPD)

X-ray powder diffraction (XRPD) was performed in transmission mode with an X-ray diffractometer (X'Pert Pro, PANalytical, The Netherlands) with Cu-K α radiation at 40 kV acceleration voltage and 40 mA current. The samples were prepared in a transmission holder between two polyimide films (PANalytical, The Netherlands). The angular range comprised 10 to 50° 2θ with sampling steps of 0.0334° and a scan speed of 0.028°/s. At the incident beam the following adjustments were applied: mask 15 mm, divergence slit 1/8°, anti-scatter slit 1/4°. At the diffracted beam an anti-scatter slit with 5.0 mm was utilised. Measurements were conducted in duplicate.

6.2.3.9. Fourier Transform-Infrared Spectroscopy (FT-IR)

Fourier transform-infrared spectroscopy (FT-IR) spectra were recorded by a Tensor 37 FT-IR instrument (Bruker Optik, Germany) equipped with a platinum ATR diamond. The spectra were recorded from 4000 to 600 cm^{-1} with a resolution of 1 cm^{-1} and by using eight scans per spectrum. Spectra were recorded in duplicate.

6.2.3.10. Differential Scanning Calorimetry (DSC)

Differential scanning calorimetry (DSC) measurements were performed with a DSC 1 (Mettler Toledo, Germany). Samples weighing approximately 5 mg were sealed into pierced aluminium pans of 40 μl . An empty, pierced aluminium pan served as reference. The calibrations of temperature and heating rate were performed with indium and zinc. Measurements were conducted in duplicate in the temperature range from 20 to 220 $^{\circ}\text{C}$ with a heating rate of 10 $^{\circ}\text{C}/\text{min}$.

For the investigation of the interaction of the coating and the matrix in the MPLRs a special DSC method was applied according to literature (Schilling and McGinity, 2010): The matrix material of the MPLRs (PEG-mixture) was either heated in pure form or mixed with an equal quantity of the film building polymer. The DSC-samples ($n = 2$) were sealed in an aluminium pan and heated at 10 $^{\circ}\text{C}/\text{min}$ to 65 $^{\circ}\text{C}$ (20 $^{\circ}\text{C}$ above the extrusion temperature of 45 $^{\circ}\text{C}$). Then, the samples were held at this temperature for 10 min simulating the filling of the barrel, the equilibration time in the barrel, and the ram extrusion. After cooling rapidly to 20 $^{\circ}\text{C}$, a second heating run was performed at 10 $^{\circ}\text{C}/\text{min}$. The melting enthalpies for both the first and the second run were calculated by peak integration (STARe SW 9.20, Mettler Toledo, Germany) and the percentage of relative polymer crystallinity after processing was calculated by dividing the melting enthalpies of the second run through the melting enthalpies of the first run.

6.2.3.11. Raman Spectroscopy

Raman spectra were collected using a Raman RXN2 System (Kaiser Optical Systems, USA). The system was either equipped with a PhAT probe as a non-contact optic sampling device or a PhAT probe with a protective cap as a contact optic sampling device. The wavelength of the excitation laser was 785 nm and the utilised laser power was 400 mW. Analysis was carried out in a spectral range of 1890 to 150 cm^{-1} . Depending on the capacity utilisation of the detector, different exposure times were selected (for mannitol, PEG 2,000, PM, MM and MM CBZ I: 30 s; for CBZ III and CBZ I: 3 s; and for formulations based on PEG, SA and PCL: 10 to 60 s depending on the CBZ content). Depicted spectra were obtained averaging 3 scans (iC Raman[®] 4.1 software, Mettler Toledo & Kaiser Optical Systems, USA).

Raw Raman spectra were treated by two simplifications: First, a CBZ characteristic spectral region (1700 - 1525 cm^{-1}) was selected. Second, a baseline correction via a standard normalised variation (SNV) transformation was accomplished and data were mean centred (SIMCA 13.0, Umetrics AB, Sweden).

The instrument wavenumber accuracy was determined according to Ph. Eur. 2.2.48 for the PhAT probe with a protective cap. Cyclohexane was measured as calibration substance ($n = 3$). Five peaks defined as characteristic in Ph. Eur. (1444.4, 1266.4, 1157.6, 1028.3, 801.3 cm^{-1}) were evaluated for shifts in the peak wavenumber [cm^{-1}] and conformance to required tolerances ($\pm 1.0 \text{ cm}^{-1}$).

6.2.3.12. CBZ Equilibrium Solubility and Partition Coefficient

The equilibrium solubility of CBZ III in molten PEG 2,000 was determined at 65.0 ± 0.5 °C ($n = 3$) based on a method from literature (Just et al., 2013). PEG 2,000 and an excess of CBZ III (carbamazepine F, BASF Pharma, Switzerland) were placed in a small beaker and stirred with a magnetic stirrer at 150 rpm. Constant temperatures were generated by a heating plate. Samples were collected with a syringe after 136 h and directly filtered via a polypropylene filter of 0.45 μm pore size. The sampling equipment was heated prior to usage to avoid recrystallisation of the PEG during the ongoing sampling.

The partition coefficients of CBZ III between PEGs and a wax-mixture (F9, section 3.2.3.1, Table 6) were determined in duplicate. Therefore, CBZ (6 % w/w, carbamazepine F, BASF Pharma, Switzerland) was dissolved in the molten mixture of 85 % PEG 2,000 and 15 % PEG 1,500. Then, the wax-mixture was added and also molten. After stirring at 80 °C for 8 h, the two phases were allowed to separate and the CBZ content was measured within the PEG-phase. A reference (without the addition of the molten wax-mixture) was treated the same way.

For both approaches, the CBZ content was quantified after dissolution of the sample in degassed, demineralised water by UV-spectroscopy at a wavelength of 285 nm (Spekol 1500, Analytik Jena, Germany). In preliminary studies it has been shown, that the excipients did not have a notable impact on the UV-spectra at the corresponding wavelength. The CBZ concentration was calculated following a calibration function (Figure 76).

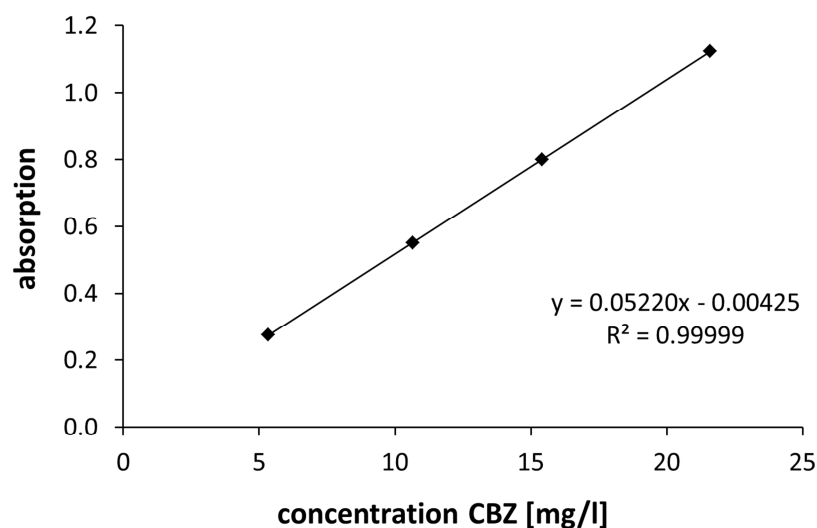


Figure 76: UV-absorption of CBZ in degassed, demineralised water at 21.0 ± 1.0 °C; Spekol 1500, Analytik Jena, Germany; wavelength of 285 nm; cuvette 1 cm

6.2.4. Application of the Solid Dosage Pen

6.2.4.1. Dosing

The rods were inserted into the SDP and ten doses with 5, 10, and 15 dose units (DU) corresponding to extrudate pieces of 2, 4, or 6 mm length were cut. One full revolution of the adjusting screw equals 0.4 mm propulsion of the drug-loaded rod and was defined as one DU.

For the small-scale ram-extrudates exemplary doses with 5 DUs (2 mm length) and for the MPLRs exemplary ten doses with 10 DUs (4 mm length) were sliced.

6.2.4.2. Mass Variation

The mass variation was analysed by weighing and by the assessment of the standard deviation of ten single doses (section 6.2.4.1). Weighing was conducted with a balance with an accuracy (d) of 0.01 mg (model MC 210P, Sartorius, Germany).

6.2.4.3. Content Uniformity

The content of ten single doses (section 6.2.4.1) was analysed spectrophotometrically in degassed, demineralised water at a wavelength of 285 nm (Spekol 1500, Analytik Jena, Germany). In preliminary experiments, it has been shown that the highly diluted excipients did not have an impact on the UV-spectra at the corresponding wavelength. The CBZ concentration was analysed spectrophotometrically as described in section 6.2.3.12.

6.2.4.4. Uniformity of Dosage Units

The uniformity of dosage units was analysed based on the content of ten single doses (6.2.4.3) and on a label claim. The CBZ concentration was analysed spectrophotometrically as described in section 6.2.3.12. Acceptance values (AV) were calculated according to Ph. Eur. 2.9.40. with M as a reference value, \bar{X} as mean of individual contents expressed as the percentage of the label claim, k as acceptability constant (for $n = 10$: $k = 2.4$), and s as the sample standard deviation (Equation 5). Ph. Eur. 2.9.40 requires $AV \leq 15$ for L1.

$$AV = |M - \bar{X}| + k * s$$

Equation 5: Formula to calculate the acceptance value (AV) according to Ph. Eur. 2.9.40.

7. Bibliography

Ager, C.L., Olivett, B.L., Johnson, C.L., 1984. Grasp and pinch strength in children 5 to 12 years old. *Am. J. Occup. Ther.* 38, 107-113.

Attia, M.A., Habib, F.S., 1985. Dissolution rates of carbamazepine and nitrazepam utilizing sugar solid dispersion system. *Drug Dev. Ind. Pharm.* 11, 1957-1969.

Auer, M.E., Griesser, U.J., Sawatzki, J., 2003. Qualitative and quantitative study of polymorphic forms in drug formulations by near infrared FT-Raman spectroscopy. *J. Mol. Struct.* 661, 307-317.

Aulton, M.E., Dyer, A.M., Khan, K.A., 1994. The strength and compaction of millispheres - the design of a controlled-release drug-delivery system for ibuprofen in the form of a tablet comprising compacted polymer-coated millispheres. *Drug Dev. Ind. Pharm.* 20, 3069-3104.

Balducci, A.G., Colombo, G., Corace, G., Cavallari, C., Rodriguez, L., Buttini, F., Colombo, P., Rossi, A., 2011. Layered lipid microcapsules for mesalazine delayed-release in children. *Int. J. Pharm.* 421, 293-300.

Behme, R.J., Brooke, D., 1991. Heat of fusion measurement of a low melting polymorph of carbamazepine that undergoes multiple-phase changes during differential scanning calorimetry analysis. *J. Pharm. Sci.* 80, 986-990.

Breitenbach, J., 2002. Melt extrusion: from process to drug delivery technology. *Eur. J. Pharm. Biopharm.* 54, 107-117.

Breitkreutz, J., Boos, J., 2007. Paediatric and geriatric drug delivery. *Expert Opin. Drug Deliv.* 4, 37-45.

Breitkreutz, J., Wessel, T., Boos, J., 1999. Dosage forms for peroral drug administration to children. *Paediatr. Perinat. Drug Ther.* 3, 25-33.

Brittain, H.G., 1999. *Drugs and the pharmaceutical sciences*. Marcel Dekker, Inc., New York, USA.

Brunner, E., 1904. Reaktionsgeschwindigkeit in heterogenen Systemen (German). *Z. Phys. Chem.* 47, 56-102.

Bühler, V., 2007. Kollicoat® grades: Functional polymers for the pharmaceutical industry. BASF Aktiengesellschaft (Ed.), Ludwigshafen, Germany.

Carlsson, K.C., Hoem, N.O., Glauser, T., Vinks, A.A., 2005. Development of a population pharmacokinetic model for carbamazepine based on sparse therapeutic monitoring data from pediatric patients with epilepsy. *Clin. Ther.* 27, 618-626.

Cheng, L., Lei, L., Guo, S.R., 2010. In vitro and in vivo evaluation of praziquantel loaded implants based on PEG/PCL blends. *Int. J. Pharm.* 387, 129-138.

Cloyd, J., Hauser, W., Towne, A., Ramsay, R., Mattson, R., Gilliam, F., Walczak, T., 2006. Epidemiological and medical aspects of epilepsy in the elderly. *Epilepsy Res.* 68, 39-48.

-
- Corrigan, O.I., Murphy, C.A., Timoney, R.F., 1979. Dissolution properties of polyethylene glycols and polyethylene glycol-drug systems. *Int. J. Pharm.* 4, 67-74.
- Covas, J.A., Costa, P., 2004. A miniature extrusion line for small scale processing studies. *Polym. Test* 23, 763-773.
- Crowley, M.M., Zhang, F., Koleng, J.J., McGinity, J.W., 2002. Stability of polyethylene oxide in matrix tablets prepared by hot-melt extrusion. *Biomaterials* 23, 4241-4248.
- Crowley, M.M., Zhang, F., Repka, M.A., Thumma, S., Upadhye, S.B., Battu, S.K., McGinity, J.W., Martin, C., 2007. Pharmaceutical applications of hot-melt extrusion: Part I. *Drug Dev. Ind. Pharm.* 33, 909-926.
- Cuppok, Y., Muschert, S., Marucci, M., Hjaertstam, J., Siepmann, F., Axelsson, A., Siepmann, J., 2011. Drug release mechanisms from Kollicoat SR:Eudragit NE coated pellets. *Int. J. Pharm.* 409, 30-37.
- Dashevsky, A., Kolter, K., Bodmeier, R., 2004. Compression of pellets coated with various aqueous polymer dispersions. *Int. J. Pharm.* 279, 19-26.
- Dierickx, L., Remon, J.P., Vervaet, C., 2013. Co-extrusion as manufacturing technique for multilayer mini-matrices with dual drug release. *Eur. J. Pharm. Biopharm.* 85, 1157-1163.
- Dierickx, L., Saerens, L., Almeida, A., De Beer, T., Remon, J.P., Vervaet, C., 2012. Co-extrusion as manufacturing technique for fixed-dose combination mini-matrices. *Eur. J. Pharm. Biopharm.* 81, 683-689.
- Doshi, D.H., Ravis, W.R., Betageri, G.V., 1997. Carbamazepine and polyethylene glycol solid dispersions: Preparation, in vitro dissolution, and characterization. *Drug Dev. Ind. Pharm.* 23, 1167-1176.
- Douglas, P., Andrews, G., Jones, D., Walker, G., 2010. Analysis of in vitro drug dissolution from PCL melt extrusion. *Chem. Eng. J.* 164, 359-370.
- Eadie, M.J., 1998. Therapeutic drug monitoring - antiepileptic drugs. *Br. J. Clin. Pharmacol.* 46, 185-193.
- El-Zein, H., Riad, L., El-Bary, A.A., 1998. Enhancement of carbamazepine dissolution: in vitro and in vivo evaluation. *Int. J. Pharm.* 168, 209-220.
- EMA/CHPM, 2013. Guideline on pharmaceutical development of medicines for paediatric use. European Medicines Agency/Committee for Medicinal Products for Human Use, London. EMA/CHMP/QWP/805880/2012 Rev. 2.
- Ensslin, S., Moll, K.P., Haefele-Racin, T., Mader, K., 2009. Safety and robustness of coated pellets: Self-healing film properties and storage stability. *Pharm. Res.* 26, 1534-1543.
- Ensslin, S., Moll, K.P., Paulus, K., Mader, K., 2008. New insight into modified release pellets - Internal structure and drug release mechanism. *J. Control. Release* 128, 149-156.
- Fischer, G., Bar-Shalom, D., Slot, L., Lademann, A.M., Jensen, C., 2003. Polymer release system. WO 03/024429A024421.

Fischer, M.A., 2008. Implanon: A new contraceptive implant. *J. Obstet. Gynecol. Neonatal. Nurs.* 37, 361-368.

Florence, A.T., Lee, V.H.L., 2011. Personalised medicines: More tailored drugs, more tailored delivery. *Int. J. Pharm.* 415, 29-33.

Granger, P., Biton, B., Faure, C., Vige, X., Depoortere, H., Graham, D., Langer, S.Z., Scatton, B., Avenet, P., 1995. Modulation of the gamma-aminobutyric-acid type-a receptor by the antiepileptic drugs carbamazepine and phenytoin. *Mol. Pharmacol.* 47, 1189-1196.

Grassi, M., Voinovich, D., Franceschinis, E., Perissutti, B., Filipovic-Grcic, J., 2003. Theoretical and experimental study on theophylline release from stearic acid cylindrical delivery systems. *J. Control. Release* 92, 275-289.

Griessmann, K., Breitzkreutz, J., Schoettler, F., Schubert-Zsilavec, M., Abdel-Tawab, M., 2005. Amoxicillin powder for syrup. Dosing accuracy and reliable measurement. *Monatsschr. Kinderheilkd.* 153, 735-740.

Groenewegen, R.J.J., 1999. Thermoplastic polymer core and skin containing steroidal progestogenic compound and steroidal estrogenic compound. US 5989581 A.

Grzesiak, A.L., Lang, M.D., Kim, K., Matzger, A.J., 2003. Comparison of the four anhydrous polymorphs of carbamazepine and the crystal structure of form I. *J. Pharm. Sci.* 92, 2260-2271.

Güres, S., Kleinebudde, P., 2011. Dissolution from solid lipid extrudates containing release modifiers. *Int. J. Pharm.* 412, 77-84.

Haaser, M., Karrouit, Y., Velghe, C., Cuppok, Y., Gordon, K.C., Pepper, M., Siepmann, J., Rades, T., Taday, P.F., Strachan, C.J., 2013. Application of terahertz pulsed imaging to analyse film coating characteristics of sustained-release coated pellets. *Int. J. Pharm.* 457, 521-526.

Haupt, M., Thommes, M., Heidenreich, A., Breitzkreutz, J., 2013. Lipid-based intravesical drug delivery systems with controlled release of tiroprium chloride for the urinary bladder. *J. Control. Release* 170, 161-166.

Herrmann, S., Winter, G., Mohl, S., Siepmann, F., Siepmann, J., 2007. Mechanisms controlling protein release from lipidic implants: Effects of PEG addition. *J. Control. Release* 118, 161-168.

Ho, L., Cuppok, Y., Muschert, S., Gordon, K.C., Pepper, M., Shen, Y.C., Siepmann, F., Siepmann, J., Taday, P.F., Rades, T., 2009. Effects of film coating thickness and drug layer uniformity on in vitro drug release from sustained-release coated pellets: A case study using terahertz pulsed imaging. *Int. J. Pharm.* 382, 151-159.

Ingelman-Sundberg, M., Sim, S.C., Gomez, A., Rodriguez-Antona, C., 2007. Influence of cytochrome P450 polymorphisms on drug therapies: Pharmacogenetic, pharmacoepigenetic and clinical aspects. *Pharmacol. Ther.* 116, 496-526.

Iosio, T., Voinovich, D., Grassi, M., Pinto, J.F., Perissutti, B., Zacchigna, M., Quintavalle, U., Serdoz, F., 2008. Bi-layered self-emulsifying pellets prepared by co-extrusion and spheronization: Influence of

formulation variables and preliminary study on the in vivo absorption. *Eur. J. Pharm. Biopharm.* 69, 686-697.

Just, S., Sievert, F., Thommes, M., Breitzkreutz, J., 2013. Improved group contribution parameter set for the application of solubility parameters to melt extrusion. *Eur. J. Pharm. Biopharm.* 85, 1191-1199.

Kayitare, E., Vervaet, C., Ntawukulilyayo, J.D., Seminega, B., Bortel, V., Remon, J.P., 2009. Development of fixed dose combination tablets containing zidovudine and lamivudine for paediatric applications. *Int. J. Pharm.* 370, 41-46.

Kayumba, P.C., Huyghebaert, N., Cordella, C., Ntawukuliryayo, J.D., Vervaet, C., Remon, J.P., 2007. Quinine sulphate pellets for flexible pediatric drug dosing: Formulation development and evaluation of taste-masking efficiency using the electronic tongue. *Eur. J. Pharm. Biopharm.* 66, 460-465.

Kearns, G.L., Abdel-Rahman, S.M., Alander, S.W., Blowey, D.L., Leeder, J.S., Kauffman, R.E., 2003. Developmental pharmacology - Drug disposition, action, and therapy in infants and children. *N. Engl. J. Med.* 349, 1157-1167.

Kennedy, J.P., Niebergall, P.J., 1998. Evaluation of extended-release applications for solid dispersion hot-melt fluid bed coatings utilizing hydrophobic coating agents. *Pharm. Dev. Technol.* 3, 95-101.

Kerr, B.M., Thummel, K.E., Wurden, C.J., Klein, S.M., Kroetz, D.L., Gonzalez, F.J., Levy, R.H., 1994. Human liver carbamazepine metabolism - Role of CYP3A4 and CYP2C8 in 10,11-Epoxy formation. *Biochem. Pharmacol.* 47, 1969-1979.

Kircher, W., 2007. Arzneiformen richtig anwenden, Kapitel: Ergonomische Aspekte (in German). DAV, Stuttgart, 17-29.

Kleinebudde, P., Schröder, M., Schultz, P., Müller, B.W., Waaler, T., Nymo, L., 1999. Importance of the fraction of microcrystalline cellulose and spheronization speed on the properties of extruded pellets made from binary mixtures. *Pharm. Dev. Technol.* 4, 397-404.

Klingmann, V., Spomer, N., Lerch, C., Stoltenberg, I., Fromke, C., Bosse, H.M., Breitzkreutz, J., Meissner, T., 2013. Favorable acceptance of mini-tablets compared with syrup: A randomized controlled trial in infants and preschool children. *J. Pediatr.* 163, 1728-1732.

Kobayashi, Y., Ito, S., Itai, S., Yamamoto, K., 2000. Physicochemical properties and bioavailability of carbamazepine polymorphs and dihydrate. *Int. J. Pharm.* 193, 137-146.

Kogermann, K., Aaltonen, J., Strachan, C.J., Pollanen, K., Veski, P., Heinämäki, J., Yliruusi, J., Rantanen, J., 2007. Qualitative in situ analysis of multiple solid-state forms using spectroscopy and partial least squares discriminant modeling. *J. Pharm. Sci.* 96, 1802-1820.

Kolter, K., 2004. New instant release coating - viscosity and pigment binding capacity of Kollicoat® IR. *Excipients Act. Pharma* 12, 6-7.

Krueger, C., Thommes, M., Kleinebudde, P., 2013. Influence of MCC II fraction and storage conditions on pellet properties. *Eur. J. Pharm. Biopharm.* 85, 1039-1045.

- Laine, E., Tuominen, V., Ilvessalo, P., Kahela, P., 1984. Formation of dihydrate from carbamazepine anhydrate in aqueous conditions. *Int. J. Pharm.* 20, 307-314.
- Langer, M., 2003. Glasartige feste Lösungen schwerlöslicher Arzneistoffe in Zuckeralkoholen (PhD thesis in German). Institute of Pharmaceutics and Biopharmaceutics, Heinrich Heine University, Düsseldorf.
- Law, D., Schmitt, E.A., Marsh, K.C., Everitt, E.A., Wang, W.L., Fort, J.J., Krill, S.L., Qiu, Y.H., 2004. Ritonavir-PEG 8000 amorphous solid dispersions: In vitro and in vivo evaluations. *J. Pharm. Sci.* 93, 563-570.
- Lefebvre, C., Guyot-Hermann, A.M., Draguet-Brughmans, M., Bouche, R., Guyot, J.C., 1986. Polymorphic transitions of carbamazepine during grinding and compression. *Drug Dev. Ind. Pharm.* 12, 1913-1927.
- Lindenberg, M., Kopp, S., Dressman, J.B., 2004. Classification of orally administered drugs on the World Health Organization Model list of Essential Medicines according to the biopharmaceutics classification system. *Eur. J. Pharm. Biopharm.* 58, 265-278.
- Lowe, B.D., 2001. Precision grip force control of older and younger adults, revisited. *J. Occup. Rehabil.* 11, 267-279.
- Lowes, M.M.J., Caira, M.R., Lotter, A.P., Vanderwatt, J.G., 1987. Physicochemical properties and x-ray structural studies of the trigonal polymorph of carbamazepine. *J. Pharm. Sci.* 76, 744-752.
- Lyons, J.G., Blackie, P., Higginbotham, C.L., 2008. The significance of variation in extrusion speeds and temperatures on a PEO/PCL blend based matrix for oral drug delivery. *Int. J. Pharm.* 351, 201-208.
- Mathiowetz, V., Wiemer, D.M., Federman, S.M., 1986. Grip and pinch strength - norms for 6-year-olds to 19-year-olds. *Am. J. Occup. Ther.* 40, 705-711.
- McMahon, L.E., Timmins, P., Williams, A.C., York, P., 1996. Characterization of dihydrates prepared from carbamazepine polymorphs. *J. Pharm. Sci.* 85, 1064-1069.
- Meyer, M.C., Straughn, A.B., Jarvi, E.J., Wood, G.C., Pelsor, F.R., Shah, V.P., 1992. The bioequivalence of carbamazepine tablets with a history of clinical failures. *Pharm. Res.* 9, 1612-1616.
- Miller, D.A., McConville, J.T., Yang, W., Williams, R.O., McGinity, J.W., 2007. Hot-melt extrusion for enhanced delivery of drug particles. *J. Pharm. Sci.* 96, 361-376.
- Moneghini, M., Kikic, I., Voinovich, D., Perissutti, B., Filipovic-Grcic, J., 2001. Processing of carbamazepine PEG 4000 solid dispersions with supercritical carbon dioxide: preparation, characterisation, and in vitro dissolution. *Int. J. Pharm.* 222, 129-138.
- Mühlenfeld, C., Thommes, M., 2012. Miniaturization in pharmaceutical extrusion technology: Feeding as a challenge of downscaling. *AAPS PharmSciTech* 13, 94-100.
- Müller, J., Knop, K., Regdon jr., G., Makai, Z., Pintye-Hódi, K., Kleinebudde, P., 2008. Interaction between Kollicoat® SR and pore forming material in aqueous dispersion and casted films. 6th PBP World Meeting, Barcelona, Spain.

Müllers, K.C., Wahl, M.A., Pinto, J.F., 2013. Multilayer laminar co-extrudate as a novel controlled release dosage form. *Eur. J. Pharm. Sci.* 49, 491-498.

Murphy, D., Rodriguez-Cintron, F., Langevin, B., Kelly, R.C., Rodriguez-Hornedo, N., 2002. Solution-mediated phase transformation of anhydrous to dihydrate carbamazepine and the effect of lattice disorder. *Int. J. Pharm.* 246, 121-134.

Nair, R., Gonen, S., Hoag, S.W., 2002. Influence of polyethylene glycol and povidone on the polymorphic transformation and solubility of carbamazepine. *Int. J. Pharm.* 240, 11-22.

Nernst, W., 1904. Theorie der Reaktionsgeschwindigkeit in heterogenen Systemen (in German). *Z. Phys. Chem.* 47, 52-55.

O'Brien, L.E., Timmins, P., Williams, A.C., York, P., 2004. Use of in situ FT-Raman spectroscopy to study the kinetics of the transformation of carbamazepine polymorphs. *J. Pharm. Biomed. Anal.* 36, 335-340.

Oliveira, G., Wahl, M.A., Pinto, J.F., 2013. Characterization of laminar extrudates manufactured at room temperature in the absence of solvents for the delivery of drugs. *Int. J. Pharm.* 454, 90-98.

Oliveira, G., Wahl, M.A., Pinto, J.F., 2014. Delivery of drugs from laminar co-extrudates manufactured by a solvent-free process at room temperature. *J. Pharm. Sci.* 103, 3501-3510.

Pajander, J., Rensonnet, A., Overgard, M., Olsen, M.R., Fisher, G., Baldursdottir, S., Rantanen, J., 2012. Solid form change of carbamazepine during hot melt processing, 2nd Electronic Conference on Pharmaceutical Sciences.

Patil, A., Chafle, S., Khobragade, D., Umathe, S., Avari, J., 2011. Evaluation of hot melt coating as taste masking tool. *Int. Res. J. Pharm.* 8, 169-172.

Perissutti, B., Rubessa, F., Princivalle, F., 2000. Solid dispersions of carbamazepine with Gelucire 44/14 and 50/13. *STP Pharma Sci.* 10, 479-484.

Perissutti, B., Newton, J.M., Podczek, F., Rubessa, F., 2002. Preparation of extruded carbamazepine and PEG 4000 as a potential rapid release dosage form. *Eur. J. Pharm. Biopharm.* 53, 125-132.

Pinto, J.F., Lameiro, M.H., Martins, P., 2001. Investigation on the co-extrudability and spheronization properties of wet masses. *Int. J. Pharm.* 227, 71-80.

Pinto, J.F., Silverio, N.P., 2001. Assessment of the extrudability of three different mixtures of saturated polyglycolysed glycerides by determination of the "specific work of extrusion" and by capillary rheometry. *Pharm. Dev. Technol.* 6, 117-128.

Podczek, F., Alessi, P., Newton, J.M., 2008. The preparation of pellets containing non-ionic surfactants by extrusion/spheronization. *Int. J. Pharm.* 361, 33-40.

Pöllinger, N., 2013. Microparticulates as drug carriers for pediatric use. *Int. J. Pharm.* 457, 351-353.

Quintavalle, U., Voinovich, D., Perissutti, B., Serdoz, F., Grassi, M., 2007. Theoretical and experimental characterization of stearic acid-based sustained release devices obtained by hot melt co-extrusion. *J. Drug Deliv. Sci. Technol.* 17, 415-420.

- Quintavalle, U., Voinovich, D., Perissutti, B., Serdoz, F., Grassi, G., Dal Col, A., Grassi, M., 2008. Preparation of sustained release co-extrudates by hot-melt extrusion and mathematical modelling of in vitro/in vivo drug release profiles. *Eur. J. Pharm. Sci.* 33, 282-293.
- Racz, I., Dredan, J., Antal, I., Gondar, E., 1997. Comparative evaluation of microcapsules prepared by fluidization atomization and melt coating process. *Drug Dev. Ind. Pharm.* 23, 583-587.
- Ragsdale, D.S., Scheuer, T., Catterall, W.A., 1991. Frequency and voltage-dependent inhibition of type-IIa Na⁺-channels, expressed in a mammalian-cell line, by local-anesthetic, antiarrhythmic, and anticonvulsant drugs. *Mol. Pharmacol.* 40, 756-765.
- Reitz, C., Kleinebudde, P., 2007. Solid lipid extrusion of sustained release dosage forms. *Eur. J. Pharm. Biopharm.* 67, 440-448.
- Reitz, C., Strachan, C., Kleinebudde, P., 2008. Solid lipid extrudates as sustained-release matrices: The effect of surface structure on drug release properties. *Eur. J. Pharm. Sci.* 35, 335-343.
- Repka, M.A., Battu, S.K., Upadhye, S.B., Thumma, S., Crowley, M.M., Zhang, F., Martin, C., McGinity, J.W., 2007. Pharmaceutical applications of hot-melt extrusion: Part II. *Drug Dev. Ind. Pharm.* 33, 1043-1057.
- Roberts, R.J., Payne, R.S., Rowe, R.C., 2000. Mechanical property predictions for polymorphs of sulphathiazole and carbamazepine. *Eur. J. Pharm. Sci.* 9, 277-283.
- Roberts, R.J., Rowe, R.C., 1996. Influence of polymorphism on the Young's modulus and yield stress of carbamazepine, sulfathiazole and sulfanilamide. *Int. J. Pharm.* 129, 79-94.
- Rowan, A.J., Ramsay, R.E., Collins, J.F., Pryor, F., Boardman, K.D., Uthman, B.M., Spitz, M., Frederick, T., Towne, A., Carter, G.S., Marks, W., Felicetta, J., Tomyanovich, M.L., 2005. New onset geriatric epilepsy - A randomized study of gabapentin, lamotrigine, and carbamazepine. *Neurology* 64, 1868-1873.
- Rustichelli, C., Gamberini, G., Ferioli, V., Gamberini, M.C., Ficarra, R., Tommasini, S., 2000. Solid-state study of polymorphic drugs: carbamazepine. *J. Pharm. Biomed. Anal.* 23, 41-54.
- Sakai, T., Thommes, M., 2014. Investigation into mixing capability and solid dispersion preparation using the DSM Xplore Pharma Micro Extruder. *J. Pharm. Pharmacol.* 66, 218-231.
- Salunke, S., Hempenstall, J., Kendall, R., Roger, B., Mroz, C., Nunn, T., Tuleu, C., 2011. European Paediatric Formulation Initiative's (EuPFI) 2nd conference commentary - Formulating better medicines for children. *Int. J. Pharm.* 419, 235-239.
- Sawicki, W., Lunio, R., 2005. Compressibility of floating pellets with verapamil hydrochloride coated with dispersion Kollicoat[®] SR 30 D. *Eur. J. Pharm. Biopharm.* 60, 153-158.
- Scheytt, T., Mersmann, P., Lindstadt, R., Heberer, T., 2005. 1-octanol/water partition coefficients of 5 pharmaceuticals from human medical care: Carbamazepine, clofibrac acid, diclofenac, ibuprofen, and propyphenazone. *Water Air Soil Pollut.* 165, 3-11.

-
- Schilling, S.U., McGinity, J.W., 2010. Novel application of hot-melt extrusion for the preparation of monolithic matrices containing enteric-coated particles. *Int. J. Pharm.* 400, 24-31.
- Schmidt, C., Bodmeier, R., 2001. A multiparticulate drug-delivery system based on pellets incorporated into congealable polyethylene glycol carrier materials. *Int. J. Pharm.* 216, 9-16.
- Schoemakers, J., Grummel, A., 2002. Dosing stick containing rod-shaped tablets. WO 02/102296 A102291.
- Schultz, P., Tho, I., Kleinebudde, P., 1997. A new multiparticulate delayed release system. Part II: Coating formulation and properties of free films. *J. Control. Release* 47, 191-199.
- Shipway, P.H., Hutchings, I.M., 1993. Fracture of brittle spheres under compression and impact loading 1. Elastic stress distributions. *Philos. Mag. A-Phys. Condens. Matter Struct. Defect Mech. Prop.* 67, 1389-1404.
- Sobhani, P., Christopherson, J., Ambrose, P.J., Corelli, R.L., 2008. Accuracy of oral liquid measuring devices: Comparison of dosing cup and oral dosing syringe. *Ann. Pharmacother.* 42, 46-52.
- Spomer, N., Klingmann, V., Stoltenberg, I., Lerch, C., Meissner, T., Breitzkreutz, J., 2012. Acceptance of uncoated mini-tablets in young children: Results from a prospective exploratory cross-over study. *Arch. Dis. Child.* 97, 283-286.
- Standing, J.F., Tuleu, C., 2005. Paediatric formulations - Getting to the heart of the problem. *Int. J. Pharm.* 300, 56-66.
- Stegemann, S., Ecker, F., Maio, M., Kraahs, P., Wohlfart, R., Breitzkreutz, J., Zimmer, A., Bar-Shalom, D., Hettrich, P., Broegmann, B., 2010. Geriatric drug therapy: Neglecting the inevitable majority. *Ageing Res. Rev.* 9, 384-398.
- Strachan, C.J., Howell, S.L., Rades, T., Gordon, K.C., 2004a. A theoretical and spectroscopic study of carbamazepine polymorphs. *J. Raman Spectrosc.* 35, 401-408.
- Strachan, C.J., Pratiwi, D., Gordon, K.C., Rades, T., 2004b. Quantitative analysis of polymorphic mixtures of carbamazepine by Raman spectroscopy and principal components analysis. *J. Raman Spectrosc.* 35, 347-352.
- Strübing, S., Abboud, T., Contri, R.V., Metz, H., Mäder, K., 2008. New insights on poly(vinyl acetate)-based coated floating tablets: Characterisation of hydration and CO₂ generation by benchtop MRI and its relation to drug release and floating strength. *Eur. J. Pharm. Biopharm.* 69, 708-717.
- Strübing, S., Metz, H., Mäder, K., 2007. Mechanistic analysis of drug release from tablets with membrane controlled drug delivery. *Eur. J. Pharm. Biopharm.* 66, 113-119.
- Suhrenbrock, L., Radtke, G., Knop, K., Kleinebudde, P., 2011. Suspension pellet layering using PVA-PEG graft copolymer as a new binder. *Int. J. Pharm.* 412, 28-36.
- Suhrenbrock, L.R., 2011. Effizienz und Geschwindigkeit von Prozessen zur Wirkstoffbeschichtung von Pellets - ein Technologievergleich (PhD thesis in German). Institute of Pharmaceutics and Biopharmaceutics, Heinrich Heine University, Düsseldorf.

- Tanner, S., Wells, M., Scarbecz, M., McCann, B.W., 2014. Parents' understanding of and accuracy in using measuring devices to administer liquid oral pain medication. *J. Am. Dent. Assoc.* 145, 141-149.
- Thommes, M., Baert, L., Rosier, J., 2011. 800 mg Darunavir tablets prepared by hot melt extrusion. *Pharm. Dev. Technol.* 16, 645-650.
- Thommes, M., Kleinebudde, P., 2006. Use of kappa-carrageenan as alternative pelletisation aid to microcrystalline cellulose in extrusion/spheronisation. I. Influence of type and fraction of filler. *Eur. J. Pharm. Biopharm.* 63, 59-67.
- Tian, F., Zhang, F., Sandler, N., Gordon, K.C., McGoverin, C.M., Strachan, C.J., Saville, D.J., Rades, T., 2007. Influence of sample characteristics on quantification of carbamazepine hydrate formation by X-ray powder diffraction and Raman spectroscopy. *Eur. J. Pharm. Biopharm.* 66, 466-474.
- van Santen, E., Barends, D.M., Frijlink, H.W., 2002. Breaking of scored tablets: A review. *Eur. J. Pharm. Biopharm.* 53, 139-145.
- Vaz, C.M., van Doeveren, P., Reis, R.L., Cunha, A.M., 2003. Development and design of double-layer co-injection moulded soy protein based drug delivery devices. *Polymer* 44, 5983-5992.
- Verhoeven, E., De Beer, T.R.M., Schacht, E., Van den Mooter, G., Remon, J.P., Vervaet, C., 2009. Influence of polyethylene glycol/polyethylene oxide on the release characteristics of sustained-release ethylcellulose mini-matrices produced by hot-melt extrusion: In vitro and in vivo evaluations. *Eur. J. Pharm. Biopharm.* 72, 463-470.
- Vynckier, A.-K., Dierickx, L., Saerens, L., Voorspoels, J., Gonnissen, Y., De Beer, T., Vervaet, C., Remon, J.P., 2014a. Hot-melt co-extrusion for the production of fixed-dose combination products with a controlled release ethylcellulose matrix core. *Int. J. Pharm.* 464, 65-74.
- Vynckier, A.-K., Dierickx, L., Voorspoels, J., Gonnissen, Y., Remon, J.P., Vervaet, C., 2014b. Hot-melt co-extrusion: Requirements, challenges and opportunities for pharmaceutical applications. *J. Pharm. Pharmacol.* 66, 167-179.
- Vynckier, A.-K., Lin, H., Zeitler, J.A., Willart, J.-F., Bongaers, E., Voorspoels, J., Gonnissen, Y., Remon, J.P., Vervaet, C., 2014c. Calendring as a direct shaping tool for the continuous production of fixed-dose combination products via co-extrusion. 9th PBP World Meeting, Lisbon, Portugal.
- Walsh, J., Bickmann, D., Bretkreutz, J., Chariot-Goulet, M., EuPFI, 2011. Delivery devices for the administration of paediatric formulations: Overview of current practice, challenges and recent developments. *Int. J. Pharm.* 415, 221-231.
- Washburn, N.R., Simon, C.G., Tona, A., Elgandy, H.M., Karim, A., Amis, E.J., 2002. Co-extrusion of biocompatible polymers for scaffolds with co-continuous morphology. *J. Biomed. Mater. Res.* 60, 20-29.
- Wening, K., 2011. Entwicklung eines Dosiersystems für die individuelle Therapie mit neuen festen oralen Arzneiträgern (PhD thesis in German). Institute of Pharmaceutics and Biopharmaceutics, Heinrich Heine University, Düsseldorf.
- Wening, K., Bretkreutz, J., 2010. Novel delivery device for monolithical solid oral dosage forms for personalized medicine. *Int. J. Pharm.* 395, 174-181.

Wening, K., Breitzkreutz, J., 2011. Oral drug delivery in personalized medicine: Unmet needs and novel approaches. *Int. J. Pharm.* 404, 1-9.

Wening, K., Laukamp, E.J., Thommes, M., Breitzkreutz, J., 2012. Individual oral therapy with immediate release and effervescent formulations delivered by the Solid Dosage Pen. *J. Pers. Med.* 2, 217-231.

Willow, M., Gonoï, T., Catterall, W.A., 1985. Voltage clamp analysis of the inhibitory actions of diphenylhydantoin and carbamazepine on voltage-sensitive sodium-channels in neuro-blastoma cells. *Mol. Pharmacol.* 27, 549-558.

Windbergs, M., Strachan, C.J., Kleinebudde, P., 2009. Tailor-made dissolution profiles by extruded matrices based on lipid polyethylene glycol mixtures. *J. Control. Release* 137, 211-216.

Zecevic, D.E., Wagner, K.G., 2013. Rational development of solid dispersions via hot-melt extrusion using screening, material characterization, and numeric simulation tools. *J. Pharm. Sci.* 102, 2297-2310.

Zerrouk, N., Chemtob, C., Arnaud, P., Toscani, S., Dugue, J., 2001. In vitro and in vivo evaluation of carbamazepine-PEG 6000 solid dispersions. *Int. J. Pharm.* 225, 49-62.

Zhang, G.G.Z., Law, D., Schmitt, E.A., Qiu, Y.H., 2004. Phase transformation considerations during process development and manufacture of solid oral dosage forms. *Adv. Drug Deliv. Rev.* 56, 371-390.

8. Danksagung

Meinem Doktorvater, Herrn Prof. Jörg Breitzkreutz danke ich für die mir gegebene Möglichkeit, in seinem Arbeitskreis am Institut für Pharmazeutische Technologie und Biopharmazie über ein interessantes, vielseitiges und anwendungsnahe Thema promovieren zu können. Seine kreativen Ideen, seine Kenntnis über aktuelle Fragestellungen im Fachgebiet und seine Motivation haben zum Gelingen dieser Arbeit in hohem Maße beigetragen. Des Weiteren bedanke ich mich für die Möglichkeit der Teilnahme an vielen internationalen Konferenzen, Symposien und Seminaren.

Herrn Prof. Peter Kleinebudde, dem Korreferenten dieser Arbeit, danke ich für die vielen konstruktiven Fragen und Anregungen in Fokusgruppen-Sitzungen und bei Vorträgen.

Meinem Fokusgruppen-Leiter Herrn PD Dr. Markus Thommes danke ich von Herzen für seine Unterstützung während der letzten Jahre und das Korrekturlesen dieser Arbeit. Frau Dr. Miriam Pein möchte ich für die Unterstützung v.a. bei analytischen Fragestellungen danken. Herrn Dr. Klaus Knop gilt mein herzlicher Dank für die stetige Ansprechbarkeit, die konstruktiven Gespräche auf dem Gebiet des Befilmens und das Korrekturlesen dieser Arbeit.

Herrn Gerd Büttgenbach und seinem Team in der Feinmechanik-Werkstatt Chemie/Pharmazie danke ich für die stets sehr gute und immer freundliche Zusammenarbeit. Für die Konstruktion und den Bau einer Gussform sowie zweier Schnittapparaturen danke ich Herrn Stefan Stich.

Frau Karin Matthée danke ich für diverse DSC-Methodenentwicklungen und -Messungen sowie für die stets sehr gute Zusammenarbeit auch im Praktikum „Arzneiformenlehre“.

Frau Dr. Elena Reitz danke ich für die kompetente Einarbeitung in die Schmelzextrusion und das „trouble-shooting“ am Extruder. Für die Unterstützung mit der Raman-Sonde und mit dem Hüttlin-Coater danke ich Frau Friederike Foltmann. Frau Dr. Johanna Mosig danke ich für die hilfreichen Diskussionen über Biegefestigkeit und E-modul und Frau Carmen Stomberg für die Überlassung von befilmten Partikeln für Vorversuche am Hochdruck-Kapillarrheometer.

I wish to thank PhD Jody Voorspoels and especially Mrs. An-Katrien Vynckier from Conexus Pharma as well as Prof. Chris Vervaet and Prof. Jean Paul Remon from Ghent University (Belgium) for the very competent and friendly cooperation with the co-extrusion performed in Ghent.

Den studentischen Hilfskräften Herrn Raphael Wiedey, Frau Juliana Radtke, Herrn Philipp Kiefer und Frau Olga Kapelnikova danke ich für die Unterstützung bei Zerfallsbestimmungen, die Bestimmung von mechanischen Eigenschaften am Texture Analyser, die Gehaltsbestimmungen sowie die ersten Extrusionsversuchen am Hochdruck-Kapillarrheometer.

Pour la possibilité d'acquérir des expériences scientifiques en France en 2009, pour l'intégration cordiale dans l'équipe de recherche et pour avoir eu confiance en moi, je remercie le Professeur Odile Chamblin et Ali Assifaoui du Laboratoire de Pharmacie Galénique et Biopharmacie, de l'Université de Bourgogne.

Herrn Prof. Knut Baumann, Frau Prof. Ute Wittstock, Herrn Dr. Rainer Lindigkeit und Herrn Dr. Hans-Otto Burmeister danke ich für die fortwährende Unterstützung während meiner Zeit als Studiengangskoordinatorin Pharmazie. Die vielen lehrreichen Erfahrungen an der TU Braunschweig waren für mich persönlich eine unschätzbare wichtige Vorbereitung für die Promotion.

Meinen Kollegen und Kolleginnen am Institut, insbesondere meinen Bürokolleginnen Frau Dr. Daniela Brock und Frau Dr. Carolin Eckert, sowie Frau Christina Wörtz und Frau Elisabeth Lenz, möchte ich u.a. für viele hilfreiche und offene Diskussionen und viele unvergessliche Kongressreisen DANKE sagen.

Meinen Eltern, meiner Familie und besonders Markus danke ich von ganzem Herzen für die fortwährende und liebevolle Unterstützung und Ermutigung während meiner Doktorarbeit.